CHARACTERISTICS OF PROPAGATING STALL IN AXIAL-FLOW COMPRESSORS

Thesis by

David M. Benenson

In Partial Fulfillment of the Requirements

For the Degree of

Doctor of Philosophy

California Institute of Technology

Pasadena, California

1957

ACKNOWLEDGEMENTS

I wish to express my gratitude to Professor W. D. Rannie for his guidance, constructive criticism and encouragement in this research; to Professor F. E. Marble for his discussions of the propagating stall; to Professor A. J. Acosta for making available the axial-flow pump facility and for his guidance and discussions of the experiments performed in that installation.

I wish to especially thank Mr. F. Tyler Linton for his invaluable assistance in every phase of this research and in the preparation of the manuscript.

I wish to express my thanks to Mr. Carl Eastvedt for his aid in obtaining the motion pictures of the propagating stall.

I wish to thank Mr. Richard Briceland, Mr. Robert E. Devine, Mr. Arthur Henry, Mr. Edison R. Hoge, Mr. Jack R. Kingan and Mr. Haskell Shapiro for their contributions to the research.

Many others contributed to the research and to the preparation of the manuscript.

Last, but certainly not least, I wish to express my appreciation to my wife, Lydia, for her encouragement during the course of the research and for her aid in the computations and preparation of the manuscript.

The author received financial assistance from a Daniel and Florence Guggenheim Fellowship in Jet Propulsion.

The project was sponsored by the Office of Naval Research, Contract N6 ORI-102, Task Order IV.

ABSTRACT

Both small and large amplitude propagating stalls have been observed experimentally, and their characteristics distinguished. The characteristics of the small amplitude propagating stall are such that the phenomenon can be described well by linearized theory. The characteristics of the large amplitude stall (which is the propagating stall phenomenon generally found in compressors) are such that the linearized theory is not adequate to describe the stall.

The propagating stall speeds determined from the small amplitude propagating stall experiments are in good agreement with those predicted by a particular formulation of the linearized theory.

TABLE OF CONTENTS

TABLE OF CONTENTS (Cont'd)

TABLE OF CONTENTS (Cont'd)

SYMBOLS

A	Compressor annulus area
a, A_1, A_2, A_3	Constants in the hot-wire equations (King's Law)
b, B_1, B_2, B_3	Constants in the hot-wire equations (King's Law)
c	Blade chord
C_a	Mean local axial velocity
$\bar{C}_a$	Mean axial velocity in the compressor annulus
$\bar{C}_{a_o}$	Mean axial velocity in the cascade annulus, measured upstream of the guide vanes
C_P	Pressure coefficient = $\Delta P / \frac{1}{2} \rho V^2$
C_T	Torque coefficient = Torque$/\frac{1}{2} \rho U_o^2 A R_o$
C_u	Mean local whirl velocity
$\mathcal{C}_a$	Axial velocity ratio = $C_a / \bar{C}_{a_o}$
$\mathcal{C}_u$	Whirl velocity ratio = $C_u / \bar{C}_{a_o}$
F	Defined in text (Section IV)
G	Defined in text (Section IV)
H	Defined in text (Section IV)
i	Current
N_S	Number of propagating stall cells
p	Pressure perturbation = $p(x,y)$
P	Static pressure
P	Pressure surface of a blade (figure 37)
P_a	Atmospheric pressure
P_s	Static pressure
$\mathcal{P}$	Total pressure loss characteristic (Section IV)
$\mathcal{P}_o$	$\mathcal{P}$ evaluated at (V_o/U) (Section IV)
$\mathcal{P}_o'$	Slope of loss characteristic evaluated at (V_o/U) (Section IV)
ΔP	Static pressure rise across cascade

ΔP_s	Peak-to-peak value of the static pressure fluctuation = $P_{s\max.} - P_{s\min.}$
$\frac{\Delta P_s}{\frac{1}{2}\rho U_o^2}$	Static pressure fluctuation ratio
r	Radius
R	Hot-wire resistance
R_a	Hot-wire resistance at air temperature
R_{known}	Known value of a resistance
R_o	Hot-wire resistance at $0^\circ C$
R_t	Tip radius
s	Blade spacing
S	Suction surface of a blade (figure 37)
u	Velocity perturbation in axial direction = $u(x,y)$
U	Axial velocity
U_o	Velocity of rotor blade tip
v	Velocity perturbation in whirl direction = $v(x,y)$
V	Magnitude of the total local velocity
$\bar{V}$	Magnitude of the mean total local velocity
V_s	Propagating stall speed
V_o	Whirl velocity measured far upstream of a blade row
V_∞	Whirl velocity measured far downstream of a blade row
ΔV	Peak-to-peak value of the magnitude of the velocity fluctuation = $V_{max.} - V_{min.}$
$\frac{\Delta V}{\bar{V}}$	Velocity fluctuation ratio
w	Mean total local velocity
$\mathcal{W}$	Total velocity ratio = $w/\bar{C}_{a_o}$
α	Temperature coefficient of resistance of hot-wire

β Flow angle, measured from the axial direction. Increasing the flow angle results in an increase of the blade angle of attack, for a given cascade geometry.

β_1 Flow angle measured far upstream of a blade row

β_2 Flow angle measured far downstream of a blade row

δ Cascade stagger angle, measured from the axial direction. Increasing the stagger angle results in a decrease of the blade angle of attack, for a given flow angle.

Δ Change of a quantity

θ Angle measured in the circumferential direction

θ_p Circumferential angle of separation of two hot-wire probes

ξ Radius ratio $= r/R_t$

ρ Fluid density

σ Solidity $= c/s$

σ_o Solidity with full complement of blades installed

σ/σ_o Solidity ratio

$\bar{\phi}$ Average flow coefficient $= \bar{C}_a/U_o$

$\bar{\psi}$ Average power coefficient = shaft power $/ \frac{1}{2} \rho \bar{C}_a U_o^2 A$

ψ_s Static pressure rise coefficient $= P_s - P_a / \frac{1}{2} \rho U_o^2$

ω_s Angular frequency of a stall cell, measured with respect to a stationary system

Ω_R Angular frequency of the rotor

ω_s/Ω_R Absolute stall frequency ratio

Subscripts:

1 Perturbed quantities (u, v, p) evaluated immediately in front of cascade, along the y-axis (Section IV)

2 Perturbed quantities (u, v, p) evaluated immediately behind cascade, along the y-axis (Section IV)

a Quantities (c_a, c_u) evaluated in front of the annular cascade guide vanes (figure 32)

b Quantities (c_a, c_u, w) evaluated behind the annular cascade guide vanes (figure 32)

SUMMARY

All compressors and pumps (radial flow, mixed flow and axial flow) stall as the flow rate is reduced. The stall is characterized by a dropping off of the average outlet pressure from the linear rate of increase of pressure as the flow rate is reduced near design values. The efficiency also drops sharply and surging, a self induced oscillation of the flow rate, may occur depending on the configuration of the ducting associated with the compressor. The stalling phenomena became of great interest to engineers as design pressure ratios of compressors were increased because the first stages of high pressure ratio machines invariably ran stalled during starting. This condition made starting of turbojets, for instance, quite difficult. A further difficulty was that blade failure frequently occurred during starting procedure.

Until six or seven years ago, it was assumed that the stall occurred uniformly circumferentially on all blades similarly to the stall of an isolated airfoil. The blade failures were thought to be fatigue failures resulting from stalled flutter as had been observed in single airfoils. In an attempt to discover the source of a low frequency sound that accompanied stalled operation, hot-wire anemometers were introduced near the blades and it was soon found that the stall was asymmetric and consisted of severely stalled regions or cells separated by unstalled flow, the entire pattern rotating unchanged in shape at a constant speed, less than the rotor speed.

This phenomenon, which became known as propagating stall, or rotating stall was discovered at the California Institute by Iura and

Rannie in the latter part of 1951 and was announced simultaneously and independently by Emmons at Harvard and by investigators at the NACA. Iura made a systematic study of the phenomenon in an axial flow compressor during the next two years. About this time theories of the phenomenon were proposed by Sears and Marble. The theories were based on the assumption that the disturbances were of small amplitude, hence allowing linearization of the equations of motion upstream and downstream of an infinite cascade. The flow field upstream was irrotational, where as that downstream was rotational. The theories showed the possibility of disturbances travelling unchanged in shape with constant speed, and the propagating speed was determined.

The comparison of theoretical and experimental stall speeds was not very satisfactory and it was usually necessary to introduce a time lag or other parameters to allow for possible unsteady effects that were believed to be responsible for the differences between calculated and measured propagation speeds. Iura's measurements indicated that the stall disturbance amplitudes were quite large, although the instrumentation he used was not suitable for determination of amplitudes of velocity fluctuations that were not small compared with the mean velocity. Hence there appeared to be a possibility that the linearized theory was not adequate for description of the observed stall phenomena.

The present author continued Iura's investigations with modified and later improved instrumentation, and geometrically simpler blading configurations, in an attempt to find a propagating stall disturbance with amplitude small enough to make comparison with theory more realistic. In spite of extensive search, no propagating stall disturbance was found that did not involve velocity fluctuations as large as

the mean velocity. As a result, a firm conviction grew that small disturbance stall could not occur. Experiments made by other investigators did not give any evidence to the contrary. Other theories were proposed but all were based on the linearizing assumption of small amplitudes.

Attempts were made to discover and describe the detailed nature of the stalled regions of the disturbances in the compressor in the hopes that this would give suggestions for an appropriate theoretical model of the large amplitude stall. Such a variety of stall patterns were found with minor changes of blade configuration, and the hot-wire data were so difficult to interpret that it was decided to investigate the stall phenomena in a fixed annular cascade of very high solidity and high hub ratio. It was hoped that in this way some of the unsteady effects and three-dimensional effects that were possibly complicating the compressor stall would disappear or at least be reduced.

At first no propagating stall could be found. Several changes of chord length and spacing of the flat plate blades first installed in the annular cascade were made with no sign of propagating stall. After auxiliary experiments on a cascade of five blades, blades of simple airfoil shape were installed in the annular cascade and a propagating stall of small amplitude (velocity fluctuations of 10 $^{o}/o$ or less of the mean velocity) was found. This finding was of very great significance because it clarified the status of the linearized theory. There appears to be no doubt that a linearized theory based on an assumption that the losses increase sharply and in a quasi-steady manner as the angle of attack increases corresponds very closely with an observed phenomenon. Amplitudes and disturbance wave length are not determined by the

simplest form of the linearized theory; all other results of the theory including propagating speed, agree remarkably well with observations.

There is still no convincing theory for large amplitude stall, the type that seems to occur almost invariably in actual turbomachines, and hence the type that is of practical importance. The small amplitude stall would be of academic importance except that the close agreement of linearized theory and experiment make it seem most unlikely that the large amplitude stall can be represented by a linearized theory. Many attempts of such representation have been made and perhaps are still being made. The results of the investigations reported herein are of great importance since they present a convincing argument that this representation is unsatisfactory.

The major part of this thesis is concerned with the experiments on the small amplitude stall and in particular the comparison with theory. The observations of large amplitude stall were very extensive but the difficulties of interpretation were such that the results described in what follows are confined to demonstrating the principal difference between the two types of propagating stall. To intrepret the measurements of the large amplitude stall in a consistent manner requires a satisfactory model and so far this has not been devised.

I. INTRODUCTION

As the flow rate through a compressor is reduced with rotor speed constant, the angle of attack of the fluid on the blades is increased to the point that the flow cannot be turned through the blade channel; a stall then occurs, which is similar to the stall of an isolated airfoil. Two types of stall have been observed in compressors: (1) the uniform, or symmetric stall in which all blades are stalled in the same way. The stalled regions remain fixed to the blades. (2) The non-uniform, or asymmetric stall in which the stalled regions occur in well defined patches over the annulus of the blade row, the remaining portion of the annulus being unstalled. The stalled regions are observed to rotate (or propagate) along the blade row at constant speed and unchanged in shape. This stall is termed the propagating (or rotating) stall. Both types of stall occur in compressors. Generally, however, during the stalled operation of a compressor, the propagating stall occurs over a much wider range of flow rates than does the uniform stall.

The periodicity of the propagating stall seems to be the principal cause of blade failure in compressors. It is important therefore, to understand the phenomenon so as to be able to control or at least circumvent its destructive characteristics. Of general interest, it is important to understand propagating stall in order to describe the operation of compressors under stalled conditions.

Propagating stall has been described qualitatively as the periodic stalling and unstalling of the blades. When a blade (or blades) stalls, the resulting separation (and high resistance to the flow) in the channel causes the flow approaching the blade row to be diverted about

the stalled region, as shown in figure 1. Thus, the angle of attack to the left of the stalled blades is reduced, tending to unstall the blades in that region, while the angle of attack to the right of the stalled blades is increased, tending to stall the blades in this region. The stall propagates to the right.

Detailed knowledge of the propagating stall characteristics (such as: (1) conditions for the initiation of the stall, (2) propagating stall speed, (3) number of stall cells, (4) circumferential extent of the stall and (5) flow range in which the stall occurs) and of the loading effects upon the blades caused by the stall is of importance to the designer who, with the aid of such information, could design installations in which the destructive aspects of the stall are avoided. As the use of the turbojet engine has increased, the interest in the phenomenon has also become greater. The results of a number of investigations of the propagating stall, experimental and theoretical, have been published. There has been little correlation between the theoretical and experimental results; the reasons for this lack of agreement will become apparent.

The earliest recorded observation of what is now known as the propagating stall was reported by Cheshire (1) in 1945, at the time of the development of the early British jet engines. The phenomenon was observed in one series of diffuser tests for centrifugal compressors. For the diffuser tests, a low speed research unit was constructed; a window was installed to facilitate visual observations (with the aid of tufts) of the flow. Stall propagation was detected at low speeds; the stall speed was readily determined from the tuft motions. The

investigation was not carried beyond the initial observations.

Emmons and his group (2) were the first to systematically investigate the propagating stall, although their results were not published until 1953. The group was the first to distinguish between the surge and stall phenomena. In the surge phenomenon, the frequency depends primarily upon the compressor ducting; further, the flow rate averaged over the compressor annulus varies with time. In the propagating stall, the frequency is not dependent upon the ducting, but depends upon the compressor characteristics; in addition, the flow rate averaged over the annulus remains constant with time. Emmons and his group were the first to use the hot-wire anemometer extensively in stall propagation investigations. Propagating stall was detected in a single stage axial-flow compressor, a centrifugal compressor and a rectangular cascade.

In 1953, Huppert and Benser (3) reported some results of propagating stall investigations conducted in a single stage and multistage axial-flow compressor. Details of the configurations and the installations in which they were tested were not made available. They were the first to distinguish between partial stall (in which the stall zone extends only over a portion of the blade span) and full stall (in which the stall zone covers the entire blade span). The hot-wire anemometer was used to obtain measurements of the unsteady flow.

Iura and Rannie (4) published in 1953, the first systematic detailed investigations of the propagating stall. The tests were conducted at low speeds upon a compressor of low hub-tip ratio, 0.6.

Single stage and multi-stage configurations were tested; the effects of solidity and blade row interference were investigated. Compressor blading of the free-vortex and solid body type were tested. The hot-wire anemometer was used to obtain measurements of the unsteady flow.

In 1954, Smith and Fletcher (5) summarized the results of a number of tests conducted upon different installations: centrifugal compressors, axial-flow compressors and fans, and a pump. Measurements of the pressure fluctuations, only, were obtained.

Montgomery and Braun (6), in 1955 published the results of investigations of stall propagation in an axial-flow compressor of moderate hub-tip ratio, 0.7. The tests were conducted at low speeds upon a single stage configuration of free-vortex blading; the effects of removal of the stator row were determined. Measurements of the non-steady flow were obtained with a hot-wire anemometer and with a barium titanate crystal pressure transducer located in the outer casing of the compressor, before and after each blade row.

In 1955, Costilow and Hupper (7) reported the propagating stall characteristics of an isolated rotor row in a compressor of high hub-tip ratio, 0.9. A constant-temperature hot-wire anemometer was used to measure the velocity fluctuations. Pressure fluctuations were measured with a pressure pick-up. This is the first installation which was constructed so that the results of experiments could be compared directly with a two-dimensional theory, that is, the hub-tip ratio was sufficiently high such that two-dimensional flows were established.

The first detailed investigations of the propagating stall in a stationary cascade were reported by Stenning (8) in 1955. The investigations were conducted in a radial cascade in which the inlet flow angle to the test cascade was varied with the aid of a row of variable-angle guide vanes located upstream of the test cascade. The effects of Mach number, solidity and Reynolds number upon the propagating stall characteristics were determined. Measurements of the unsteady flow were obtained with a hot-wire anemometer and pressure pick-up. Visual observations of the propagating stall were made with a schlieren system.

Costilow and Huppert (9), in 1956 reported the effects of various degrees of guide vane turning and the presence of stators upon the stall characteristics of a rotor row installed in a compressor of high hub-tip ratio, 0.9 (this installation is the same as that reported in reference 7). Velocity fluctuations were measured with a constant temperature hot-wire anemometer; pressure fluctuations were obtained with the aid of a pressure pick-up.

In 1956, Kreibel (10) published the results of propagating stall investigations in an axial-flow compressor (this facility is the same as that used in reference 6) and a radial cascade (the same installation as reported in reference 8). In the compressor, tests were conducted upon an isolated rotor row; the effects of the variation of solidity and stagger angle upon the stall characteristics were obtained. A constant current hot-wire anemometer and a pressure pick-up were used to measure the fluctuations in the unsteady flow. In the radial cascade, the purpose of the investigations was to extend the data of reference 8

to include the effects of lower cascade stagger angle, higher inlet angles to the cascade and blade row interference. The velocity fluctuations were measured with a hot-wire anemometer; a pressure pick-up was used to measure the pressure fluctuations. Visual observations of the propagating stall were obtained with a schlieren and an interferometer. The use of the interferometer is the first reported of such an instrument in stall investigations; with this device, the flow patterns can not only be made "visible" but quantitative information, as well, can be obtained from the data.

The wide variation of some of the characteristics of the propagating stall, such as the stall rotation speed and number of stall cells, has confused the interpretation of the experimental results. Some of the difficulty in understanding the experimental results may be due to the facilities themselves, such as the use of a compressor of low hub-tip ratio in which three-dimensional flow effects may be important, or the use of a compressor of high hub-tip ratio in which the boundary layer effects may be significant. The use of multi-stage or multi-blade row configurations has, also, indicated considerable blade row interference effects.

The limitations of the instrumentation have contributed to the limitation of the understanding of the phenomenon. To determine adequately the detailed characteristics of the stall, instruments having high responses are required. The hot-wire anemometer has been used most extensively in the stall investigations. However, this instrument is limited in that it responds to the magnitude only, and not the direction of the velocity fluctuations. The hot-wire anemometer

can with modifications, be used as a directional instrument; however it has not yet been able to be adapted to the characteristics of the flows associated with propagating stall (large changes in velocity and flow direction). The use of the interferometer, which has the effect of making the flow "visible" and, from the use of which, quantitative data can be obtained, is an interesting development.

An important factor which limits the understanding of the propagating stall is the lack of an adequate theory through which the observed experimental results can be interpreted. This will be discussed in this section.

In the summary which follows, the experimental results are presented in a qualitative manner only, due to the considerable variation in many of the characteristics of the propagating stall. In all these tests, however, two features of the stall appear to remain the same, regardless of the configuration and installation: (1) the magnitude of the velocity (and pressure) fluctuations is large, of the order of the mean total local velocity (and stagnation pressure) and (2) during stall propagation the fluctuations in flow angle are large at the blade row which controls the stall. These two features will be shown to be significant.

The results of the previous investigations of the propagating stall are:

1. When a compressor is throttled or the angle of attack of a cascade row is increased, the propagating stall first occurs at or near the point of maximum pressure rise of a compressor or cascade system.

2. Partial stalls (stalls which cover only a portion of the blade span) or full stalls (stalls which cover the entire span) may occur. The partial stall occurs in compressors with low hub-tip ratios. In compressors of high hub-tip ratio, or in cascades, the full stall only, is detected.
3. The velocity fluctuation ratios vary considerably in axial and radial station surveys, depending upon the configuration and installation. In general, the value of the ratio is large, of the order of unity, near the blade at which the stall originates or at which the stall is being controlled.
4. Pressure fluctuations upstream of a system are much larger than those downstream of the system at low Mach numbers. As the Mach number is increased, the downstream fluctuations approach, in magnitude, those of the upstream fluctuations. Upstream of a system, the static pressure in the stall cell is of the order of the upstream total head pressure.
5. In compressors, the stalled area increases fairly uniformly as the flow is reduced.
6. In compressors, the absolute stall varies directly with the wheel speed and is independent of the Reynolds number, although the existence of some stall zones is affected by Reynolds number (10). (Effective Reynolds numbers in the multi-stage compressors are greater than those calculated using nominal values of the through-flow velocity, due to the effects of blade wakes). On the other hand, there are appreciable Reynolds number effects in tests conducted in the

radial cascade (10).

7. In compressors, the stall rotates in the direction of the wheel rotation, with respect to an observer in a stationary system, but at a speed lower than the wheel speed. In all systems, the stall propagates in the direction of increasing angle of attack.
8. The values of the absolute stall rotational speed vary considerably, depending upon the configuration and installation.
9. The number of stall cells varies considerably, depending upon the configuration and installation.
10. At the blade row which controls the stall, the flow angle changes significantly during stall propagation. There are indications that flow reversal occurs.
11. Regions of irregular fluctuation or uniform stall may occur near the shut-off condition or between stall regimes in a compressor; similar regions are observed in cascades.
12. Blade row or stage interference effects upon the characteristics of the propagating stall are appreciable. These affect the frequency of the stall zone, number of stall regions, and the angle at which the stall first occurs, but not the magnitude of the fluctuation.
13. Mach numbers large enough to cause shock waves to develop, affect the propagating stall characteristics. The effects of lower Mach numbers have not been clearly determined.

There have been several theoretical investigations of the propagating stall. However, there has been little correlation between

the results of the theories and the experimental results. As will be shown, this is due primarily, to the differences between the theoretical models and the actual stall phenomenon.

All the propagating stall theories presented to date, with but one exception, started from a linearization of upstream and downstream flow fields. Generally, only two-dimensional flow of an inviscid fluid through an isolated blade row of high solidity has been considered. Flows through cascades of high solidity have been considered to enable the propagating stall to be treated as a quasi-steady phenomenon. In the small disturbance theories, the flow upstream of the cascade is assumed to be irrotational, that downstream to be rotational, with small vorticity. At the cascade, three conditions are required to match the upstream and downstream flows. The continuity of flow through the cascade has been employed by all investigators. The remaining two conditions are expressed in terms of the cascade operating characteristics. The various investigators have, as will be seen, chosen cascade characteristics which appear to differ widely from one another; in reality, however, the cascade characteristics differ significantly only in whether the lift or drag effects during stall propagation are to be considered the dominating factor. In the lift important case, the reduction in lift during stall propagation is considered important, while in the drag important case, the increase in drag during stall propagation is of primary importance. At the same conditions, all the lift important theories yield the same results, and all drag important theories yield the same results, the results of the two classes of theories differing from one another. Owing to the linearization the amplitude of the stall

cannot be determined; due to the quasi-steady analysis, neither the shape nor the number of cells of the stall can be determined. The results of the theories are: (1) propagating stall speed and (2) conditions for stall initiation.

The first analysis of propagating stall was made by Emmons and his group (2) which published their results in 1953. The effect of the stall was represented as a restriction of the exit flow area (that is, considered a loss to occur due to the stall) in the channel between two blades. The flow at all other points in the channel was assumed to occur without loss. The flow restriction was considered to be a function of the inlet angle only, implying that the static pressure behind the cascade remained constant during stall propagation. As a consequence of the assumption of constant pressure behind the cascade, the flow pattern upstream of the cascade becomes independent of that downstream of the cascade.

The stability of the flow restriction with respect to small disturbances in the irrotational flow upstream of the cascade was investigated and a condition of neutral stability was determined, that is, a condition was found in which the disturbances neither increased nor diminished with time. During the non-steady flow associated with these disturbances, a lag, related to the separation effects, was assumed; the presence of this lag affected the stall propagation speed.

An additional result of the analysis is that the harmonics of the disturbance travel at different speeds (the higher harmonics traveling more slowly) proportional to $1/n$. Therefore, in order to preserve

the initial shape of the disturbance with time, the disturbance is required to be a pure sine wave.

The dynamic equations of motion were not solved.

Sears (11) in 1953, obtained the first solutions. The flow was considered to be quasi-steady with respect to the propagating stall. Small turning of the flow through the cascade was assumed. Two cases were considered: (1) lift important; that is, the reduction in lift during stall propagation was considered to be of dominating importance and (2) drag important; that is, the increase of drag during stall propagation was considered to be the important factor.

The cascade characteristics, for the lift important case, were assumed to be: (1) conservation of total pressure across a stationary cascade and (2) relation between circulation, lift and blade angle of attack. A phase lag, between the lift and angle of attack, was introduced in the second cascade characteristic. The phase lag was introduced on the basis of data which appeared to indicate its existence; the phase lag was assumed to depend upon the mean blade angle of attack only, and not upon the frequencies associated with stall propagation. The resulting equations are satisfied, and stall propagation can occur, only for certain values of inlet angle, phase lag and lift curve slope; the lift curve slope is required to be negative, that is, the conventional lift characteristic of an isolated airfoil is in the region of stalled flow. Stall propagation is possible for all values of phase lag.

The cascade characteristics, for the drag important case, were assumed to be: (1) total pressure loss across the cascade and (2) con-

stant leaving angle, which implies a cascade of very high solidity. In the first cascade characteristic, a phase lag, similar to the lag introduced in the lift important case, was introduced; this lag was assumed to occur in a manner similar to that observed in the phase lag associated with the lift. The solutions of the resulting equations indicate requirements, for stall propagation to occur, upon the slope of the loss characteristic, inlet angle and phase lag. Stall propagation occurs in the region in which the losses are increased beyond those in normal operation; thus a blade can be considered to be stalled. Stall propagation is possible for all values of the phase lag.

In 1954, Marble (12) presented a theory of propagating stall. The flow was considered to be quasi-steady with respect to the propagating stall. Small turning of the flow through the cascade was implied. The loss of cascade pressure rise was considered to be of dominating importance.

The cascade characteristics were assumed to be: (1) constant leaving angle of the flow from the cascade, which implies a cascade of very high solidity and (2) an abrupt decrease in pressure rise at stall conditions. During stall, the cascade pressure-rise was assumed to decrease, abruptly, to zero. An interesting feature of this second characteristic is that a clear distinction between stalled and unstalled flow regimes is made; therefore, the percent of the circumference which is stalled can be determined. The resulting stall speed obtained is identical, at the same conditions, with that determined by Sears in the drag important case.

Stenning (13), in 1954, extended Emmons' (2) approach, essentially, and solved the equations of motion to obtain a stall speed. Various time lags connected with (1) the inertia of the fluid (a) outside the cascade and (b) between the blades and (2) the boundary layer, were considered. As in Emmons' case, the stall speed depends upon the harmonics of the disturbance. Due to the assumption of constant pressure downstream of the cascade, the resulting stall speed is twice that obtained by Sears, at the same conditions, in the drag important case.

Burggraf (14) presented, in 1955, a theory of stall propagation based upon airfoil characteristics. The airfoil lift and drag characteristics were represented as functions both of the angle of attack and rate of change of angle of attack; a time constant, associated with the non-steady stalling characteristic of the airfoil was introduced. The deflection of the fluid in passing through the blade row was assumed to be small. The effect of a finite number of blades upon the stall characteristics was investigated and found to be small. Cases in which (1) the lift is important and (2) the drag is important, were considered.

The solutions to the resulting equations were represented by Fourier series. Owing to the non-linearity in the assumed lift and drag airfoil characteristics, harmonics, higher and lower than a given harmonic appeared, thereby making it difficult to evaluate the Fourier coefficients. The coefficients corresponding only to the fundamental frequency of the Fourier series were evaluated. Solutions could then be obtained.

The resulting stall speeds determined are identical, at the same conditions, with those obtained by Sears.

The first non-linear theory was presented in 1956 by Kriebel (10) who considered from observations of experimental data, that both rotors and cascade airfoils shed vortices, during stall propagation, similar to the Kármán vortex street shed from a flat plate. During stall propagation, it was assumed that all the circulation downstream of the cascade was concentrated in discrete potential vortices which were shed from the airfoils as they entered or left a stall cell. Therefore, the flow could be considered irrotational everywhere except at the singularities associated with the vortices.

The effect of a vortex near a cascade of airfoils was considered first; due to the difficulties of analysis the approach was abandoned in favor of a vortex street method. In the vortex street method, each cascade airfoil was assumed to shed all its circulation when it entered the stall cell and to regain it completely upon leaving the stall cell. The vortex street was assumed to extend indefinitely far downstream of the cascade. The width of the stall cell was considered to be the distance between the rows of vortices. With respect to the stall, the flow was considered to be quasi-steady. In the theory, it was implied that all blades outside the stall cell had no drag while those inside the stall cell had no lift. By assuming the axial through-flow velocity in the stall cell to be zero, the propagating stall speed was determined.

The results of the theoretical investigations of the propagating stall may be summarized as follows:

1. The results of the small disturbance analyses are: (1) propagating stall speed and (2) conditions for the first occurrence of stall propagation. The extent of the stall cannot be determined, except in the case of the theory according to Marble in which clear distinction was made between stalled and unstalled operation.

2. With the exception of the theories of Emmons and Stenning, all small disturbance theories assume or imply small turning of the fluid through the cascade.

3. All small disturbance theories of the same type yield, at the same conditions, the same result for the propagating stall speed:

For the theories in which the lift is important, the stall speed at zero lag is:

$$\frac{V_s}{U} = \frac{\tan \beta_1}{\cos^2 \beta_1 (\tan^2 \beta_1 - 1)} \quad .$$

For the theories in which the drag is important, the stall speed at zero lag is:

$$\frac{V_s}{U} = \csc 2\beta_1 \quad .$$

The stall speed determined according to Stenning is twice the above, due to the assumption of constant pressure downstream of the cascade.

At the time the present investigations were begun, the results of experiments performed by Huppert and Benser (3) and Iura and

Rannie (4) were available, as were the theoretical investigations of Sears (11) and Marble (12). From these experimental investigations it appeared that the observed propagating stalls were of such strength that their representation by small disturbance theories was not appropriate; that is, the theories, in order to represent the actual occurrences, would, then, be required to be non-linear theories. Accordingly, experiments were performed by the present author to determine the character of the propagating stall which is generally observed in compressors and to determine whether a propagating stall existed which could be described well by a small disturbance theory.

In the experiments which were then conducted, two types of propagating stall were detected; these stalls are differentiated from one another, experimentally, by the character of their more easily measurable quantities. In one type of propagating stall, the perturbations in velocity are found from experiments, to be small everywhere (of the order of 10 percent of the mean steady-state values) except near the suction surface of a blade and in the blade wake; this stall is called the small amplitude propagating stall. In the second type of propagating stall, the perturbations are observed to be large everywhere (of the order of the mean steady-state values); hence, the stall is identified as the large amplitude propagating stall. The propagating stall phenomenon which has been encountered in compressors and reported in the literature is the large amplitude stall. The characteristics of the small and large amplitude stalls will be shown to differ completely from one another. Propagating stalls of intermediate character have not been detected.

In discussing the characteristics of these propagating stalls, consider the steady-state performance of a cascade. At low incidence angles and within a small range of angles (about 5 degrees), the cascade losses (analogous to the drag losses of an isolated airfoil) are small; the cascade blade is unstalled in this region. Beyond this range, the losses increase quite rapidly with changes in incidence angle; in this region, therefore, the steady-state losses are greater than those encountered in the unstalled region, and the slope of the loss characteristic is much larger than observed in the unstalled region. At some point in this region of high loss, the cascade stalls, and the propagating stall occurs. With the cascade loss characteristic as a reference, the distinguishing characteristics between the small and large amplitude propagating stalls will become clearly evident.

Consider first the small amplitude propagating stall.

Just prior to the cascade stall, the incidence angle of the cascade is large, resulting, during steady-state operation, in greater losses than encountered at small incidence angles. At these large incidence angles, the tendency for the boundary layer along the suction surface of a blade to separate, due to a disturbance, is much more pronounced than at the small incidence angles. Disturbances, due to stream and/or wake turbulence, are always present, and at a sufficiently large incidence angle, depending upon the blade shape, the disturbances will be of the right order to trigger the separation of the boundary layer along the suction surface of a blade. The resulting perturbations will cause other blades to stall and a propagating stall then occurs; that is, at a given blade, the boundary layer along the

suction surface will periodically separate and reattach. In the small disturbance stall, only the boundary layer along the suction surface separates (and reattaches); the flow along the pressure surface of a blade always remains smooth and attached. Therefore, the disturbances in velocity and pressure are everywhere small, except (1) at the suction surface of a blade, where the differences between separated and attached flows are considerable, and (2) in the wake regions downstream, where the same differences occur. Examining the previously described cascade loss characteristics, the cascade is then seen to operate at an incidence angle such that, for a small change in incidence angle, the cascade loss increases rapidly.

Propagating stall would not occur at low incidence angles since the normally encountered disturbances, previously described, are not of sufficiently large magnitude to trigger the boundary layer separation.

At a sufficiently low cascade solidity, perturbations, due to the separation of the boundary layer from the blade suction surface, would be of insufficient strength to induce separation upon an adjacent blade; the small amplitude propagating stall would not then occur.

The angle range in which the small amplitude propagating stall occurs is limited by the ability of the boundary layer to reattach to the suction surface following separation. At sufficiently large angles, complete, non-reattaching separation of the suction surface boundary layer (uniform stall) would then occur, similar to that of an isolated airfoil.

The airfoil shape, insofar as it influences the boundary layer and its transition characteristics, affects both the actual occurrence and the range of angle in which the small amplitude stall occurs. Consider a blade of rectangular profile, for example. There is appreciable separation of the flow along the suction surface at most incidence angles; consequently, the propagating stall, if it occurs at all, would do so only in a narrow range of incidence angles.

Experimental observations of the small amplitude propagating stall in a large rectangular cascade have shown, with the aid of tufts, periodic separation and reattachment of the boundary layer along the suction surface of a blade, practically from its leading edge. The flow along the pressure surface is smooth and virtually unperturbed at all times.

Tests, in this installation, upon a cascade of airfoils of rectangular profile, have shown that the boundary layer along the suction surface is separated at very low incidence angles; propagating stall is not detected at any incidence angle.

The small disturbance propagating stall was also detected in an annular cascade and in the stator row of an axial-flow compressor. The small amplitude stall was not detected upon the rotors of rotating machines.

In all experiments, the velocity disturbances were everywhere of the order of $\pm$ 10 percent of the mean total local velocity, except in the wake regions previously described, in which the disturbances were of the order of the mean total local velocity.

The effects of the variation of solidity were investigated in the annular cascade and the compressor cascade. Below a solidity of the order, $\sigma = 1/2$, propagating stall was not detected.

In all installations, there was a maximum incidence angle, beyond which propagating stall did not occur. For a given configuration, the propagating stall was detected in about a 10 degree range of incidence angles.

A minimum Reynolds number was detected, below which propagating stall did not occur.

A quasi-steady small disturbance theory of propagating stall, proposed by Professor W. D. Rannie, is presented in this thesis. As previously discussed, for the stall to be treated as quasi-steady, the stall wavelength is required to be long compared to a characteristic length, such as the spacing between blades. In the theory, the flow upstream of the cascade is considered to be irrotational, that downstream of the cascade to be rotational with small vorticity. Three conditions at the cascade are required to match the upstream and downstream flows. One condition is that of the continuity of the flow through the cascade. The two remaining conditions are considered in terms of assumed cascade operating characteristics: (1) the leaving angle of the flow from the cascade is assumed to be constant at all times; this implies a cascade of very high solidity and (2) the cascade characteristics are represented by the loss characteristics; the losses (drag) are considered to be of importance in determining the propagating stall characteristics. In the theory, the turning of the flow through the cascade is <u>not</u> assumed to be small. The results of the analysis are:

(1) propagating stall speed, (2) occurrence of the stall at but one inlet angle and (3) value of the loss and slope of the loss characteristic at the stalling inlet angle.

The characteristics of the experimentally observed small amplitude stalls satisfy well the requirements of the theory. Therefore, comparison between theory and experiment becomes significant. The experimentally measured propagating stall speeds agree, generally within 10 percent, with the results predicted according to the theory.

The occurrence of the stall in a fairly large range of incidence angles, as compared to the theoretical restriction, is due both to the finite, though small, amplitude of the stall and to the manner in which the variation of incidence angle is obtained.

Values of the loss and slope of the loss characteristic, calculated according to the theory, using the experimentally measured flow angles, are of the order which are observed during cascade operation at large incidence angles.

The small disturbance theory can be adapted to determine the effects of asymmetrical inlet flows upon the performance of a cascade or compressor. Experimental results confirm the theory.

Consider now, the large amplitude propagating stall.

During stall propagation of a stall covering many blades, consider the flow through these blades to be blocked, causing the flow to be diverted to both sides of the stalled region. The angle of attack at one side of the stalled region is increased so that the blades are positively stalled, that is, stalled in the normal manner. On the

opposite side of the stalled region, due to the extensive flow blockage, the angle of attack is reduced to such an extent that the blades in this neighborhood are negatively stalled. Thus, the distinction between the small and large amplitude propagating stalls becomes evident. In the former, during stall propagation, the cascade operates under positively stalled conditions. During large amplitude stall propagation, however, the cascade operation covers the entire region from positive to negative blade stall. In about the center of the stalled region, the incoming flow is at an angle such that the cascade could be expected to be unstalled; however, this does not occur due, probably, to the large loss which exists at this angle. In other words, due to the stall, there must be a significant hysteresis effect such that at low incidence angles the cascade still remains stalled. Such a hysteresis effect has not been detected in cascades probably because the appropriate tests have not been performed.

The flow blockage during stall propagation results in large perturbations in velocities and pressure, of the order of the mean values of these quantities, upstream and downstream of the blade row. The through-flow velocity during stall propagation is small; flow reversal may occur.

The extent of the flow blockage associated with the large amplitude propagating stall results in the occurrence of the stall (1) to solidities lower than those encountered in the small amplitude stall and (2) over a larger range of angles than observed with the small amplitude stall.

Since the extent of the flow blockage is so great in the large amplitude stall, little effect of blade shape upon the stall occurs.

In the experiments, two types of large amplitude propagating stall were detected: the partial stall and full stall. Such stalls have occurred in many installations, as previously noted. In the partial stall, the propagating stall occurs only over a portion of the blade span (from blade tip to the blade mid-span, for example), whereas the full stall occurs over the entire blade span. The partial stall occurs in compressors of low hub-tip ratio, of the order of 0.5, in which the blade twist is such that stall propagation occurs over only a portion of the blade span. In compressors of high hub-tip ratio, of the order of 0.9, only the full stall occurs; the full stall occurs in all compressors.

The velocity and pressure fluctuations associated with the large amplitude propagating stall are of the order of the mean steady-state values of these quantities in the vicinity of the blade row which controls the stall.

The investigations performed on an axial-flow compressor show that the minimum velocities during stall propagation are small. Upstream of the blade row, during stall propagation, hot-wire anemometer measurements reveal considerable turbulence which would most probably arise if the flow through the blade row were reversed. Visual observations of the motions of tufts attached to rotor and stator blades, and to rakes in the blade passages of an axial-flow pump indicate (1) flow reversal in the blade passage during stall propagation and (2) positive and negative blade stall during stall propagation.

Blade row interference affects considerably the stall propagation speed and the number of stall cells, but not the amplitude of the disturbance.

The experimentally observed characteristics of the large amplitude propagating stall immediately indicates that the use of the small disturbance theories of propagating stall are not applicable to the large amplitude stall. As was previously described, the use of any small disturbance theory requires that, during propagating stall, the cascade operate under positively stalled conditions and that the perturbations in velocity and pressure be small. The experimentally observed characteristics of the large amplitude stall do not at all agree with the basic requirements of the small disturbance theories; during stall propagation, the cascade operating conditions vary from positive to negative blade stall and the perturbations are large.

A non-linear stall propagation theory is, therefore, required.

The experimental evidence previously described indicates that the stall can be considered to be a bluff body, vortices being formed downstream of the body, as in a vortex street, as a result of the loss and regaining of circulation of the blades as they enter and leave the region of stalled flow. The first non-linear theory was presented by Kriebel (10), who used the above model.

II. EXPERIMENTAL OBSERVATIONS OF THE SMALL AMPLITUDE PROPAGATING STALL

2:1 Introduction

Before the first example of a small amplitude propagating stall was discovered, extensive experimental investigations had been conducted upon various guide vane-rotor and isolated rotor row configurations in the axial-flow compressor described in Appendix I:1.2 and I:2.1 in unsuccessful attempts to find such a stall. All stalls observed were of the large amplitude type, that is the velocity fluctuations associated with the stalls were of the order of the mean total local velocity.

The small amplitude stall was first detected in the rectangular cascade described in Appendix I:1.3. The fairly large size of the blades in this cascade (8 1/2 inch chord) permitted detailed observations of the cascade stall characteristics. Several characteristics of the small amplitude stall: separation of the boundary layer along the suction surface only, of a blade; smooth attached flow along the blade pressure surface at all times; and effect of blade shape were observed clearly in this installation. However, two characteristics of this installation: the small number of blades in the cascade (five) and the abrupt change to a large flow area downstream restricted the use of this cascade to the description of the qualitative characteristics only of the small amplitude stall.

An annular cascade of high hub-tip ratio, 0.8, was constructed so as to obtain two-dimensional flow; the cascade is described in Appendix I:1.1 of this thesis. A reduced, scaled version of one of the

blade shapes tested in the rectangular cascade was employed in the annular cascade. Well defined, stable small amplitude propagating stall was observed in this installation. The effects of solidity upon the stall characteristics were determined. The stall propagation speed and number of stall cells (one) were readily determined. From these observations of the propagating stall, it became apparent that a small amplitude stall should be detected in the stator row, at least, of the previously described axial-flow compressor. Accordingly, a guide vane-rotor configuration was employed to vary the inlet flow angle to the stator row; the stator row was separated as much as possible from the guide vane-rotor combination to minimize blade row interference effects. This configuration is described in Appendix I: 1. 2. Small amplitude propagating stall was observed in the stator row. The stall was not as stable as that observed in the annular cascade, perhaps due to the radial variation of blade twist occasioned by the low compressor hub-tip ratio, 0. 6; in addition, multi-cell stall patterns were observed, in contrast to the single cell stall pattern detected in the annular cascade.

The small disturbance propagating stall was not detected on the rotors of the axial-flow compressor.

From the observations of the small disturbance propagating stall, the distinguishing characteristics between the small and large amplitude stalls became clear. Consider the cascade performance to be represented in terms of losses (analogous to the drag losses of an isolated airfoil). Within a small range of incidence angles, the losses are small; outside this region the losses increase rapidly with small

changes in incidence angle. At some point within the latter region the cascade is considered to be in the stalled condition.

In the small amplitude propagating stall, the cascade is considered to be operating in the region of high loss (near positive blade stall), and experiences small changes from the mean operating condition. When a blade stalls, the boundary layer along the suction surface only separates; the resulting perturbations then induce the same boundary layer separation at the adjacent blades. The flow along the pressure surface of the adjacent blades remains attached and smooth at all times. Thus, the perturbations are small everywhere except near the blade suction surface and in the wake regions. At a given blade, during stall propagation, the boundary layer periodically separates and reattaches. Therefore, there will be a maximum incidence angle beyond which the boundary layer becomes permanently separated and propagating stall no longer occurs. The blade shape or profile, insofar as it affects the boundary layer transition characteristics, will influence both the actual occurrence and the range of angles in which stall propagation occurs. Since the perturbations associated with the stall are small, there will be a minimum solidity below which these perturbations will not be of sufficient strength to induce boundary layer separation at the adjacent blades; at such conditions propagating stall will not occur.

At about the time the small amplitude stall was first detected, a quasi-steady small disturbance theory of propagating stall was proposed by Professor Rannie (see Section IV of this thesis). The

quasi-steady condition implies a stall whose wavelength is much greater than the blade spacing. Two-dimensional flow of an inviscid fluid through an infinitely long isolated cascade row is considered. The turning of the fluid through the cascade is not assumed to be small. The flow upstream of the cascade is assumed to be irrotational, while that downstream is considered to be rotational with small vorticity. Three conditions at the cascade are required to match the upstream and downstream flows. One of the conditions employed is that of the continuity of flow through the cascade. The two remaining conditions are specified in terms of the cascade characteristics: (1) constant leaving angle of the flow from the cascade. This implies a cascade of very high solidity and (2) representation of the cascade losses as an unspecified function of the inlet angle. Condition (1) is satisfied experimentally to solidities as low as the order of unity. Solution of the resulting equations yields the following results: (1) stall propagation speed, (2) occurrence of the stall at but one value of the inlet angle and (3) total pressure loss and slope of the loss characteristic at the stalling inlet angle.

The experimental results in the annular cascade showed that the stall was indeed quasi-steady, the stall wavelength being 60 blade spacings. Inasmuch as the cascade leaving angle was the variable during these tests, the cascade matching condition (1) could not be checked. In the compressor cascade tests the stall wavelength was of the order of 5 blade spacings which satisfies less well the quasi-steady requirements of the theory. The flow leaving angle was nearly constant regardless of the inlet angle in the range of inlet angles tested.

The requirements of the theory having been satisfied in general by the experimental results, the comparison of the stall speeds according to theory and experiment, becomes significant. In general the theoretical and experimental results agree within 10 percent.

In the large amplitude propagating stall, the flow through the stall cell is essentially blocked. The flow which is diverted about this region causes positive stall at one end of the stall zone and negative stall at the other. Thus the cascade operates over a much wider range of conditions than is the case in the small amplitude stall. In the region of the stall zone in which the flow is at a low incidence angle, the cascade losses are still probably too great to permit the cascade to unstall. In other words, a hysteresis effect, similar to that observed with isolated airfoils, undoubtedly occurs. That such an effect has not been observed is simply due to the fact that the appropriate tests have not been conducted. In the stall cell, the through-flow velocity is small, or very possibly reversed. The perturbations associated with the stall are sufficiently large so that propagating stall occurs to solidities lower than is observed with the small amplitude stall.

The striking differences between the small and large amplitude propagating stalls and the agreement of theory and experiment for small amplitude stall make it seem unlikely that a linearized theory can represent large amplitude stall adequately. Comparison of large amplitude stall experimental results with the results of the small disturbance theories (essentially the stall propagation speed) is not meaningful since the theoretical model does not represent the actual

stall phenomena. A non-linear approach therefore, is required to describe the large amplitude stall.

2:2 Tests at Solidity Ratio, $\sigma/\sigma_o = 1.$

In the five-bladed rectangular cascade, described in Appendix I:1.3, using the design blades, the small amplitude propagating stall was clearly detected in the region between blades 3 - 5 only; between blades 1 - 3, the stall was detected upstream of the cascade but was not clearly observed downstream of the cascade. The propagating stall occurred over the entire blade span. Representative oscillograph records of the velocity fluctuations between blades 3 - 5 are shown in figure 43. The velocity fluctuations are small everywhere, of the order of 10 percent of the mean total local velocity, except in the neighborhood of the blade suction surface and in the blade wakes. The mean velocity, velocity fluctuations and velocity fluctuation ratios are presented in figure 37.

From observations of tufts attached to the suction and pressure surface of a blade, it was clearly observed that the boundary layer along the suction surface of the blade periodically separated at or near the blade leading edge and reattached during stall propagation. The flow along the pressure surface was smooth and attached to the blade at all times. The motions of a tuft attached to a rod which was inserted in the blade passage indicated large periodic fluctuations near the suction surface of a blade and very small disturbances away from the blade.

Propagating stall of definite periodicity was detected above a

Reynolds number (based upon the blade chord and the mean total inlet velocity) of 36,000. Below a Reynolds number of about 20,000, irregular fluctuations were detected; intermittently periodic fluctuations were observed at intermediate Reynolds numbers.

The propagating stall was detected within a range of incidence angle of about 4 degrees. The inlet angle to the cascade was changed by varying the cascade stagger angle while maintaining a fixed angle of the inlet flow.

At a mean total inlet velocity of approximately 32 feet per second, a single cell stall pattern with a stall frequency of approximately 2.0 cycles per second, having a propagation speed of about 5 feet per second, was detected.

Due to the small number of blades in the cascade (five), the stall speed varied along the cascade, being greatest near blade 5. The stall speed noted in the preceding paragraph was measured near blade 5. Further, the open flow area downstream of the cascade tends to make the downstream pressure field constant and this does not satisfy the conditions of the small disturbance theory for two-dimensional flow. For these reasons, comparison between stall speeds determined from the experiments and according to the theory was not made.

In the annular cascade and compressor cascade, neither of the limitations of the rectangular cascade were encountered.

The 60-bladed annular cascade, described in Appendix I: 1.1, was designed with a high hub-tip ratio equal to 0.8 to obtain two-dimensional flow. The inlet angle to the cascade was changed by varying the cascade stagger angle, while maintaining a fixed angle of the

inlet flow. Guide vanes, located upstream of the test cascade, turned the axial inlet flow to an angle of approximately 48 degrees from the axial direction. Due to the large turning for the particular blade design, flow separation occurred in the guide vanes; the resulting unbalance between the inertia and pressure forces directed the separated fluid towards the hub, creating a distorted velocity profile. A comparison between the theoretical and experimental velocity profiles is presented in figure 32.

The cascade performance, as indicated by the static pressure rise across the cascade, was determined qualitatively only, for the range of stagger angles which at the extremes indicated that the cascade was operating at either unstalled or uniformly stalled (non-propagating) conditions; at intermediate angles propagating stall occurred. The cascade static pressure rise coefficient is presented in figure 40a as a function of the stagger angle. Tests were conducted at an inlet velocity to the cascade of about 150 feet per second at mid-radius, or a mean inlet axial velocity into the guide vanes of about 90 feet per second. Propagating stall occurred at the peak of the cascade pressure characteristic and could not be detected at the minimum of the characteristic. The cascade was observed to be in the uniformly stalled condition as shown by the low value of the cascade static pressure rise coefficient as well as the hot-wire anemometer data.

The variation of the flow inlet angle to the test cascade and the flow exit angle measured at mid-radius, is shown in figure 38; the data were taken at a characteristic inlet velocity to the guide vanes of the order of 90 feet per second only.

With the aid of the hot-wire anemometer propagating stall was detected over the entire blade span. Very close to the hub and tip portions of the blades the presence of the stall is obscured by the boundary layer effects. Quantitative measurements of the velocity fluctuations at various radial positions about one inch in front of the cascade were obtained for a stagger angle δ = 29 degrees only. A circumferential survey, approximately 12 degrees in extent (about two blade passages) was made about one inch behind the cascade, also at stagger angle δ = 29 degrees only. The data obtained at this stagger angle are representative of all stagger angles at which stall propagation occurs. Representative Brush oscillograph records of the velocity fluctuations are shown in figure 41.

In figure 33, the average velocities in front of the test cascade, determined by the pitot-static pressure and hot-wire anemometer measurements, are compared. The results are in agreement within 7 percent.

The magnitude of the velocity fluctuations in front of the cascade, determined from Brush oscillograph records and oscilloscope data, are presented in figure 33. The trends of the two methods of measurement are in agreement; the differences are due to the presence of high frequency components associated with the wakes of the upstream guide vanes. The oscilloscope system, with its high frequency response characteristics, can detect components that are suppressed in the oscillograph.

The velocity fluctuation ratios in front of the cascade are shown in figure 33, for both the oscillograph and oscilloscope recording

methods. The results show clearly that the disturbance is indeed small, of the order of 10 percent of the mean total local velocity.

The mean velocity, velocity fluctuations, and velocity fluctuation ratios determined from the circumferential survey conducted behind the test cascade, are presented in figure 34. The effect of the blade wakes upon the mean velocity is seen; some mixing has occurred by the time the fluid has reached the measuring station, thus smoothing the differences between the wakes and the unstalled flow regions. Increasing circumferential angle corresponds to a crossing of the blade from suction to pressure surface.

Measurements obtained at a given cascade stagger angle show that the stall propagation frequency is directly proportional to the inlet velocity to the test cascade; this is shown in figure 31.

Phase measurements with two hot-wires separated circumferentially indicated the presence of a one cell stall pattern only for all conditions at which propagating stall occurred. Therefore, the stall wave length is 60 blade spacings.

Thus the occurrence of the small amplitude and long wave length (60 blade gaps) satisfies the assumptions of the theory. The theoretical values of the stall speed ratio were calculated according to equation 38 of Section IV. By using this equation: (1) it is implied that equation 35 has been satisfied and (2) the total pressure loss coefficient is considered small with respect to the slope of the loss coefficient. Calculations of the total pressure loss coefficient using the qualitative, measured values of C_p as a guide indicate that (2) is probably reasonable. Since propagating stall was detected in a 12 degree range of stagger angle and since

a result of the linearized theory is that propagating stall can occur at but one value of the inlet angle, for a given cascade configuration (stagger angle), it is not at all clear that (1) has been satisfied. However in these tests the cascade configuration was changed at each point, the results of which are that the cascade loss characteristics are also different for each cascade stagger angle. Therefore stall propagation becomes possible for a range of stagger angles. Further, due to the small, though finite, amplitude of the stall, the change in the local value of the inlet angle is probably sufficient to cause propagating stall to occur over a range of mean inlet angles. It therefore appears reasonable to consider (1) to have been satisfied. Thus equation 38 is employed and theory and experiment are compared at each point.

The theoretical and experimental values of the stall speed ratio are shown in figure 29a as a function of the cascade stagger angle; the results are presented for the mid-radius position. The theoretical values of the stall speed ratio were calculated using the experimentally measured inlet and exit flow angles presented in figure 38. The experimental propagating stall speed was determined from the measured value of the stall frequency and the results of the phase measurements. The axial velocity, U, at mid-radius was determined from the measured flow inlet angle to the cascade and from measured values of the total inlet velocity to the cascade.

The theoretical and experimental values of the stall speed ratio agree within 10 percent; the trends of both curves are the same. By including the value of the total pressure loss in the theoretical calculations of the stall speed ratio, the agreement between theory and

experiment would be further improved.

Propagating stall was not detected below a Reynolds number (based upon the blade chord and total inlet velocity to the cascade at mid-radius) of 19,400; the lowest Reynolds number at which measurements were made was 34,800. Intermediate values of the Reynolds number were not investigated due to the difficulty of adjusting the speed control device.

With the occurrence of the small amplitude propagating stall clearly established in the rectangular and annular cascades, it was felt that such a stall might occur in the stator row of an axial-flow compressor. It was necessary only to find a compressor configuration such that the stator row would stall before stall occurred on a rotor row. To insure this early stator stall, the stagger angle of the stator row was changed so that its angle of attack at a given inlet angle was greater than when the blades were set at their design value. A guide vane-rotor combination was employed to vary the inlet flow angle to the 32-bladed stator row. The hub-tip ratio of the compressor is 0.6; the configuration is described in Appendix I: 1.2. The spacing between the stator row and the guide vane-rotor combination was made a maximum to reduce interference effects. Tests were conducted at stagger angles 10 and 5 degrees from the design setting. Measurements of the flow were obtained about 1/4 inch upstream of the stator row; a circumferential survey 15 degrees in extent (slightly greater than one blade spacing) was performed about one inch behind the stator row. The measuring stations were sufficiently close to the row that the measurements were influenced by the presence of the blade row.

This effect was small; for example, in the measurements of the flow angles, the maximum effect was of the order of two degrees.

The inlet flow to the stator row was appreciably smoother than that observed in the annular cascade, since flow separation had not occurred in the upstream blade rows. During stall propagation, however, there was separation of the flow from the suction surface of the stator blades, resulting in the formation of a boundary layer which was considerably thicker at the hub than near the tip.

The stator inlet angle and exit angle characteristics, for both the 10 and 5 degree changes in stagger angle setting, are shown in figures 69a and 69b, respectively. In the range of inlet angles tested the leaving angle is nearly constant, regardless of the inlet angle. This is in good agreement with one of the assumptions of the linearized theory; that the leaving angle be constant. Beyond a stator inlet angle of approximately 51 degrees, a large amplitude propagating stall occurred in the rotor row; this stall was detected throughout the machine and therefore limited the angle range in which the small amplitude propagating stall could be investigated.

Propagating stall was detected over the entire span; very close to the hub and tip portions of the blades the presence of the stall was obscured by the boundary layer effects. Because of the relatively high stall frequencies, 15 to 20 cycles per second, a Miller photographic recording oscillograph was employed for the frequency and phase measurements. A representative Miller oscillograph record of the velocity fluctuations, obtained upstream of the blade row, at radius ratio $\xi = 0.700$, is shown in figure 44a.

The observed propagating stalls were not as stable as those detected in the annular cascade. This may be due to the radial variation of blade stagger angle and flow incidence angle associated with the low hub-tip ratio, which would give different stall propagation speeds at different radii. Due both to the variation of the stall frequencies (see figure 44a, for example) and to the difficulties in the measuring technique, the determination of the frequency and number of stall cells and consequently the stall speed is subject to some uncertainty. The average number of stall cells detected was seven, resulting in a stall wave length of the order of 5 blade passages. The indicated number of stall cells varied between six and eight. The wave length of the stall was sufficiently short that the velocity fluctuations were damped rapidly upstream of the stator row. One of the assumptions of the theory, that the stall wave length be long compared to the blade spacing, is not satisfied as well as in the tests conducted upon the annular cascade.

The results of the tests conducted at both stagger angle settings were quite similar. In the tests at the 5 degree change in stagger angle setting, the range of inlet angles in which the stall could be investigated before the large amplitude stall occurred was appreciably smaller than was the case with the tests conducted at the 10 degree change in stagger angle setting. Accordingly, the number of data points presented are less for the tests conducted at the 5 degree change in stagger angle setting than at the 10 degree change.

For the larger stagger angle setting propagating stall occurred, initially, at an inlet angle of approximately 44.0 degrees. At this

angle, the velocity fluctuations indicated that the stall occurred in bursts. As the stator inlet angle was increased beyond the initial stalling angle, the continuous, periodic velocity fluctuations associated with the propagating stall rapidly dominated the flow characteristics.

The mean velocity, velocity fluctuations, and velocity fluctuation ratios, in front of the stator row, at various inlet angles, are presented in figure 35. In the measurements of the mean velocity, comparison is made between hot-wire anemometer and velocity head measurements; the results are in agreement within 10 percent. The velocity fluctuations due to stall propagation increase as the inlet angle is increased; at stall initiation, the stall amplitude is about 5 percent of the mean total local velocity, while at the highest inlet angle tested, the disturbance amplitude is about 12 percent of the mean total local velocity. Thus, under all conditions tested, the observed propagating stalls are of small amplitude.

The mean velocity, velocity fluctuations and velocity fluctuation ratios during propagating stall, determined from the circumferential survey conducted behind the stator row, are presented in figure 36 for the mid-radius position. The velocity fluctuation ratio is small except in the region of the blade wakes. In crossing a blade from the suction to the pressure surface, the circumferential angle is increased.

A comparison between theory and experiment can be made although some questions arise in so doing. The assumption in the theory of long wave length is not nearly as well satisfied as in the annular cascade; the rather short wave length, 5 blade gaps, may cause significant non-steady flow effects. Further, in these tests the stall

occurred over 7 degree range of inlet angles. This is not in agreement with a result of the linearized theory. In the annular cascade, the cascade configuration was changed at each point, which could then permit stall propagation to occur in a range of stagger angles; in the compressor cascade, the configuration is maintained constant and the inlet angle only is varied. Therefore, for a single valued loss curve, the stall should occur at but one value of the inlet angle for a stall of infinitesimal amplitude. For a stall of finite amplitude, the local inlet angle could vary sufficiently so that propagating stall could occur over a range of mean inlet angles. Further, since the loss curve is not known, it becomes very questionable as to where to make the comparison between theory and experiment. It is not correct to make a comparison at each point. For these reasons, the theoretical curve in figure 30a is shown as a dashed line; the stall speed was calculated according to equation 38 of Section IV. The theoretical "point" shown in figure 30a was obtained by taking an average value of the theoretical stall speed.

The stall speed ratio is shown in figure 30a as a function of the inlet angle; the results are presented for the mid-radius position. Values were calculated as previously described in the annular cascade. The axial velocity at mid-radius was taken as the average velocity in the compressor annulus, determined from the flow calibration.

Propagating stall was not detected below a Reynolds number (based upon the blade chord and total inlet velocity to the stator row at mid-radius) of 12,700; the lowest Reynolds number at which measurements were made was 30,600. Data was not obtained at intermediate values of the Reynolds number.

Propagating stall was not detected on the rotors of the compressor due possibly to the large radial variation of blade stagger angle and flow incidence angle associated with the low hub-tip ratio.

The stall speed ratio characteristic, for the tests conducted at the 5 degree change in stagger angle setting, are presented in figure 30b.

2:3 Effects of Variation of Solidity.

The effects of variation of solidity were investigated in both the annular and compressor cascades. The results showed that a minimum solidity existed, below which the perturbations caused by the separation of the boundary layer along the suction surface of a blade were not of sufficient strength to induce separation at an adjacent blade; at this condition, stall propagation no longer occurs.

In the annular cascade, configurations having 50, 40 and 30 blades (corresponding to solidity ratios $\sigma/\sigma_0 = 5/6$, 2/3 and 1/2, respectively) were tested. Quantitative measurements of the stall frequencies and number of stall cells was obtained; a single stall cell pattern only was found at all conditions at which propagating stall occurred. Quantitative hot-wire anemometer measurements of the mean velocity and velocity fluctuations were not obtained; the velocity fluctuations are of the same order as those observed in the tests conducted at full solidity. Measurements of the flow angles were not obtained; the flow inlet angle to the test cascade was assumed not to have changed from that measured in the tests conducted at full solidity, and was assumed to be equal to 47.5 degrees for the purposes of

calculations. The mean total local inlet velocity to the cascade was measured near mid-radius with pressure measuring instrumentation.

At solidity ratio, $\sigma/\sigma_o = 5/6$, stable propagating stall occurs in a manner entirely similar to that previously described in the tests conducted at full solidity. The propagating stall speed is increased slightly in comparison to that observed in the tests at full solidity. The stall speed ratio is shown in figure 29b. The propagating stall was detected in a 12 degree range of cascade stagger angles. The cascade static pressure rise characteristic is shown in figure 40b.

At solidity ratio, $\sigma/\sigma_o = 2/3$, propagating stall occurred, but did so only intermittently. The oscillograph records of the velocity fluctuations indicated that the stall occurred in bursts; at other times, irregular fluctuations were detected. A representative oscillograph record is shown in figure 42a. The stall speed ratio as a function of the cascade stagger angle is shown in figure 29c. The stall speed ratio is somewhat greater than observed in the tests at higher solidities. Stall propagation was detected over an 11 degree range of cascade stagger angles. The cascade static pressure rise characteristic is presented in figure 40c.

At solidity ratio, $\sigma/\sigma_o = 1/2$ propagating stall was very difficult to detect. The effects noted in the tests conducted at solidity ratio $\sigma/\sigma_o = 2/3$ were greatly accentuated. The time duration of the bursts of propagating stall was very small compared to the length of time in which irregular fluctuations only were detected. A representative oscillograph record of the velocity fluctuations is shown in figure 42b. The stall speed ratio characteristic is presented in figure 29d; the stall

speed ratio is greater than those observed in the tests conducted at higher solidities. Definite evidence of propagating stall was found in a 5 degree range of cascade stagger angles. The cascade static pressure rise characteristic is presented in figure 40d.

Using the small disturbance theory as a guide, the expected stall speed is seen to increase as the turning of the fluid through the blade row is decreased. With a reduction of solidity, the turning of the fluid through a blade row is, indeed, decreased; therefore, the experimentally observed stall speeds increase as the solidity is reduced as is predicted by theory.

In the compressor cascade tests were conducted at solidity ratios $\sigma/\sigma_0 = 1/2$ and $1/4$; propagating stall was not detected at solidity ratio $\sigma/\sigma_0 = 1/4$. During the tests at reduced solidity, the change in cascade stagger angle was maintained at the 10 degree setting.

Quantitative measurements of the flow and flow parameters were recorded.

The inlet angle-exit angle characteristic is shown in figure 39c for solidity ratio $\sigma/\sigma_0 = 1/2$. The exit angle is nearly independent of the inlet angle; this is in good agreement with the assumption of the linearized theory.

The propagating stall frequencies were of the order of 50 cycles per second; the frequencies were higher, by a factor of about three, than those detected in the tests conducted at full solidity. A representative Miller oscillograph record of the velocity fluctuations obtained in front of the stator row at radius ratio $\xi = 0.700$ is shown in figure 44b. The measurements gave an average of 10 stall cells (9 cells to 11 cells

indicated). The stall speeds, therefore, were considerably greater in these tests than in the tests conducted at full solidity. Further, the stall wave length is of the order of two blade passages, which does not satisfy the assumption of the theory that the stall wave length be long compared to the blade spacing.

The stall speed ratio characteristic is shown in figure 30c, for the mid-radius position. The theoretical curve and "point" were calculated as previously described for the tests conducted at full solidity. Due to the short wave length, the application of the quasi-steady theory becomes very questionable; comparison between theory and experiment is probably not appropriate. Hence the large differences between the theory and experiment are not at all unexpected. Data were recorded at two inlet angles only.

At solidity ratio $\sigma/\sigma_0 = 1/4$, no propagating stall was found. High frequency fluctuations, apparently random, were the only type observed.

2:4 Effects of Variation of Blade Shape.

The effects of variation of blade shape were investigated in the rectangular cascade. The influence of the blade shape, insofar as it affects the boundary layer along the suction surface of a blade and its transition characteristics, is significant.

A set of blades of flat plate, rectangular profile, described in Appendix I:1.3.1 was tested in a range of angle attack from 0 to 40 degrees. At very low angles of attack, even at 0 degrees, a wake thickness (corresponding to a flow separation) of the order of 5/8 inches was observed at the blade trailing edge; at 5 degrees angle of attack,

the thickness was about 1 inch; at 9 degrees angle of attack, the thickness was about 2 inches. Propagating stall was not found with this set of blades. The boundary layer along the suction surface was separated at all times, thereby precluding any occurrence of the propagating stall.

Tests were also conducted upon blades of shape intermediate between the design blades and the blades of flat plate profile. These blades are the models from which the blades employed in the annular cascade were designed; they are described in Appendix I:1.3.1.

Tests were conducted upon these blades covered with a smooth fabric over the entire surface; the results indicated that stall propagation occurred in an angle of attack range of about 2 degrees (with the design blades, stall propagation was detected in a range of angle of attack of about 4 degrees). The wake thickness at the trailing edge was about twice as great as that observed in the tests conducted upon the design blades.

When these intermediate shape blades were tested in their original condition (not covered with fabric), the results obtained were quite similar to those noted when the blades were covered with the fabric. The wake thickness was slightly greater than that observed in the tests conducted upon the fabric covered blades.

2:5 Summary.

The results of the investigations of the small amplitude propagating stall may be summarized as follows:

1. A propagating stall of small amplitude can occur under certain circumstances.

2. The small amplitude propagating stall was detected only in stationary cascades. The small amplitude stall was not detected in the rotors of rotating machines.
3. The characteristics of the small amplitude stall are:
    a. During stall propagation, the cascade operates under conditions of positive blade stall.
    b. During stall propagation, the boundary layer along the suction surface, only, of a blade periodically separates and reattaches. The resulting perturbations induce similar separation upon adjacent blades. The flow along the pressure surface is smooth and attached to the blade at all times.
    c. The perturbations are small everywhere (of the order of 10 percent of the mean total local velocity) except in the neighborhood of the suction surface of a blade and the blade wakes.
    d. A minimum solidity exists, below which stall propagation will not occur. At the low solidities, evidently, perturbations caused by the boundary layer separation are not of sufficient strength to induce separation at the adjacent blades. This solidity is of the order of $\sigma = 1/2$.
    e. The blade shape, insofar as it affects the boundary layer and its transition characteristics, influences both the occurrence of the stall and the range of angles in which stall propagation occurs. The more nearly the profile is to rectangular, the narrower the angle range in which stall

propagation occurs.

f. A maximum inlet angle exists, beyond which the boundary layer along the suction surface of a blade cannot reattach following separation. Beyond this angle, propagating stall does not occur. Stall propagation occurs in a narrow range of angles.

g. A minimum Reynolds number exists, below which propagating stall does not occur; this minimum Reynolds number is of the order of 25,000.

4. Comparison of the observed stall speed ratios with those predicted according to the quasi-steady, linearized theory shows agreement, generally within 10 percent. The assumptions of the theory are:

   a. Wave length of the stall is long compared to the blade spacing (to enable treatment of the stall as quasi-steady).

   b. Constant leaving angle, which implies a cascade of very high solidity.

   c. Cascade losses dominate the stall characteristics.

In all cases, except one, the assumptions of the theory were satisfied, resulting in the agreement mentioned above. At low solidity ratio ($\sigma/\sigma_0 = 1/2$) and with a stall wave length of the order of 2 blade spacings, agreement between theory and experiment was poor.

A result of the theory is that stall propagation can occur at but one inlet angle for a given configuration for a stall of vanishing amplitude. Due to the finite, though small, amplitude of the stall: (1) stall propagation could occur over a range of inlet angles for a given

configuration (compressor cascade); (2) for a cascade in which the inlet angle is fixed and the stagger angle varied (annular cascade), a different loss characteristic is obtained for each setting of the stagger angle; thus, in conjunction with (1) stall propagation could occur in a range of stagger angles.

III. EXPERIMENTAL OBSERVATIONS OF THE LARGE AMPLITUDE PROPAGATING STALL

3:1 Introduction

Experiments conducted upon configurations of single stage and single row in the axial-flow compressor described in Appendix I:2.1, and upon single stage configurations in the axial flow pump described in Appendix I:2.2 have shown that the propagating stalls are all of the large amplitude type. In no case was a small amplitude stall detected.

Two different types of large amplitude stall were observed: the partial stall (in which the stall covers only a portion of the blade span) and the full stall (in which the stall covers the entire blade span). In some guide vane-rotor configurations, a stall of intermediate character, the modified partial stall, was detected. At the beginning of stall, for this type, the stall is of the partial stall character; as the flow is reduced, the stall covers an increasingly larger portion of the blade span.

Blade row interference effects upon the stall characteristics are significant, and vary appreciably, depending upon the configuration tested; in all cases however the amplitude of the stall remains large.

Measurements obtained visually and with the hot-wire anemometer indicate that the minimum velocities associated with the stall are small. Hot-wire anemometer recordings taken in front of the blade row which controls the stall indicate that flow reversal undoubtedly occurs during stall propagation. This is inferred from the premise that shear flow upstream of a blade row, where the incoming flow far upstream is irrotational, is evidence of flow reversal. The flow reversal extends

only a small distance upstream of the controlling blade row, perhaps of the order of a chord length or two. Visual observations (studies of tuft motions) in the pump clearly indicate flow reversal in the rotor passages during stall propagation. Further, these visual studies show the presence of positive and negative stall upon a blade during stall propagation.

From the above observations, it becomes clear that the large amplitude stall is completely different from the small amplitude stall and should be so treated. The characteristics of the large amplitude stall: (1) positive and negative blade stall and (2) complete flow blockage and flow reversal, are such that it becomes inappropriate to use a linearized theory, as described in Section IV and in the Introduction. The mechanisms of the small and large amplitude stalls are different.

The characteristics of the large amplitude stall strongly suggest a model in which the stall can be considered to be a bluff body, with respect to which, a vortex street is formed downstream of the body due to the loss and regaining of the circulation of the blades as they enter and leave the stall cell. The first attempt at a non-linear theory is that of Kriebel (10); the model described above was used.

With the strong effects of positive and negative stall, the stall occurs to solidities lower than, and in a range of angles greater than, was the case in the small amplitude stall.

3:2 Tests at Solidity Ratio, $\sigma/\sigma_0 = 1$.

The tests which will be described were conducted upon single stage configurations in both the compressor and pump, and upon an

isolated rotor row in the compressor. The stall amplitudes in all tests were found to be large, of the order of the mean total local velocity in the compressor and of the order of the design head rise in the pump. Both partial and full stalls were detected. The effects upon the stall propagation of blade row interference were significant; however, in all tests, the perturbations due to the stall were large.

Observations of the tuft motions show that the propagating stall occurs as a partial stall at the rotor tip. Clear flow reversal in the rotor passages near the blade tip is observed. Observations of the tuft motions indicate that positive and negative blade stall occurs during stall propagation.

The absolute stall frequency ratios are shown in figures 51a and 51b as functions of flow coefficient for the single stage and single stage expanded configurations, respectively. Partial stalls only (at the rotor tip), occurred in the tests conducted in these configurations. Irregular fluctuations were found over wide ranges of flow coefficient; their origin and significance are not understood at this time.

The effect of blade row interference is clearly seen in the comparison of the number of stall cells for the single stage and single stage expanded configurations. In the former, phase measurements indicate the presence of a single cell stall pattern, while for the single stage expanded configuration a two cell stall pattern is observed.

The static pressure fluctuation characteristics are shown in figure 47 for both configurations. The pressure fluctuations upstream

of the rotor row are always greater than those downstream of the rotor row. During stall propagation, the pressure fluctuations upstream of the rotor row are of the order of the pump design head rise.

Tests were conducted upon the identical configurations in the axial-flow compressor; those conducted upon the single stage configuration were reported by Iura and Rannie (4), while those conducted upon the single stage expanded configuration were performed by the writer. The blade aspect ratio and physical dimensions of the compressor are larger than in the pump; in all other respects the blading is identical. The results of the experiments conducted in the compressor are similar, but not identical, to those reported in the pump tests.

The steady-state aft duct static pressure rise coefficient and torque coefficient characteristics are presented in figures 48 and 49, respectively, for the single stage expanded configuration. The characteristics are representative of those which were obtained for all configurations tested. The observed hysteresis effects are due to the propagating stall.

Near the rotor row, for both the single stage and single stage expanded configuration tests, the velocity fluctuations are large. The mean velocities, velocity fluctuations, and velocity fluctuation ratios are shown in figure 46 at various flow coefficients, for the single stage expanded configuration. The velocity fluctuation ratios for the single stage configuration is shown in figure 45, at various flow coefficients; this data is reproduced from reference 4.

In contrast to the occurrence of only the partial stalls in the pump tests, both partial and full stalls were detected in the tests

conducted upon the two compressor configurations. The absolute stall frequency ratio characteristics for the single stage and single stage expanded configurations are presented in figures 50a and 50b respectively. As was noted in the pump tests, irregular fluctuations were found over wide ranges of flow coefficient; the causes and significance of these fluctuations are not understood at this time.

Phase measurements show that, in the partial stall regime, a single cell stall pattern (and an unstable two cell stall pattern) occurs in the single stage configuration. A five cell stall pattern occurs in the tests conducted upon the single stage expanded configuration; unstable one, two, three and four cell stall patterns occur at the flow rate at which stall begins.

In the partial stall regime, the absolute stall frequency ratios for identical configurations in the pump and compressor are nearly the same.

Examination of the oscillograph records of the velocity fluctuations upstream of the rotor row during the full stall, in the tests conducted upon the single stage expanded configuration, shows that flow reversal undoubtedly occurs in the rotor passages during propagating stall. A representative oscillograph record is shown in figure 54.

Tests were also conducted upon an isolated rotor row configuration in the axial-flow compressor. The velocity fluctuations associated with the stall are observed to be large, as is the case with all configurations tested in the compressor and pump.

The absolute stall frequency ratio as a function of flow rate is presented in figure 52a. Unstable partial stalls of one, two and three cell patterns occur at the rotor tip at the flow rate at which stall begins. Eventually, while maintaining a given throttle setting in this flow regime, the partial stalls change to a single cell full stall pattern.

A representative oscillograph record of the velocity fluctuations during the full stall is shown in figure 55. As was noted in the tests conducted upon the single stage configurations, the shear flow in the patterns measured upstream of the rotor row indicate the presence of reverse flow.

There is no effect of Reynolds number upon the occurrence of the propagating stall in the range of Reynolds numbers investigated. The lowest tip Reynolds number (based upon rotor chord and rotor tip speed) at which detailed tests were conducted was about 10,000.

3:3 Effects of Variation of Solidity.

The effects of the variation of solidity were determined for the isolated rotor row configuration. Propagating stall was detected with as few as two blades in the rotor row (solidity ratio $\sigma/\sigma_o = 1/15$).

Quantitative measurements of the velocity fluctuations reveal that with as few as two blades in the rotor row, the velocity perturbations due to the propagating stall are still large close to the rotor row.

The absolute stall frequency ratios are presented for the various solidities tested: configurations tested with five, three and two blades installed in the rotor row (solidity ratios $\sigma/\sigma_o = 1/6$, $1/10$ and $1/15$), in figures 52b, 52c and 52d, respectively.

3:4 Summary

The results of the investigations of the large amplitude propagating stall may be summarized as follows:

1. Only large amplitude propagating stall occurs in the axial-flow compressor and pump.
2. The characteristics of the large amplitude stall are:
   a. During stall propagation, the blades operate under conditions varying from positive to negative stall.
   b. The perturbations due to the stall are everywhere large in the vicinity of the blade controlling the stall. In the compressor, the velocity fluctuations are of the order of the mean total local velocity. In the pump, the pressure fluctuations are of the order of the design head rise.
   c. Clear indications of flow reversals in the blade passages are found.
   d. The effect of variations of solidity upon the occurrence of stall propagation is not pronounced. Propagating stall occurs with as few as two blades in an isolated rotor row.
   e. For a given configuration, propagating stall occurs in a wide range of flow coefficients and therefore, in a wide range of inlet angles.
   f. The large amplitude propagating stall is not sensitive to Reynolds number. The lowest tip Reynolds number at which detailed tests were conducted was about 10,000.

3. A non-linear theory is required to describe appropriately the large amplitude propagating stall.

IV. THEORETICAL MODEL OF THE SMALL AMPLITUDE PROPAGATING STALL

4:1 Introduction

Several formulations of linearized propagating stall theory have appeared, as mentioned in Section I. All are based on the assumption of small disturbances on uniform flow upstream and downstream of the cascade, with various assumptions for matching the flow fields over the cascade. A variety of results have been obtained depending primarily on the method of matching at the cascade. The form of the theory described below is a recent one due to W. D. Rannie. The reason that it is believed to be "correct" in contrast to the others is that it agrees with experiment in all details that can be checked. Until the experiments on small amplitude stall were made by the present author, it was not possible to tell which of the various theories was correct.

The theory assumes that the wave length of the stall disturbance is large compared with the blade gap. This assumption is required if the flow through the cascade is to be quasi-steady. Unsteady flow through the cascade is much more difficult to treat; in fact it is not certain that we know how to do it correctly. The three conditions for matching upstream and downstream flows over the cascade are: (1) continuity, (2) leaving angle constant, independent of entering flow angle, and (3) a total pressure loss that is low over a range of incidence angle and rises very sharply at the ends of the range. The first of these conditions is quite obvious; the second condition is applicable to cascades of high solidity, and eliminates difficulties of unsteady flow; the third condition

introduces the non-linearity that is required for existence of the travelling disturbance.

These conditions, including the assumption of long wave length, are chosen to give the theory as sound a physical basis as possible. Stall disturbances with short wave length or stall disturbances in low solidity cascades may occur, but a theory for such cases is much less certain. From the experiments described in Section II, it appears that small amplitude stall does not occur at very low solidities. With but one exception no disturbances of very short wave length were found; in the test conducted at reduced solidity, solidity ratio $\sigma/\sigma_o = 1/2$, in the compressor cascade, the disturbances were of the order of one or two blade passages. The evidence is not conclusive but the indications are that the assumptions of the theory are the only ones that lead to an actually realizable stall disturbance of small amplitude.

4:2 Upstream of the Cascade

Consider an infinitely long, two-dimensional cascade. One can, also, consider the cascade to have been formed by unwrapping an annular blade row at radius, R, and extending the cascade in $2\pi R$ increments.

Consider a disturbance travelling unchanged in shape with a velocity V_s in the direction of the y-axis. The wave length of the disturbance is assumed much greater than the blade gap s. Therefore, with respect to the propagating stall, the flow is steady and with respect to the blades, the flow is quasi-steady.

Let the fluid be incompressible and inviscid.

Let the velocity and pressure perturbations upstream be

$$u(x,y),\ v(x,y),\ p(x,y)$$

Assume the approaching flow far upstream of the cascade is uniform, with velocities and pressure U_o , V_o , P_o (figure 2), relative to the cascade.

Assume the flow upstream of the cascade to be irrotational. This assumption is valid as long as flow reversal does not occur.

Far enough upstream, the influence of individual blades is negligible and the flow can be considered steady. This distance is of the order of a blade gap. The disturbances are assumed periodic in the y-direction.

From the continuity relation

$$\frac{\partial u}{\partial x} = -\frac{\partial v}{\partial y} \tag{1}$$

and the assumption of irrotationality

$$\frac{\partial u}{\partial y} = \frac{\partial v}{\partial x} \tag{2}$$

the velocity field can be determined from the solutions of the resulting Laplace equation. The pressure field can be obtained from the Bernoulli equation.

Thus

$$\nabla^2 u = \nabla^2 v = 0 \tag{3}$$

and from the Bernoulli equation for axes moving with the stall

$$\frac{2P_o}{\rho} + U^2 + (V_o - V_S)^2 = \frac{2(P_o + p)}{\rho} + (U+u)^2 + (V_o - V_S + v)^2 \qquad (4)$$

Far upstream $u = v = p = 0$

4:3 Downstream of the Cascade

Far downstream of the cascade the average velocities and pressure are U , V_∞ , P_∞ (figure 2); the axial velocity U , far downstream, is equal to that far upstream as a consequence of the continuity relation.

Downstream of the cascade, the flow is rotational, due to the unsteady flow and cascade losses. Therefore, it is necessary to employ the equations of motion.

Far downstream of the cascade, the boundary conditions upon the perturbations are the same as those imposed upstream of the cascade. Consider any constant value of an average perturbation far downstream to be included in the uniform flow conditions far downstream of the cascade.

With respect to the stall, consider the equations of motion: Conservation of total pressure along a streamline

$$\left[(U+u)\frac{\partial}{\partial x} + (V_\infty - V_S + v)\frac{\partial}{\partial y}\right]\left[\frac{P_\infty + p}{\rho} + \frac{1}{2}(U+u)^2 + \frac{1}{2}(V_\infty - V_S + v)^2\right] = 0 \qquad (5)$$

and the two momentum relations, into which the continuity relation has been inserted

$$(U+u)\frac{\partial v}{\partial y} - (V_\infty - V_s + v)\frac{\partial u}{\partial y} = \frac{\partial}{\partial x}\left(\frac{p}{\rho}\right) \tag{6}$$

and

$$(U+u)\frac{\partial v}{\partial x} - (V_\infty - V_s + v)\frac{\partial u}{\partial x} = -\frac{\partial}{\partial y}\left(\frac{p}{\rho}\right) \tag{7}$$

Equations 5 - 7 are exact and non-linear; by assuming small disturbances and hence linearizing the equations, the problem is simplified greatly.

Therefore, linearizing equations 5 - 7

$$\left[U\frac{\partial}{\partial x} + (V_\infty - V_s)\frac{\partial}{\partial y}\right]\left[\frac{p}{\rho} + Uu + (V_\infty - V_s)v\right] = 0 \tag{8}$$

$$\frac{\partial}{\partial y}\left[Uv - (V_\infty - V_s)u\right] = \frac{\partial}{\partial x}\left(\frac{p}{\rho}\right) \tag{9}$$

$$\frac{\partial}{\partial x}\left[Uv - (V_\infty - V_s)u\right] = \frac{\partial}{\partial y}\left(\frac{p}{\rho}\right) \tag{10}$$

Define

$$\frac{p}{\rho} + Uu + (V_\infty - V_s)v = H \tag{11}$$

$$u v - (V_\infty - V_s) u = F \tag{12}$$

$$\frac{p}{\rho} = G \tag{13}$$

Substituting equations 11 - 13 into equations 8 - 10

$$\left[u \frac{\partial}{\partial x} + (V_\infty - V_s) \frac{\partial}{\partial y} \right] H = 0 \tag{14}$$

$$\frac{\partial}{\partial y} F = \frac{\partial}{\partial x} G \tag{15}$$

$$\frac{\partial}{\partial x} F = -\frac{\partial}{\partial y} G \tag{16}$$

Therefore, the downstream flow is described in terms of a function H that is constant along the mean stream lines and two functions F and G that satisfy the Cunchy-Riemann conditions.

4:4 Flow Through the Cascade

It has been shown that the flow field upstream due to the perturbation can be described completely in terms of a single function u_1, say, given along the y-axis. The corresponding flow field downstream can be described completely in terms of two functions H_2 and F_2, say, given along the y-axis. Three conditions across the cascade are required to determine these three functions.

Subscripts 1 and 2 denote quantities u, v, p evaluated immediately upstream and downstream of the cascade, respectively, along the y-axis.

1. Continuity of flow through the cascade Therefore

$$u_1 = u_2 \tag{17}$$

2. Constant leaving angle Assume that the flow leaves the cascade at a constant angle, regardless of the inlet flow conditions. This implies that the cascade solidity is very high; this assumption appears to be reasonable for solidities as low as the order of unity.

Therefore

$$V_\infty + v_2 = \left[U + u_2\right] \tan \beta_2$$

But, since the mean values of v_2 and u_2 are zero

$$v_2 = \frac{V_\infty}{U} \times u_1 \tag{18}$$

3. Total pressure loss through the cascade Assume that the total pressure loss through the cascade can be represented as a function of the inlet angle; it is also assumed that the propagating stall does not affect the shape of this curve. The first assumption is obvious while that of the second is, probably, also reasonable for flows approaching the quasi-steady condition.

Let $$2\Delta P_{t_1} = 2\left(U + u_1\right)^2 P\left(\frac{V_o + v_1}{U + u_1}\right) \tag{19}$$

Expanding the right hand side of equation 19 about $\frac{V_o}{U}$, and linearizing

$$2\Delta P_{t_1} = 2U^2 P_o + 2P_o'(Uv_1 - V_o u_1 + 4Uu_1 P_o) \tag{20}$$

where $P_o = P$ evaluated at $\frac{V_o}{U}$ and P_o' = slope of the P characteristic, evaluated at $\frac{V_o}{U}$.

The total pressure loss through the cascade is, according to equation 19,

$$\frac{2(P_o + p_1)}{\rho} + (U+u_1)^2 + (V_o + v_1)^2 - \frac{2(P_\infty + p_2)}{\rho} - (U+u_2)^2 - (V_\infty + v_2)^2 = 2(U+u_1)^2 P \tag{21}$$

With respect to the stall, substituting equation 21 into equation 4 and eliminating $\frac{2(P_o + p_1)}{\rho}$:

$$\frac{2P_o}{\rho} + U^2 + (V_o - V_s)^2 - (U+u_1)^2 - (V_o - V_s + v_1)^2 - \frac{2(P_\infty + p_2)}{\rho} - (V_\infty + v_2)^2 + (V_o + v_1)^2 = 2(U+u_1)^2 P \tag{22}$$

Substituting equation 18 into equation 22, and rearranging terms

$$\frac{2p_2}{\rho} + 2\left(\frac{U^2 + V_\infty^2}{U}\right) \times u_1 - 2V_s v_1 + \frac{U^2 + V_\infty^2}{U^2} = -2(U+u_1)^2 P - (V_\infty^2 - V_o^2) - 2\left(\frac{P_\infty - P_o}{\rho}\right) \tag{23}$$

Linearizing equation 23 and rearranging the equation

$$\frac{2p_2}{\rho} + 2\left(\frac{U^2 + V_\infty^2}{U}\right) \times u_1 - 2V_s v_1 + \left[4Uu_1 P_o + 2P_o'(Uv_1 - V_o u_1)\right] = \text{constant}$$

But since $\bar{u}_1 = 0$, $\bar{v}_1 = 0$, therefore, to the first order, the constant of the above equation is equal to zero. Hence

$$\frac{2}{\rho}p_2 + 2\left(\frac{U^2+V_\infty^2}{U}\right)\times u_1 - 2V_s v_1 + \left[4U u_1 P_o + 2P_o'\left(U v_1 - V_o u_1\right)\right] = 0 \tag{24}$$

The procedure for evaluating $\frac{p_2}{\rho}$, in equation 24 will be indicated. Since an F and G set of functions satisfy Laplace's equation both upstream and downstream of the cascade, F , for example, can be expressed in the forms:

Upstream

$$F(x,y) = \sum_{n=1}^{\infty}\left(a_n \cos\frac{2n\pi}{L}y + b_n \sin\frac{2n\pi}{L}y\right)e^{\frac{2n\pi}{L}x} \tag{25}$$

Downstream

$$F(x,y) = \sum_{n=1}^{\infty}\left(c_n \cos\frac{2n\pi}{L}y + d_n \sin\frac{2n\pi}{L}y\right)e^{-\frac{2n\pi}{L}x} \tag{26}$$

Expressions for G can then be determined using equation 15. The Fourier constants a_n, b_n, c_n, d_n can be evaluated by employing the orthogonality characteristics of the functions and by assuming, for example, that $F(x,y)$ is known at $(0,y)$; thus, G can be determined in terms of F . By assuming $G(x,y)$ is known at $(0,y)$, F can be determined in terms of G . The expressions contain a series which can be summed; the resulting equations are

Upstream

$$\left.\begin{aligned} G(0,y) &= -\frac{1}{L}\int_0^L F_1(\alpha)\cot\frac{\pi}{L}(y-\alpha)\,d\alpha \\ F(0,y) &= +\frac{1}{L}\int_0^L G_1(\alpha)\cot\frac{\pi}{L}(y-\alpha)\,d\alpha \end{aligned}\right\} \quad (27)$$

Downstream

$$\left.\begin{aligned} G(0,y) &= +\frac{1}{L}\int_0^L F_1(\alpha)\cot\frac{\pi}{L}(y-\alpha)\,d\alpha \\ F(0,y) &= -\frac{1}{L}\int_0^L G_1(\alpha)\cot\frac{\pi}{L}(y-\alpha)\,d\alpha \end{aligned}\right\} \quad (28)$$

Define a function, K, and its conjugate, K^*:

$$K^*(y) = \frac{1}{L}\int_0^L K(\alpha)\cot\frac{\pi}{L}(y-\alpha)\,d\alpha \quad (29)$$

Therefore

Upstream

$$\left.\begin{aligned} G(0,y) &= -F^*(0,y) \\ F(0,y) &= +G^*(0,y) \end{aligned}\right\} \quad (30)$$

Downstream

$$\left.\begin{aligned} G(0,y) &= +F^*(0,y) \\ F(0,y) &= -G^*(0,y) \end{aligned}\right\} \quad (31)$$

Thus, from equations 12 and 18

$$F_2 = -(V_\infty - V_s)u_2 + U v_2$$

$$= -(V_\infty - V_s)u_2 + V_\infty u_1$$

Therefore,

$$F_2 = V_s u_1 \tag{32}$$

From equations 13, 31 and 32

$$\frac{p_2}{\rho} = G_2$$
$$= +F_2^*$$
$$= +V_s u_1^*$$

Therefore,

$$\frac{p_2}{\rho} = -V_s v_1 \tag{33}$$

Substituting equation 33 into equation 25, and rearranging terms:

$$\left[\frac{U^2+V_\infty^2}{U} + 2P_o U - P_o' V_o\right] u_1 + \left[-2V_s + UP_o'\right] v_1 = 0 \tag{34}$$

Since u_1 and v_1 are conjugate functions (such as sine and cosine), they cannot be such that equation 34 is generally satisfied unless the coefficients of u_1 and v_1 are each equal to zero:

$$P_o' - 2\frac{U}{V_o} P_o = \frac{U^2+V_\infty^2}{U V_o} \tag{35}$$

and

$$V_s = \frac{1}{2} U P_o' \tag{36}$$

Equation 35 describes the conditions at which stall propagation could occur. To solve this equation, the inlet and outlet flow angles

and the total pressure loss characteristic must be known; a solution to the equation is obtained when, for the variables chosen, the left and right hand sides of the equation are equal. The stall propagation speed is then determined from equation 36. A solution to these equations does not necessarily mean that propagating stall will occur at the conditions indicated; higher order terms that have been neglected might rule out a solution.

Generally, the stall speed and flow angles can be determined reasonably conveniently in an experiment; the measurements of the total pressure characteristic are obtained less conveniently. With the aid of equations 24, 35 and 36, the individual terms of the equations can be determined experimentally. As can be seen from the nature of the loss characteristic (figure 3), for a given leaving angle, there is generally only one inlet angle at which stall propagation can occur; that is, there is in general only one inlet angle at which the slope and loss characteristics would satisfy equation 35.

Propagating stall would be expected to occur at blade incidence angles at which the total pressure loss characteristic is in the region of relatively steep rise; in this region, however, the slope of the loss characteristic is seen to be, generally, much greater than the value of the loss. Accordingly, if the value of the loss is neglected in comparison with the slope of the loss characteristic:

$$P_o' \approx \frac{U^2 + V_\infty^2}{U V_o}$$

Therefore

$$V_s \approx \frac{U^2 + V_\infty^2}{2V_o} \qquad (P_o \text{ neglected}) \tag{37}$$

or

$$\frac{V_s}{U} \approx \frac{\cos^2\beta_1}{\cos^2\beta_2} \times \csc 2\beta_1 \qquad (P_o \text{ neglected}) \tag{38}$$

All calculations of the stall speed for comparison with experiment were carried out employing equation 38.

All other forms of linearized theory give results which, at the same conditions, are similar. In most of these theories, the cascade turning is considered to be small; the effect of finite turning, as noted in equation 38, can be seen to be significant for the turning angles applicable to cascades of solidity one or so.

The theory can be applied to determine the effects of asymmetrical inlet flows upon cascade or compressor performance. The problem is formulated in a manner similar to that employed in the propagating stall theory. The equations of motion upstream and downstream of the cascade are similar to those developed downstream of the cascade in the propagating stall theory. Therefore, Cauchy-Riemann conditions for functions F and G are obtained upstream and downstream of the cascade; the total pressure perturbation, H, is constant along mean stream lines upstream and downstream. Assuming the same boundary conditions across the cascade as in the propagating stall theory, and assuming the upstream total pressure to be known, the remaining variables can be determined.

Results of experiments performed by Mr. R. Katz in a compressor of 0.6 hub-tip ratio show that the theory can be successfully applied to such asymmetrical inlet flow conditions.

REFERENCES

1. Cheshire, L. J., "The Design and Development of Centrifugal Compressors for Aircraft Gas Turbines", Proceedings of the Institution of Mechanical Engineers, (1945), Vol. 153, pp. 426-440.

2. Emmons, H. W., Pearson, C. E., and Grant, H. P., "Compressor Surge and Stall Propagation", Transactions of the American Society of Mechanical Engineers, (1953), Vol. 77, pp. 453-467.

3. Huppert, M. C. and Benser, W. A., "Some Stall and Surge Phenomena in Axial-Flow Compressors", Journal of the Aeronautical Sciences, (1953), Vol. 20, pp. 833-845.

4. Iura, T. and Rannie, W. D., "Observations of Propagating Stall in Axial-Flow Compressors", Mechanical Engineering Laboratory, California Institute of Technology, Pasadena, California, Report No. 4, prepared under Navy Contract N6-ORI-102, Task Order IV, (1953).

5. Smith, A. G. and Fletcher, P. J., "Observations on the Surging of Various Low Speed Fans and Compressors", National Gas Turbine Establishment Memorandum No. 219, (1954).

6. Montgomery, S. R. and Braun, Lt. J. J., "An Investigation of Rotating Stall in a Single Stage Axial Compressor", Gas Turbine Laboratory, Massachusetts Institute of Technology, Cambridge, Massachusetts, Report No. 29, prepared under NACA Contract NAw-6375, (1955).

7. Costilow, E. L. and Huppert, M. C., "Rotating Stall Characteristics of a Rotor with High Hub-Tip Ratio", NACA Technical Note No. 3518, (1955).

8. Stenning, A. H., "Stall Propagation in Axial Compressors", Gas Turbine Laboratory, Massachusetts Institute of Technology, Cambridge, Massachusetts, Report No. 28, prepared under NACA Contract NAw-6375, (1955).

9. Costilow, E. L. and Huppert, M. C., "Some Effects of Guide-Vane Turning and Stators on the Rotating Stall Characteristics of a High Hub-Tip Ratio Single Stage Compressor", NACA Technical Note No. 3711, (1956).

10. Kriebel, A. R., "Stall Propagation in a Cascade of Airfoils", Gas Turbine Laboratory, Massachusetts Institute of Technology, Cambridge, Massachusetts, Report No. 36, prepared under NACA Contract NAw-6446, (1956).

REFERENCES (Cont'd)

11. Sears, W. R., "A Theory of 'Rotating Stall' in Axial-Flow Compressors", Graduate School of Aeronautical Engineering, Cornell University, Ithaca, New York, prepared under Contract AF33(038)-21406, U. S. Air Force, Office of Scientific Research and Development Command, Baltimore, Maryland, (1953).

12. Marble, F. E., "Propagation of Stall in a Compressor Blade Row", Daniel and Florence Guggenheim Jet Propulsion Center, California Institute of Technology, Pasadena, California, Technical Report No. 4, prepared under Contract AF18(600)-178, U. S. Air Force, Office of Scientific Research, Air Research and Development Command, (1954).

13. Stenning, A. H., "Stall Propagation in a Cascade of Airfoils", Gas Turbine Laboratory, Massachusetts Institute of Technology, Cambridge, Massachusetts, Report No. 25, prepared under NACA Contract NAw-6303, (1954).

14. Burggraf, O. R., "A Theory of Stall Propagation in Axial Compressors on the Basis of Airfoil Characteristics", Ph.D. Thesis, California Institute of Technology, Pasadena, California, (1955).

15. "Forced Draft Blowers and Auxiliary Turbines", L. J. Wing Mfg. Co., New York, New York, Bulletin SW-1.

16. Gates, Calligeros, Evenson, Hayne, and Grube, "Axial Flow Blower Test", Engineering Laboratories, California Institute of Technology, Pasadena, California, (1946).

17. Lieblein, S., "Turning-Angle Design Rules for Constant-Thickness Circular-Arc Inlet Guide Vanes in Axial Annular Flow", NACA Technical Note No. 2179, (1950).

18. Bowen, J. T., Sabersky, R. H., and Rannie, W. D., "Theoretical and Experimental Investigation of Axial Flow Compressors", Mechanical Engineering Laboratory, California Institute of Technology, Pasadena, California, prepared under Navy Contract N6-ORI-102, Task Order IV, (1949).

19. Alsworth, C. C. and Iura, T., "Theoretical and Experimental Investigations of Axial Flow Compressors, Part 3, Progress Report on Loss Measurements in Vortex Blading", Mechanical Engineering Laboratory, California Institute of Technology, Pasadena, California, prepared under Navy Contract N6-ORI-102, Task Order IV, (1951).

REFERENCES (Cont'd)

20. Kovásznay, L. S. G., "Simple Analysis of the Constant Temperature Feedback Hot-Wire Anemometer", Department of Aeronautics, The Johns Hopkins University, Baltimore, Maryland, (1948).

21. Dryden, H. L. and Kuethe, A. M., "The Measurement of Fluctuations of Air Speed by the Hot Wire Anemometer", NACA Report No. 320, (1929).

22. Lindley, C. A., "Secondary Flow in Compressor Cascades", Ph. D. Thesis, California Institute of Technology, Pasadena, California, (1956).

23. Fuller, T. W. and Acosta, A. J., "Report on Design and Construction of the Axial Flow Pump Test Facility", Report No. E-12.13, Hydrodynamics Laboratory, California Instiute of Technology, Pasadena, California, (1953).

24. Rains, D. A., "Tip Clearance Flow in Axial Flow Compressors and Pumps", Report No. 5, Hydrodynamics and Mechanical Engineering Laboratories, California Institute of Technology, Pasadena, California, prepared under Navy Contract N6-ORI-102, Task Order IV and Nord 9612, (1954).

25. Li, Y. T., "High-Frequency Pressure Indicators for Aerodynamic Problems", NACA Technical Note No. 3042, (1953).

APPENDIX I

INSTALLATIONS AND EQUIPMENT

I:1 Small Amplitude Propagating Stall Investigations

I:1.1 Annular Cascade

I:1.1.1 Description of the Installation

The annular cascade system was designed to simulate two-dimensional flows; therefore an installation of moderately high hub-tip ratio, 0.8, was constructed. The tip diameter was 25.56 inches. The cascade system rested on wheels and was completely portable. The system was attached with two large clamps to a blower system. The exit of the blower system was adjacent to a window which was kept completely open during practically all the tests. A photograph of the installation is shown in figure 4; the attaching clamps are not shown.

The overall dimensions of the system are given in figure 16.

I:1.1.1.1 Cascade and Blower System

Due to the small thickness of the cylindrical shell of the cascade system, 0.060 inches, its shape was maintained with the aid of three flanges. The entrance portion of the cascade system was formed in the shape of a bell mouth. The hub portion of the cascade system was supported by the guide vanes and by two 0.050 inch steel wires which were located in the upper portion of the duct, approximately four inches upstream of the downstream flange. One end of these wires was terminated inside the hub; the other end was terminated outside the shell. The orientation of the hub with respect to the shell was achieved by adjustments of the two wires, and was checked periodically. More

detailed information is presented in figure 17.

The hub portion was constructed of wood; the surface was finished with several coats of lacquer and sanded smooth. The hub was constructed in several sections: entrance fairing, guide vane-eight inch straight portion, two separate eight inch straight sections, and exit fairing which was the same shape as the entrance fairing. The sections were held together with a rod located at the center of the hub and which extended at least the full length of the hub. The details of the installation are presented in figure 17. It was believed that the portion of the weight of the hub installation acting through the guide vanes would be sufficient at the speeds of operation to maintain the hub at a fixed axial location; this was found to be the case.

The cascade test section was designed so that different test sections could be installed conveniently. Therefore, the tip portions (outer diameter sections) of all cascade test sections were fitted to the flanges located at the exit section of the cascade system. Each cascade blade was attached to a shank which was inserted through a hole drilled radially in the tip portion of the test section; the blades were then butted against the hub section. The friction force along the shank was sufficient to maintain each blade at its prescribed setting. The clearances at the hub, caused by using a straight blade on a curved surface, are of the order of 0.003 inches. With the blades butted against the hub, the maximum extension of the shank into the airstream or above the tip diameter was of the order of 0.02 inches. The blades could be set to any angle with the aid of an adjustable

protractor to within $\pm$ 1/2 degree. The details of the test section installation are presented in figure 7. A photograph of the cascade test section is shown in figure 5.

A type 15A-COM 7.5 horsepower two stage axial blower, manufactured by the L. J. Wing Manufacturing Company of New York, New York, provided the source of power for the system. The blower contained adjustable gates between stages and fixed discharge vanes. The blower motor is run at constant speed. The air speed is regulated, in a crude fashion, by varying the gate setting. Additional physical information is given in reference 15; a calibration of the blower system was performed and is reported in reference 16.

Upstream of the blower are two ducts, separated from each other by a six inch length of one inch diameter steel honeycombs. An exit duct, downstream of the blower, guides the air leaving the system.

I:1.1.1.2 Blade Design and Construction

The guide vane blades were 3.74 percent thickness ratio circular arc airfoils. The blade chord was 5.35 inches and was constant radially; there was no blade twist. There was a complement of 30 blades; thus a solidity of 2.22 was obtained at mid-radius. The guide vanes were designed for 45 degrees (nominal) turning of the inlet flow from the axial direction. The work of Lieblein (17) was used as a basis for the guide vane design. The blades were constructed of wood, finished with several coats of lacquer and sanded smooth. Details of the guide vanes are presented in figure 17.

The cascade blades were one inch constant chord, approximately 9 percent maximum thickness ratio airfoils; the blades were

untwisted. At mean radius for the full complement of 60 blades installed, the solidity was 0.830. The blade camber angle was approximately 20 degrees. The lower surface of the blade was made flat to simplify the manufacturing process; the upper surface was then determined by the desired camber and thickness ratio. At the leading edge, the upper and lower surfaces were joined with a combination of leading edge radii; the trailing edge was blunted slightly. A photograph of a typical cascade blade is shown in figure 6; details of the cascade blade are presented in figure 17. The cascade blades are reduced scale reproductions of blades which were tested in the rectangular cascade tunnel, and which will be described later in this section.

I:1.1.2 Instrumentation

I:1.1.2.1 Probe Supports

A simple probe support was devised for surveys which were performed upstream and downstream of the cascade test section. The probe support rests upon the metallic outer shell. The base of the support is V-shaped, which enables the support to be positioned in a repeatable fashion with respect to the shell, and the probe to be oriented radially. The support is maintained in position with the aid of two magnets. The probe support position is repeatable within $\pm$ 1 degree.

A probe is fastened in a probe holder which in turn is inserted into the probe support. A spring-clip, from the probe support to the probe holder, maintains sufficient force on the holder to maintain its position; the probe holder can be turned by hand to any whirl orientation. A portion of the probe holder is milled flat along its length.

An angle scale was attached to the top surface of the probe support; a vernier arrangement, fixed to the probe holder, enabled the angle to be read in increments of one degree, while smaller increments could be estimated. A photograph of the probe support is shown in figure 7.

For surveys conducted in the (wooden) cascade test section, the probes were fitted to probe holders which were inserted into holes drilled radially into the test section; the holes were countersunk, such that the center of the base of the probe holder would lie flush with the outer diameter of the duct. In figure 7, a probe is shown installed in the cascade test section.

I:1.1.2.2 Steady-State Instrumentation

A cylindrical yaw probe was employed for measurements of the mean flow direction. The probe is 0.158 inches in diameter; its three pressure orifices are 0.015 inches in diameter. The orifices are spaced 55 degrees apart; the two side holes are used in determining the flow direction. Details of the probe are presented in figure 24a. Additional information concerning the probe may be obtained from reference 18. The probe was purchased from the Whitney Instrument Co., East Long Meadow, Massachusetts. A flat collar was permanently installed on the yaw probe. The yaw probe was always oriented in the same manner to the probe holder by aligning the flat collar of the probe with the flat portion of the probe holder. This was done with the aid of a flat plate and was checked before and after each data point. A reference mark on the probe holder consistently oriented the yaw probe and the instrument support.

Measurements of the mean velocity were obtained with a pitot-static probe. The probe has a diameter of 0.158 inches and the measuring tip is 0.058 inches in diameter. The total head orifice and the static pressure orifices are 0.028 inches and 0.009 inches in diameter, respectively. The probe indicates velocity head within about 1 percent if it is pointing within 3 degrees of the flow direction. To determine the velocity head, the probes were oriented in the air stream at a given location until a maximum reading by the probe was obtained, this reading then being taken to be the velocity head. Details of the probe are presented in figure 24b. Additional information concerning the probe may be obtained from reference 18. The probe was purchased from the Whitney Instrument Company.

The cascade static pressure rise was measured by means of static pressure taps. The installation of these taps was crude enough so that the results of these measurements are to be used only as a guide.

All pressures were measured with an electric pressure transducer manufactured by the Statham Company, Los Angeles, California. The pressure detecting unit consisted of a bridge and a Brown "Electronic" precision indicator; the unit is described in detail in reference 19. A photograph of the system is shown in figure 9.

The dry air density was determined with the aid of dry bulb temperature measurements; the temperature was measured in the entrance of the bell mouth. The accuracy of measurement was approximately $\pm$ 0.1^{o}F. The barometric pressure is measured by a standard mercury barometer. No density correction for humidity was made; experience has indicated this correction to be of the order of

1/2 percent of the density level.

I:1.1.2.3 Hot-Wire Anemometer Instrumentation

Quantitative measurements of unsteady flows were obtained with a constant temperature hot-wire anemometer, Model 60A, manufactured by the Shapiro and Edwards Company, South Pasadena, California. In this instrument, the hot wire forms one arm of a bridge which is balanced at some reference condition. Bridge unbalance, caused by changes in hot-wire resistance, are fed to an electronic control system which adjusts the current flowing through the hot-wire so as to return the wire to its original resistance, thereby restoring the bridge balance. The frequency response of the system is essentially uniform from at least 0 to 5000 cycles per second. The stability of the system was satisfactory. At the time of this writing, no circuit diagrams were available. The hot-wire anemometer is shown in figure 14. The theory of the constant temperature hot-wire anemometer operation is similar to that reported by Kovásznay (20).

The hot-wire was oriented radially in the airstream. Since the radial components of the velocity were small, the system was sensitive primarily to the magnitude of the total velocity perpendicular to the wire. The hot-wire was made of platinum wire 0.0004 inches diameter and 3/16 inch in length. The wire was manufactured by the Wollaston process, that is, the wire was covered with a silver jacket. Before using the wire, the jacket was removed by immersing the wire in a nitric acid solution. The wire was then soft soldered to the supports; results indicated that a good mechanical and electrical bond was achieved. Details of the probe are presented in figure 24c.

The hot-wire was calibrated by finding the values of current, or of the voltage obtained by this current flow through a known resistance (ix R_{known}), under conditions of constant temperature at several known values of the airstream velocity. The hot-wire was maintained at a temperature of approximately 200°C during the test runs; the temperature was considered satisfactory for sensitivity purposes and for continuous operation at which repeatable calibrations could be achieved. The hot-wire was calibrated in the entrance duct of an axial compressor; the wire was located at mid-radius in the compressor annulus. Velocities at this radius, but displaced approximately 12 degrees in the circumferential direction, were measured by the pitot-static probe. The flow conditions in the compressor were essentially uniform circumferentially. By plotting i^2, or $(i \times R_{known})^2$, against $\sqrt{V}$, a straight line relationship was obtained; this relationship is the conventional King's equation for the wire oriented normal to the airstream:

$$i^2 \alpha R_0 \frac{R}{R - R_a} = a + b\sqrt{V}$$

or, for constant temperature operation:

$$i^2 = A_1 + B_1\sqrt{V}$$

or

$$(i \times R_{known})^2 = A_2 + B_2\sqrt{V}$$

A typical constant temperature hot-wire calibration curve is shown in figure 26a. The velocity calculated from the above equation,

as a function of i^2 or $(i \times R_{known})^2$, is shown in figure 26b. The values of the output at zero speed in the compressor were difficult to obtain in a repeatable fashion due to the effects of free convection currents. In this particular anemometer system, the repeatability of the measurements of $(i \times R_{known})$ was far greater than that which was obtained by direct measurement of the current; the approximate value of the current was displayed visually by an ammeter, whereas the $(i \times R_{known})$ voltage was essentially the output of the system, which could be measured accurately and repeatedly with suitable instrumentation. Accordingly, $(i \times R_{known})$, the system voltage output, was used as the basis for all velocity calculations; the direct measurement of the current was used only for qualitative information.

Velocity measurements during unsteady flow were also obtained with a constant current hot-wire anemometer. In this system, the hot-wire forms one arm of a bridge which is always brought to balance. Changes in the velocity level result in changes of the hot-wire resistance which then unbalance the bridge; known changes of the known resistances of the other arms of the bridge are introduced, which then restore the bridge balance. The value of the resistance of the hot-wire can then be determined.

A 90 volt source was employed which, together with the large circuit resistance, enabled the current to be maintained constant to within about $\pm$ 2 percent under conditions in which the largest fluctuations in hot—wire resistance were encountered, and to within less than $\pm$ 1/2 percent for all other conditions. The hot-wire apparatus is shown in figure 15; details of the circuit are presented in figure 25b.

This system is not compensated for the thermal inertia of the wire. Consequently the response of the hot-wire in this system, while adequate at low frequencies (10 to 20 cycles per second), is greatly reduced at higher frequencies (about 100 cycles per second). Further, due to this inertia a phase lag is introduced, which becomes greater as the frequency is increased; thus, not only is the amplitude of a high frequency signal reduced, but its shape is distorted as well (21). This effect becomes greater as the wire temperature is increased.

To obtain an adequate hot-wire sensitivity, the wire temperature was usually maintained at a fairly high level. In a constant current system, the wire temperature increases as the velocity is reduced; therefore a wire, maintained at a reasonably high temperature at high speeds, could at low speeds incur temperatures large enough to cause changes in the calibration curve, or to cause the wire to break. This drawback to the use of the constant current hot-wire anemometer can be offset, somewhat, by calibrating the system at different values of wire current, and then using the appropriate current for the expected velocity levels.

The constant current hot-wire was calibrated in the entrance duct of an axial compressor; the calibration procedure is similar to that used for the constant temperature hot-wire anemometer. In this case, the values of hot-wire resistance, under conditions of constant current and at known values of the airstream velocity, are obtained. By plotting $\frac{R}{R-R_a}$ against $\sqrt{V}$, a straight line relationship was obtained. King's equation for a wire oriented normal to the airstream can then be expressed:

$$\frac{R}{R-R_a} = A_3 + B_3\sqrt{V}$$

A typical constant-current hot-wire calibration curve is shown in figure 27a; the velocity calculated from the above equation, as a function of the wire resistance, is shown in figure 27b.

For measurements of the number of stall cells (this procedure is known as "phase measurements"), two identical hot-wire circuits were employed. The two circuits were checked for identity in response time by feeding a common oscillator signal into both channels and observing the output with suitable instrumentation. Two hot-wire probes were located at different circumferential positions, and simultaneous readings of their outputs were recorded. The phase relationship of the signals, together with the known circumferential spacing of the probes, enables the number of stall cells to be determined.

The constant temperature hot-wire anemometer was employed whenever quantitative measurements of the magnitude of the velocity and velocity fluctuations during stall propagation were to be obtained. The constant current hot-wire anemometer was used for all qualitative estimates of the magnitude of the velocity and velocity fluctuations and for the measurements of the stall frequency and number of stall cells.

Hot-wire anemometer surveys were performed upstream and downstream of the test cascade; a survey was conducted in the circumferential direction behind the cascade.

The mean output voltage of the constant temperature hot-wire anemometer was measured by a direct current milliameter (one

milliampere full scale deflection) manufactured by the General Electric Company, West Lynn, Massachusetts; the milliammeter was used as a voltmeter.

The bridge circuit of the constant current hot-wire anemometer was balanced with the aid of a Wheelco portable slide wire potentiometer manufactured by the Wheelco Instrument Division of the Barber-Colman Company, Rockford, Illinois. A Speedomax self-balancing potentiometer, manufactured by the Leeds and Northrup Company, Philadelphia, Pennsylvania, was employed to balance the bridge circuit when the cold resistance of the hot-wire was determined.

The outputs of both types of anemometers were recorded by two instruments:

1. Magnitudes of the velocity fluctuations were recorded by a direct-inking type oscillograph coupled with an A-C amplifier, manufactured by the Brush Development Company, Cleveland, Ohio (Models BL-202 and BL-905, respectively). The response of the amplifier-oscillograph system is flat from approximately 0.5 to 80 cycles per second. A photograph of the Brush system is shown in figure 15. The fundamental frequencies of the propagating stall were sufficiently low so that several harmonics of the fundamental frequency could be reproduced accurately by the Brush system.
2. For the purpose of obtaining a higher frequency response in the recording instruments, the anemometer output was displayed on a dual-beam oscilloscope, Model 322-A, manufactured by the

Instrument Division of the Allen B. DuMont Laboratories, Inc., Clifton, New Jersey. The high frequency response of the oscilloscope is superior to that of the Brush system. The high frequency response of the oscilloscope is such that the hot-wire system determines the overall limiting frequency response characteristics. The signal trace which was displayed on the oscilloscope was photographed with an Oscillograph Record Camera, Type 297, purchased from the Instrument Division of the Allen B. DuMont Laboratories, Inc. A photograph of the oscilloscope camera system is shown in figure 14.

I:1.2 Axial-Flow Compressor Cascade, Stator Row

I:1.2.1 Description of the Installation

The compressor used in this investigation of the propagating stall is the same as that employed in the stall investigations reported by Iura and Rannie (4). The compressor hub-tip ratio is 0.6; the tip diameter is 36 inches. A 125 horsepower electric dynamometer drives the compressor by means of a shaft which passes through the rear duct. The air flows into the compressor through a cylindrical entrance duct, the entrance portion of which is formed in the shape of a bell mouth. A screen is installed on the bellmouth to prevent foreign objects from entering the compressor air stream. Following the flow through the compressor test section, the air enters the exit portion which consists of a short cylindrical duct, an elbow section, and a transition section which connects the elbow to the throttle valve. The throttle valve, which regulates the flow resistance and thus the com-

pressor flow volume, consists of two rectangular doors which are actuated by a variable speed motor to vary the throttle opening and therefore the flow rate. A photograph of the compressor is shown in figure 8. The details of the installation are presented in figure 18.

Most of the tests were conducted at a compressor rotative speed of 750 rpm ($U_o \approx$ 118 fps), at which speed compressibility effects were negligible, and the blades could be considered rigid as far as aerodynamic forces were concerned.

Provisions are made for the installation of three complete stages, one row of guide vanes, and two rows of straightening vanes, as shown in figure 18; each blade is separately removable which therefore enables a variety of blade and stage configurations to be tested. At full solidity there are 30 rotor blades and 32 stationary blades per row, resulting in solidities at mid-radius of 0.862 and 0.920, respectively; the axial spacing between adjacent blade rows is 2.875 inches.

Free-vortex compressor blading was used during these tests. The blade system was designed for an average power coefficient, $\bar{\psi} = 0.40$, at a flow coefficient, $\bar{\Phi} = 0.45$; due to the influence of the wall boundary layers, the design power coefficient was attained at $\bar{\Phi} = 0.43$. The design geometrical characteristics of the blades are presented in Table 1. The root and tip sections of the blades are shown in figure 19.

Additional details of the compressor installation are presented in reference (18).

To achieve the optimum compressor configuration for the detection of the small amplitude propagating stall on the stator row, a distorted single stage configuration was installed. In this configuration the rotor row was located in the third stator row position and its stagger angle was changed from that at design condition. The guide vane-rotor combination was employed to provide a simple and convenient means by which the inlet angle to the stator could be varied. Previous investigations of the propagating stall on similar configurations (Section III) have indicated that, with all blade rows set at design angles, stall propagation first occurs on the rotor and is detected throughout the machine. Therefore, the stagger angle of the stator row was changed so that it would stall before the rotor row. The separation was made a maximum in order to reduce blade row interference effects.

I:1.2.2 Instrumentation

The mean mass flow through the compressor, or the mean velocity through the compressor annulus, was determined from the measurements of an interconnected set of four wall static pressure orifices which were calibrated with respect to the flow through the entrance duct; the orifices were located midway through the entrance duct, as shown in figure 18. The air density, corrected for humidity, was determined with the aid of wet-dry bulb thermometer measurements; the thermometer was located on the screen in the entrance of the bell mouth. Barometric pressure was measured by a standard mercury barometer.

The rotational speed of the compressor was measured by means of a meter manufactured by the Standard Electric Time Company, Springfield, Massachusetts; the speed can be measured to within 1/2 rpm. Details of the instrument are presented in reference (18).

The flow through the compressor was surveyed through the use of six rectangular instrument ports located near the top of the outer case of the compressor, and a number of radially directed survey holes located at several circumferential positions near each blade row. A traversing carriage, manufactured by the Boller and Chivens Engineering Company, South Pasadena, California, was used to position the instrument probe in the compressor ports. With the aid of this carriage, a continuous survey in the circumferential direction, fifteen degrees in extent, could be conducted; in addition, the probes could be continuously and accurately positioned in both the radial and whirl directions. The instrument is described in reference (18). A radial survey carriage, manufactured by the Astro-Physics machine shop at the Institute, was used to position the probes in the radial survey holes; the probes could be continuously and accurately positioned in both the radial and whirl directions. In addition, a crude probe support was constructed by drilling a hole of the appropriate diameter through a plug of the type which were fitted to the radial survey holes; with the aid of a scale, the probe could be set with reasonable accuracy to known discrete radii. The probe supports are shown in figure 9.

Measurements of the mean velocity head and the mean flow angle were obtained with the probes described in Appendix I: 1. 1. 2. 2.

These probes were designed to fit the probe supports described in the preceding paragraph. The cylindrical yaw probe-radial survey carriage system was calibrated directionally using the method described in reference (18).

All pressures were measured with the pressure transducer-detecting unit-indicator system described in Appendix I:1.1.2.2.

Measurements of unsteady flow were obtained with the constant resistance and constant current hot-wire anemometers described in Appendix I:1.1.2.3.

The mean and fluctuating outputs of the hot-wire anemometers were measured and recorded by the voltmeter, oscillograph, oscilloscope and camera instrumentation described in Appendix I:1.2.2.3. In addition to these instruments, an amplifier and photographic recording oscillograph, (type A-3 and Model H multi-channel, respectively) manufactured by the William Miller Corporation, Pasadena, California, was employed during most of the phase measurements tests. The response of this system was essentially uniform throughout the range of interest. A photograph of the oscillograph system is shown in figure 15.

I:1.3 Rectangular Cascade

I:1.3.1 Description of the Installation

The small amplitude propagating stall was also investigated in a large, low-speed, open-return rectangular cascade tunnel originally constructed for the study of secondary flow and critical Reynolds number effects in conventional subsonic compressor cascades (22).

The inlet bell has a large area contraction ratio, the inlet to which is faced with a layer of honeycomb paper, followed by two layers of screening. The resulting flow is quite steady and the turbulence level is quite low compared to most cascade tunnels; the boundary layer thickness is of the order of 1/4 inch. The tunnel is powered by an electric motor driving a fan; the speed is controlled by a drum switch and grid resistor box. The control system permits the speed to be set to discrete values only; fine adjustments cannot be performed. In addition, fluctuations in line voltage cause small fluctuations in the speed; for the purposes of the stall investigation, this effect is not considered important. A photograph of the cascade tunnel is shown in figure 10; detailed information is presented in figure 20.

The cascade test section is 2 ft x 3 ft, with five blades of 8 1/2 inch chord length. A photograph of the test section is shown in figure 11.

Additional information regarding the installation may be obtained from reference (22).

Tests were conducted on blade sets of three different shapes:

1. One set of blades used were those which were originally installed and tested in this cascade tunnel. The blade is shown in figure 21. The cascade geometry at an angle of attack of 14.98 degrees is identical to the mean section of the free-vortex stator of the axial-flow compressor previously described. The cascade had a solidity of 0.920, a blade camber angle of 29.98 degrees, a design turning angle of 21.85 degrees at

14.98 degrees angle of attack, with a parabolic mean line, 10 percent thickness ratio, and an entrance flow angle of 46.22 degrees measured from the stagger line.

2. A second set of blades (intermediate shape) employed were those from which the annular cascade tunnel test section blades were constructed. The blade is shown in figure 21. This cascade had a solidity of 0.920, a blade camber angle of about 20 degrees, with a flat lower surface, 8.8 percent thickness ratio, and an inlet flow angle of 46.22 degrees measured from the stagger line. The lower surface of these blades was made flat. The leading edge of the upper surface was made of wood and sanded smooth. The remainder of the upper surface was made of smooth cardboard which was fitted to ribs which were attached to the flat lower surface. The resulting joints were joined together as smoothly as possible. Tests were conducted with the blades in both the above condition, and with a smooth fabric covering the entire blade surface.

3. The third set of blades employed were flat plate type blades. The blade is shown in figure 21. This cascade had a solidity of 0.920, with a rectangular profile section of 1.5 percent thickness ratio, and an entrance flow angle of 46.22 degrees measured from the stagger line.

I:1.3.2 Instrumentation

The probe support was basically a "barn door hanger" suspension parallel to the cascade stagger plane, held in place by its

own weight, and rolling on ball bearings on machined rails. Probes were clamped to a small fixture, with the probe tip located at the desired depth in the channel. Hand cranks moved the carriage in a direction parallel to the stagger line, and the probe clamping fixture in a direction parallel to the blade span. The probes could be accurately positioned; the repeatability of the probe positions was within .002 inches. The probes were generally sting mounted such that practically the entire volume of the cascade could be surveyed. Additional information regarding the probe support may be obtained from reference (22). The support is shown in figure 11. A second similar probe support was constructed for use during the stall investigation.

Measurements of unsteady flow were obtained with the constant resistance and constant current hot-wire anemometer described in Appendix I:1.1.2.3. During all tests the major axis of the hot-wire was oriented in the vertical direction (see figure 24d).

The mean and fluctuating outputs of the hot-wire anemometer were measured and recorded by the voltmeter, Brush oscillograph, oscilloscope and camera instrumentation described in Appendix I:1.1.2.3.

Measurements of the mean velocity, from velocity head data, were recorded at a location approximately one chord length upstream of the blades, at about the center of the channel.

Measurements of the flow angles were not obtained.

I:2 Large Amplitude Propagating Stall Investigations

I:2.1 Axial-Flow Compressor

I:2.1.1 Description of the Installation

The compressor used in this investigation of the propagating stall has been previously described in Appendix I:1.2.

During some of the tests conducted upon this installation a honeycomb was installed in the inlet bell mouth to reduce the velocity fluctuations entering the compressor annulus. A loss of total pressure across the screen was observed, proportional to the square of the total velocity. Consequently, for a given compressor configuration and flow coefficient, the magnitudes of the compressor pressure-rise were reduced below those observed when the honeycomb was not installed.

Practically all tests were conducted at a rotor rotative frequency of 750 rpm.

All tests were conducted with free-vortex blading.

I:2.1.2 Instrumentation

Measurements of the mean velocity through the compressor annulus were obtained by the method previously described in Appendix I:1.2.2.

During most of the runs conducted with the honeycomb installed, a compressor calibration, similar to that previously described in Appendix I:1.2.2, was not available. The velocity, measured with a pitot-static probe located at mid-radius in front of the guide vanes, was assumed to be the mean velocity through the compressor annulus. Such an assumption was sufficiently accurate for the purposes of these

stall investigations, with the possible exceptions of the effects of the full stall upon the pitot-static readings. Under these latter conditions, the instrument readings may have been inaccurate due to the occurrence of reverse flows. In this case, measurements of the mean velocity were obtained by determining the mass flow through the throttling doors. This was accomplished by judiciously locating a pitot-static probe in the throttle door, at a representative location, relatively free from all wall effects. The results were checked, with the honeycomb removed, by comparing the mean speeds obtained by this method with the results obtained from the known compressor calibration; the agreement was satisfactory. A calibration with the honeycomb installed was subsequently performed and the results employed.

The dry air density, barometric pressure and rotational speed of the compressor were determined with the aid of the instruments previously described in Appendix I: 1. 2. 2.

The power input to the compressor could be found from accurate measurements of the rotative speed and of the driving torque, which was determined by means of a diaphragm type force meter manufactured by the Hagan Corporation, Pittsburgh, Pennsylvania; additional details of this instrument may be obtained from reference (18).

Measurements of the exit-duct wall static pressure were obtained to present an indication of the compressor pressure rise. The location of the orifice is shown in figure 18.

All probe supports employed were identical to those described in Appendix I: 1. 2. 2.

Measurements of the mean velocity head and the mean flow angle were obtained with the probes described in Appendix I:1.1.2.2 and I:1.2.2.

Measurements of the unsteady flows were obtained with the constant temperature and constant current hot-wire anemometers described in Appendix I:1.1.2.3. During most of the tests, the constant temperature hot-wire anemometer was not available; consequently most of the measurements, quantitative and qualitative, were obtained using the constant current hot-wire anemometer.

In addition, during many of the tests, a constant current hot-wire anemometer identical to that described in reference (4), was employed; a schematic diagram of this unit is shown in figure 25a. In this system the hot-wire was essentially merely another resistance in series with a very large resistor. The resistance of the hot-wire was determined by measuring the potential drop across the hot-wire and the potential drop across a one ohm precision resistance in series with the hot-wire, the latter measurement indicating the current through the hot-wire. The hot-wire resistance was then determined from Ohm's law. The calibration of the hot-wire system was performed exactly as described in Appendix I:1.1.2.3, and in reference (4). The repeatability of the system was not satisfactory; the design was revised to the bridge-circuit constant current anemometer previously described.

The mean and fluctuating outputs of the hot-wire anemometer were measured and recorded by the voltmeter, potentiometer,

oscillograph, oscilloscope and camera instrumentation described in Appendix I: 1. 1. 2. 3.

I:2. 2 Axial-Flow Pump

I:2. 2. 1 Description of the Installation

The axial-flow pump used in the propagating stall investigations was designed for internal flow studies, performance investigations and cavitation experiments. The requirements led to the design of a vertically mounted test unit installed in a simple closed hydraulic circuit using water, generally, as the working fluid. The rotor is externally driven by a D. C. dynamometer which provides the only power for flow circulation.

Most of the tests were conducted at a rotative frequency of 171 rpm ($U_o \approx$ 10 ft/sec.).

The circuit consists of the test pump which discharges into a vaned elbow and thence into a diffuser section. Another vaned elbow directs the flow downward through a diffuser and then into a "lattice" type throttling device. The circuit is closed through two more vaned elbows and a 6:1 contraction ratio nozzle. A photograph of the installation is shown in figure 12; general dimensions are presented in figure 22.

A feature of the closed circuit design is that the system pressure level may be controlled; during these investigations the pressure level was maintained at atmospheric pressure.

The test section is 14 inches inside diameter with a hub-tip ratio of 0. 6; the unit can accommodate up to three complete stages of

blading. Details of the installation are shown in figure 23. A lucite window runs the full length of the rotor and extends circumferentially over two blade passages.

The blade design in this installation is the same as that employed in the axial-flow compressor previously described in Appendix I:1.2 and I:2.1. The geometrical characteristics of the blades are shown in Table I. The design flow coefficient is, $\bar{\Phi} = 0.45$, and power coefficient is $\bar{\Psi} = 0.40$. The blades are of free-vortex design. For constructional reasons, the number of blades in the installation was reduced from that in the compressor; therefore the blade aspect ratio was also reduced. Rotor blade aspect ratio is about 1.5 and that of the stator blade is about 1.1. There are 18 stationary blades (guide vanes, stator and exit blades) per row and 16 rotor blades per row.

Additional information concerning the installation may be obtained from references 23 and 24.

Due to the flow leakage caused by the lattice-type throttle construction, flow coefficients less than about $\bar{\Phi} \sim 0.09$ could not be obtained. To investigate the system characteristics at lower flow coefficients, a "flapper" valve throttle device was installed at the vaned elbow located between the two diffuser sections.

Tests were conducted upon a complete single stage (guide vanes, rotor and stator) configuration; effects of blade row separation were determined.

I:2.2.2 Instrumentation

I:2.2.2.1 Steady-State Instrumentation

The flow rate through the pump was determined from the

measurements of the pressure drop across the contraction nozzle upstream of the pump; the nozzle was calibrated from velocity surveys conducted at its exit.

An indication of the pump head rise was obtained from measurements of the difference between the total pressure measured in the center of the nozzle exit survey plate, and the static pressure measured at a static pressure ring located downstream of the test section proper.

Facilities are provided for more detailed flow measurements, none of which were employed during the stall investigations.

All pressures were measured on a standard U-tube manometer to which a scale was attached. With the aid of a vernier attachment, readings repeatable to within $\pm$.001 inches of water were obtained.

At rotative frequencies above about 100 rpm, the speed is established in unit rpm increments and controlled with the aid of a differential gear box. With this controller speed regulation is maintained to within one part in ten thousand. Below about 100 rpm the performance of the speed controller diminishes and it then becomes difficult to maintain speed with the device; manual control proves satisfactory in this range.

A torque arm and pan weight system is used to measure the torque. An electrical displacement pickup gives the location of the arm between stages 0.004 inches apart. The signal from the pickup is used as a null indicator so that the arm is returned to its original balance position for each reading. The sensitivity of the torque measuring equipment is about 0.25 inch-pounds.

Additional information regarding the instrumentation may be obtained from references (23) and (24).

I:2.2.2.2 Dynamic Instrumentation

Dynamic measurements of the pressure fluctuations were obtained with the aid of two barium titanate crystal pressure transducers. This transducer operates on the principle that a polarized crystal, when stressed, produces a charge across its surface; appropriate connections on each surface transform this charge into an electric signal related to the pressure which initially stressed the crystal. The transducer is quite sensitive to temperature changes and has rather poor low frequency response characteristics (25). The gages used in the present investigations were not compensated for temperature change; at about room temperature, the calibration changes about one percent per degree Farenheit. The low frequency response characterisitcs were improved by employing a cathode follower in conjunction with the transducer.

The gages (including the cathode followers) were calibrated in air. The gage was placed in a circuit whose pressure level was accurately known and which was different from the atmospheric pressure level. (Connections in the circuit were made using taigon tubing). A quick-opening switch was actuated which then established this pressure difference across the gage; the output of the gage was recorded on an oscilloscope and photographed with a Polaroid land camera. The switch was connected to the oscilloscope in such a fashion that, while it was being actuated, the horizontal sweep circuit of the oscilloscope was

triggered; thus a base reference was placed on the screen. At least three runs per calibration point were performed. There was some leakage of the air through the switch; the resulting changes in pressure differences were small, and considered negligible, during the time required to perform a calibration run. A representative gage calibration is presented in figure 28c.

A representative calibration test run is shown in figure 28a. A significant portion of the indicated rise time is due to the quick-opening switch. A measure of the maximum usable frequency may be obtained from the rise time; the resulting frequency is far in excess of the requirements of this investigation. The response of the gage is indicated by the level of the initial pattern. Succeeding changes in level are caused by reflected waves in the circuit.

The minimum usable frequency was determined by observing the rate of decay of the resulting system output. This frequency was found to be considerably smaller than required for this investigation. A representative oscillograph record of such tests is shown in figure 28b.

The barium titanate crystals were 0.50 inches in diameter and 0.08 inches in thickness. The crystals were obtained from the Brush Development Company; the electronic circuits were designed, and the gages constructed at the Institute. The gage installation is shown in figure 13.

The gages were located about 1/4 inch upstream and downstream of the rotor row; the gages were located circumferentially so as to be

in the same rotor passage. Provisions were made for locating the gages at the same axial location, but displaced circumferentially, for the purpose of obtaining phase measurements.

The gages were inserted radially into the tip casing. To accomodate the gages, a hole, 0.825 inches in diameter was drilled (and threaded) to within 0.19 inches of the inside tip diameter; a hole, 0.15 inches in diameter, was then drilled through to the inside tip diameter. Silicone grease was placed on the gage face prior to installation, both as space filler material and to prevent contact of the water with the crystal surface. When the gage was butted against the inside face the grease filled the hole; excess grease collected inside the pump annulus and was washed away by the moving fluid, leaving a smooth contour at the wall. An O-ring sealed against water leakage.

The output of a gage was amplified and recorded by a Brush amplifier and oscillograph system previously described in Appendix I:1.1.2.3.

The repeatability in performance of both gages during test runs was not satisfactory due to shifts in gage calibration, gage installation technique and/or electric instrumentation difficulties. The observed scatter in pressure fluctuations was, in some cases, of the order of 100 percent. Accordingly, all pressure fluctuations presented are to be considered only as guides.

I:2.2.2.3 Flow Visualization Instrumentation

All rotor blades and visible stationary blades were painted with white enamel, and tufted on both the pressure and suction surfaces and

trailing edges with about 1/64 inch diameter, 1/2 inch long black thread. The tufts were placed at various radii along the blade surface and at three chordwise locations. During some of the tests, rakes about 1/32 inch in diameter, were tufted and inserted at various locations in the blade passages and between blade rows. Tufts were also placed on the hub and tip portions of the pump, at various locations.

To facilitate the observation of the tuft motions, the segments of the stationary blades which were located in the viewing window were constructed of lucite. To avoid high stresses on the lucite, especially during propagating stall, it was required to maintain the rotative frequency of the pump below 200 rpm; practically all tests were conducted at a rotative frequency of 171 rpm.

Motion pictures of the behavior were recorded at various flow conditions. Motion pictures of the tuft motions on the stationary blades were recorded with a 16 mm Cine-Kodak Special camera manufactured by the Eastman Kodak Company, Rochester, New York; frame speeds of 16 frames/second and 64 frames/second generally were employed. Motion pictures of the tuft motions on the rotor row were recorded with a 16 mm Eastman High Speed Camera manufactured by the Eastman Kodak Company; a frame speed of 2500 frames/second was employed.

Motion pictures showing the behavior of the tufts at various flow conditions are on file at the Institute.

FREE VORTEX $\left[C_{u1} = .145 \frac{r_0}{r} u_0 ;\ C_{u2} = .345 \frac{r_0}{r} u_0\right]$

	ROTOR					STATOR				
SECTION LOCATION - r - INCHES	10.8	12.6	14.4	16.2	18.0	10.8	12.6	14.4	16.2	18.0
DESIGN ENT. ANGLE - ROTOR - β_1 - DEG.	51° 21′	42° 24′	36° 2′	31° 21′	27° 45′					
DESIGN ENT. ANGLE - STATOR - γ_2 - DEG.						38° 3′	42° 24′	46° 13′	49° 34′	52° 31′
DESIGN EXIT ANGLE - ROTOR - β_2 - DEG.	86° 49′	65° 17′	50° 40′	41° 3′	34° 29′					
DESIGN EXIT ANGLE - STATOR - γ_1 - DEG.						61° 46′	65° 17′	68° 4′	70° 18′	72° 8′
SECTION CAMBER - θ - DEGREES	46° 40′	31° 0′	20° 19′	13° 47′	9° 48′	31° 53′	31° 6′	29° 59′	28° 41′	27° 20′
CASCADE STAGGER ANGLE - β' - DEG.	74° 48′	57° 54′	46° 12′	38° 15′	32° 36′					
CASCADE STAGGER ANGLE - γ - DEG.						54° 0′	57° 57′	61° 12′	63° 55′	66° 11′
SOLIDITY - C/S	1.150	.985	.862	.766	.690	1.035	.970	.920	.880	.849
MAXIMUM THICKNESS - % C	12	11	10	9	8	10	10	10	10	10

Table 1 Geometrical Characteristics of Free-Vortex Blading, Axial-Flow Compressor

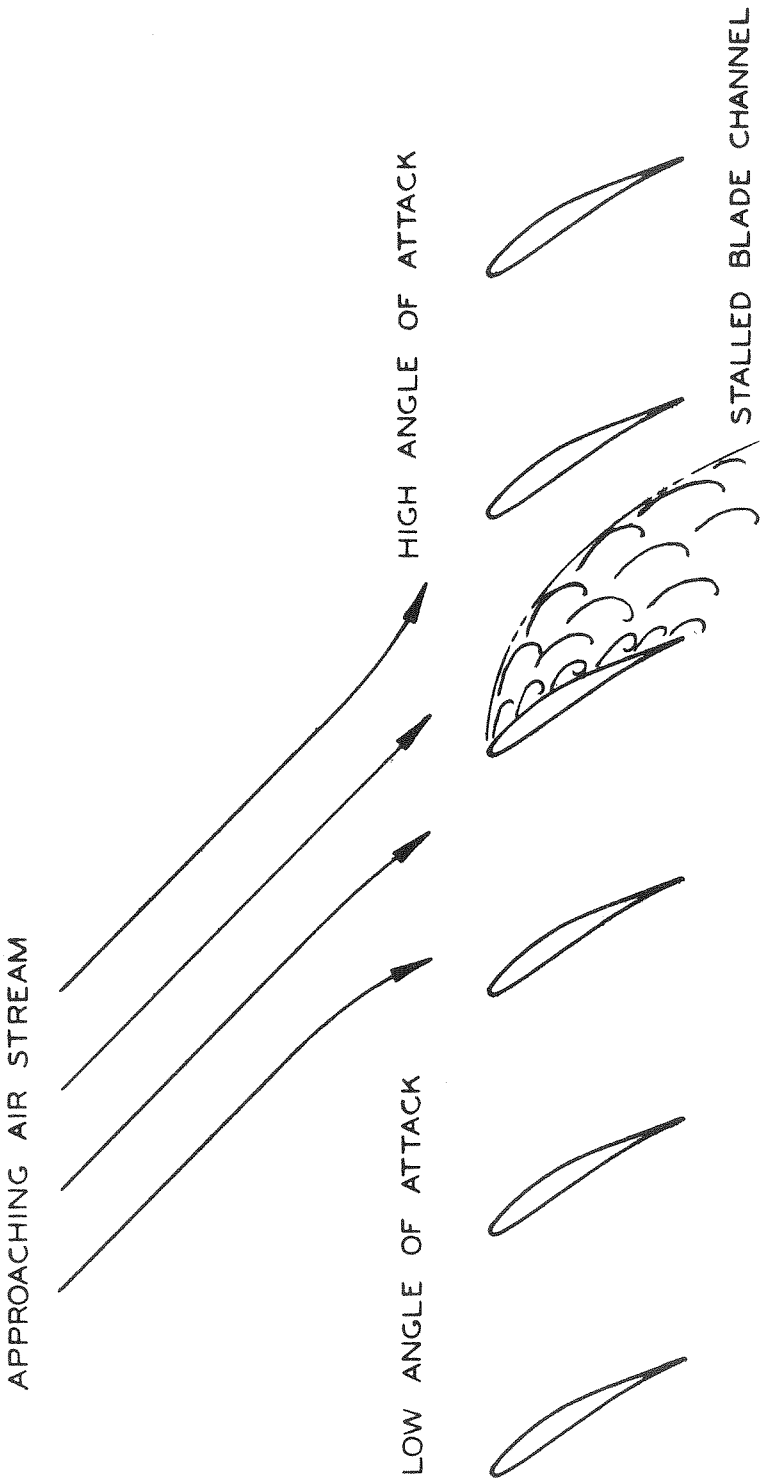

Fig. 1 Stall Propagation

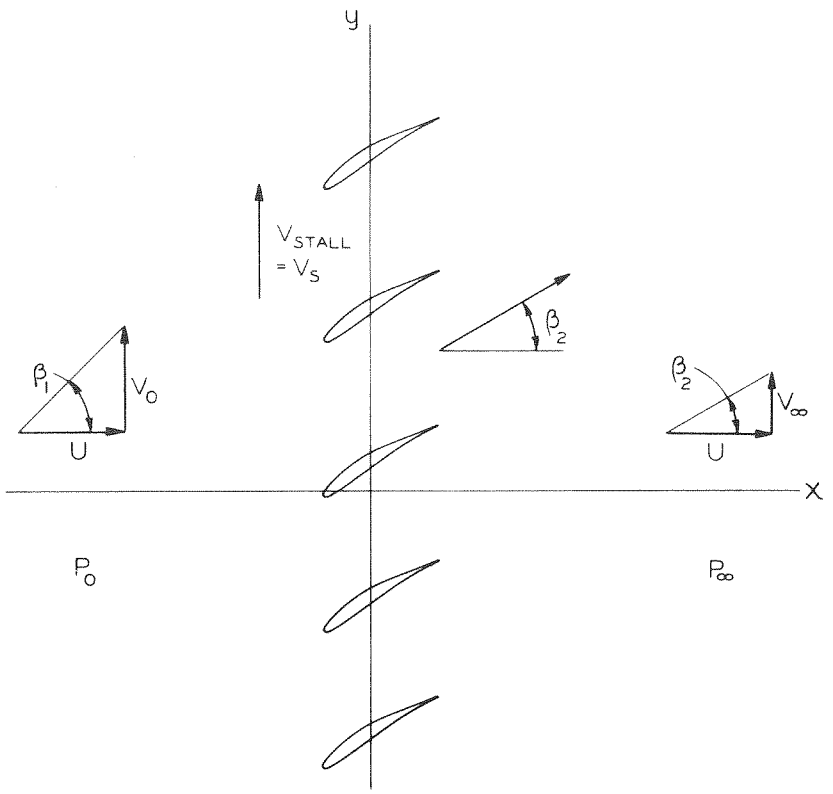

Fig. 2 Cascade Representation and Notation for Propagating Stall Theory

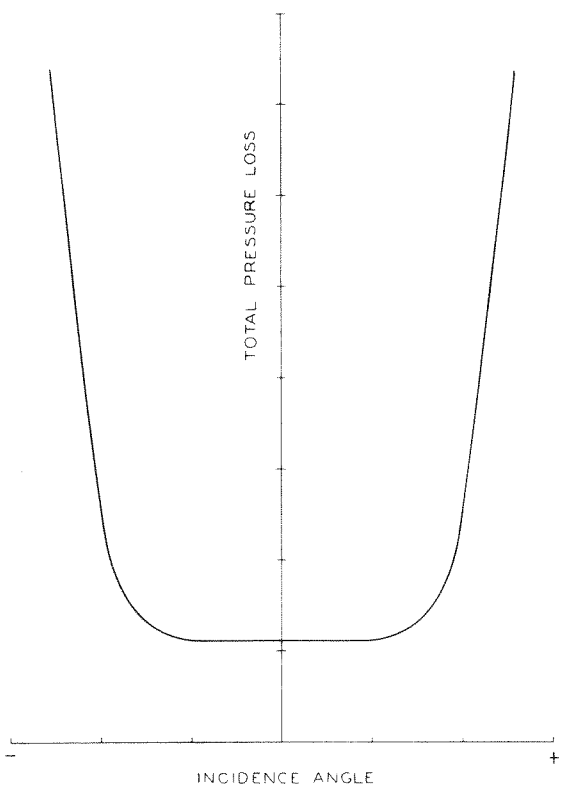

Fig. 3 Representative Cascade Total Pressure Loss Characteristic

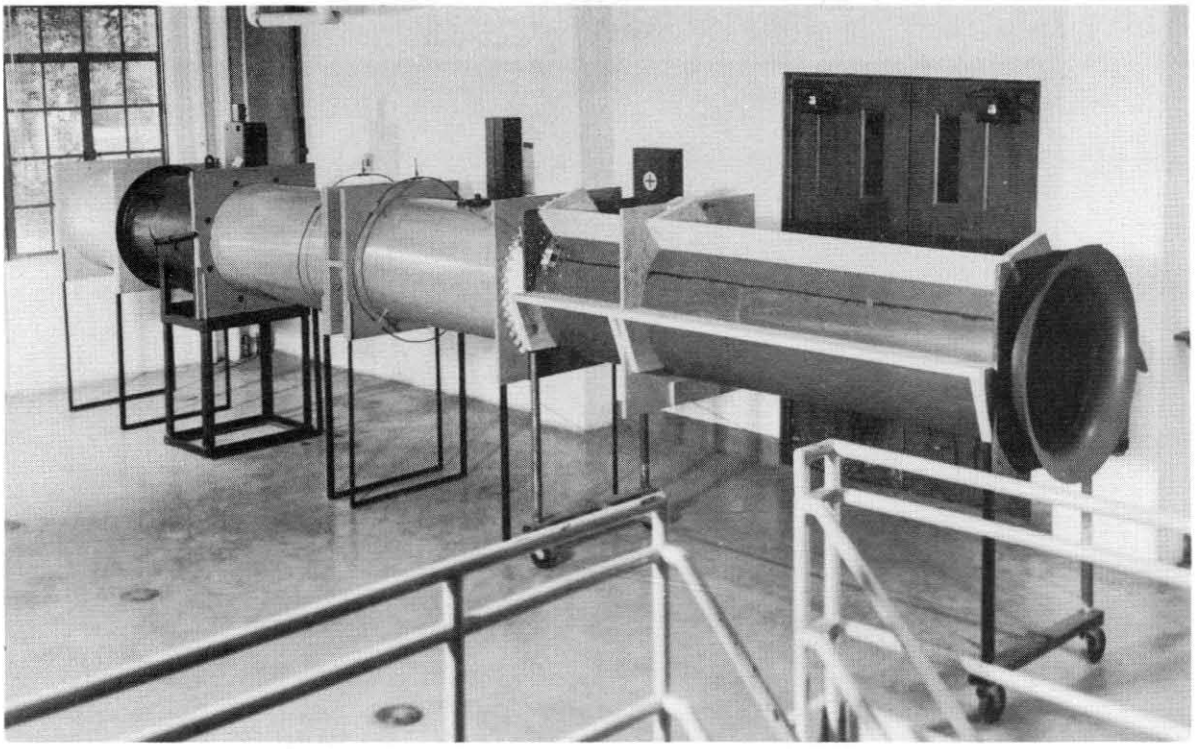

Fig. 4 Annular Cascade Tunnel.

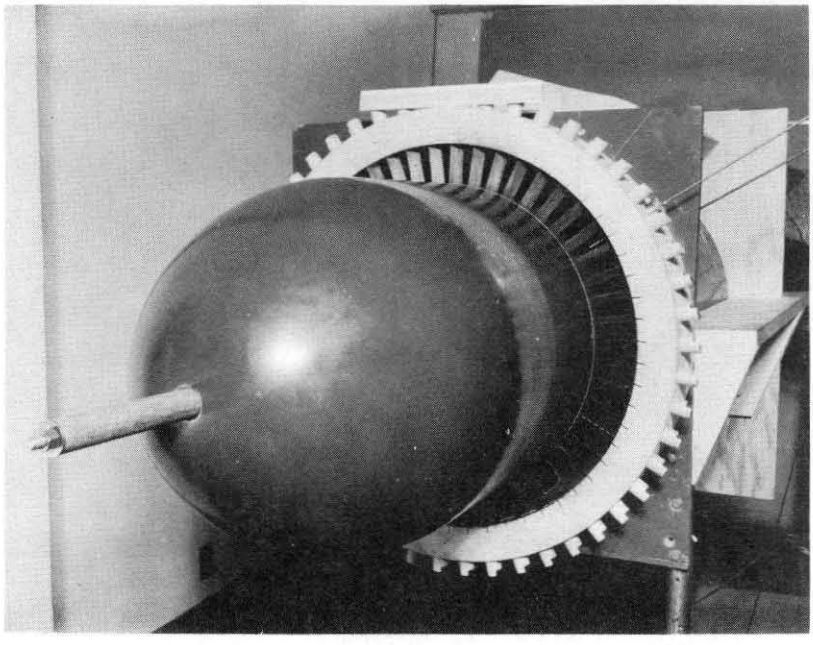

Fig. 5 Test Section and Hub Exit Fairing Annular Cascade.

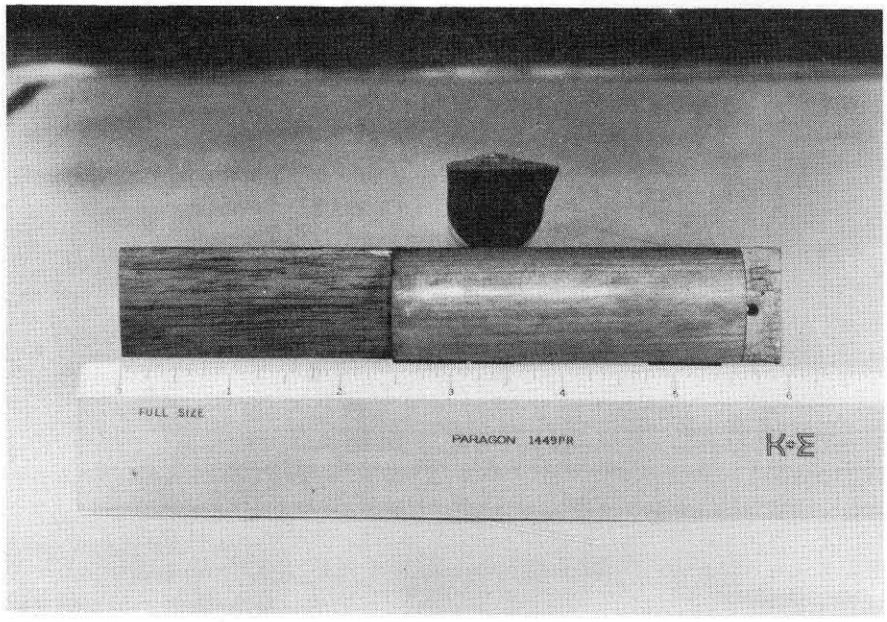

Fig. 6 Representative Test Blade.
Annular Cascade.

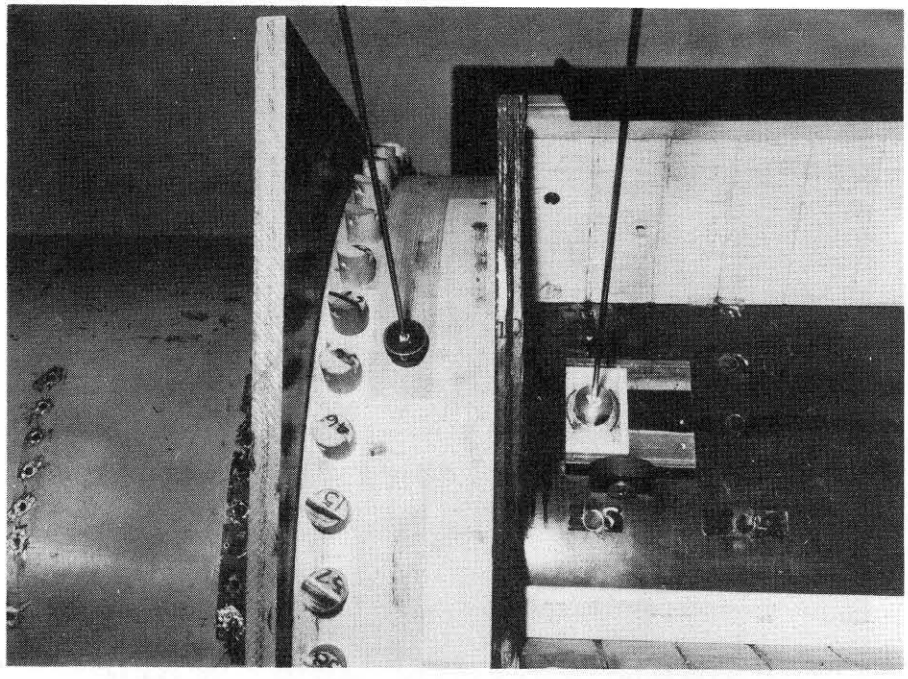

Fig. 7 Probe Supports.
Annular Cascade.

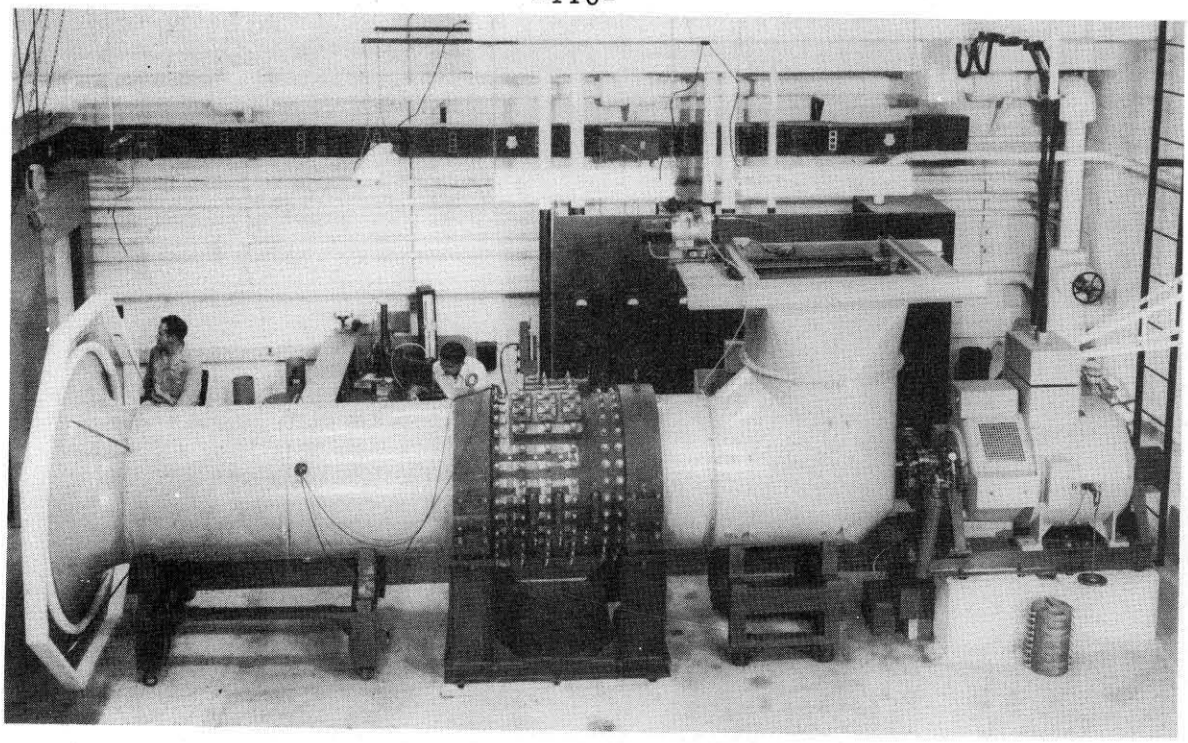

Fig. 8 Axial-Flow Compressor.

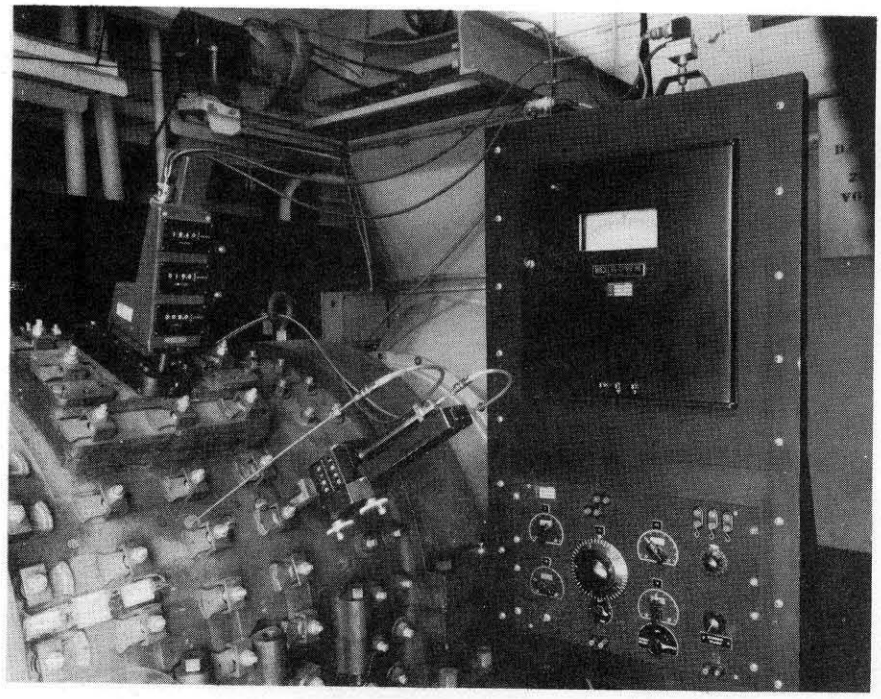

Fig. 9 Instrumentation: Survey Carriages, Pressure Detecting Unit .

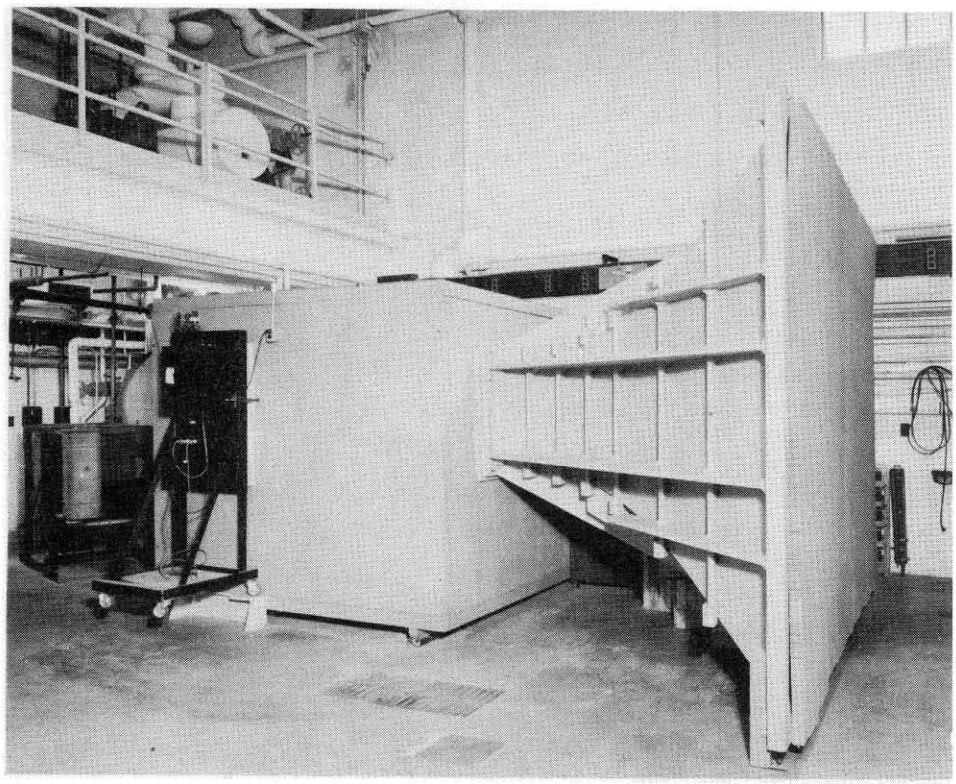

Fig. 10 Rectangular Cascade Tunnel.

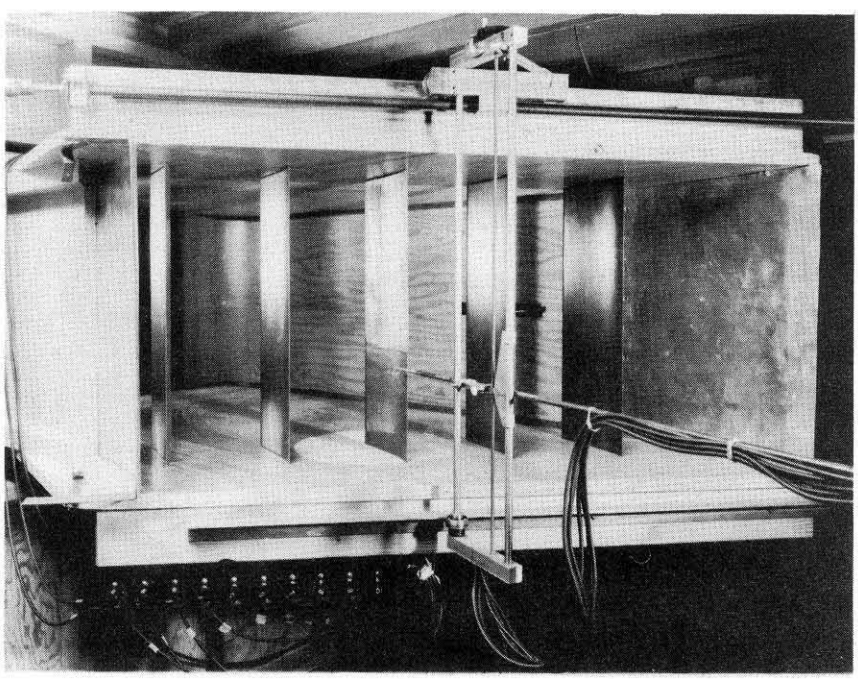

Fig. 11 Test Section. Rectangular Cascade.

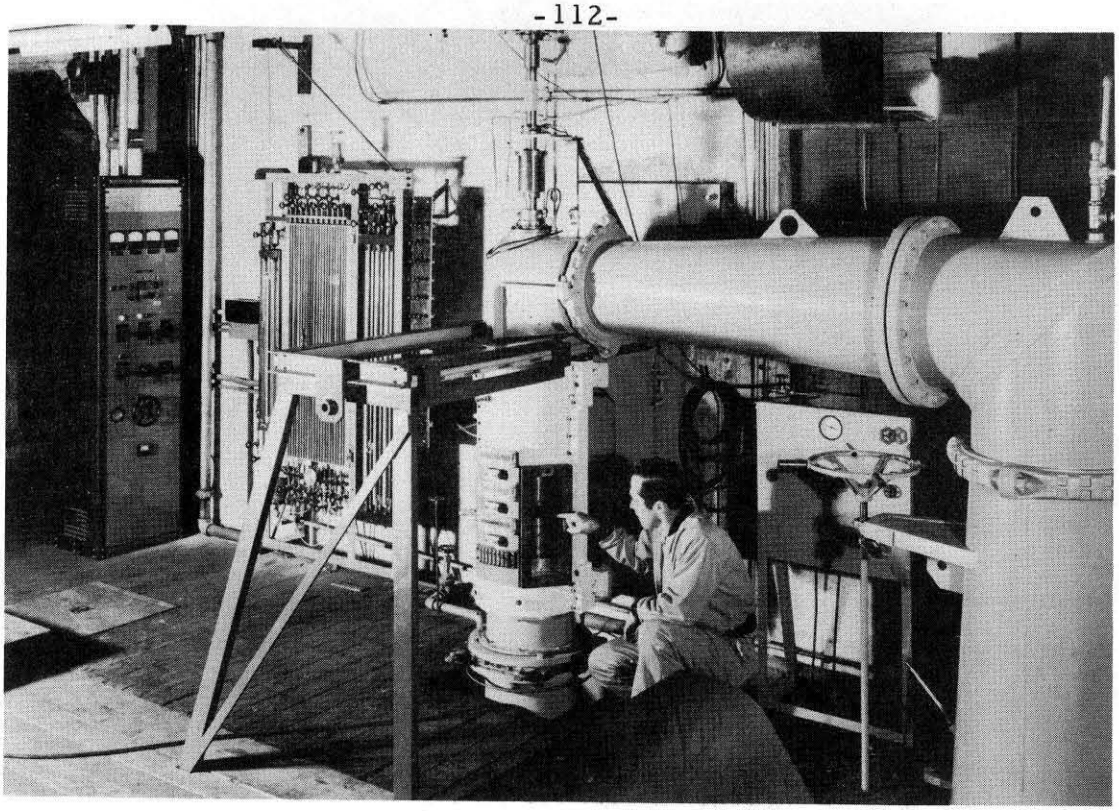

Fig. 12 Axial-Flow Pump.

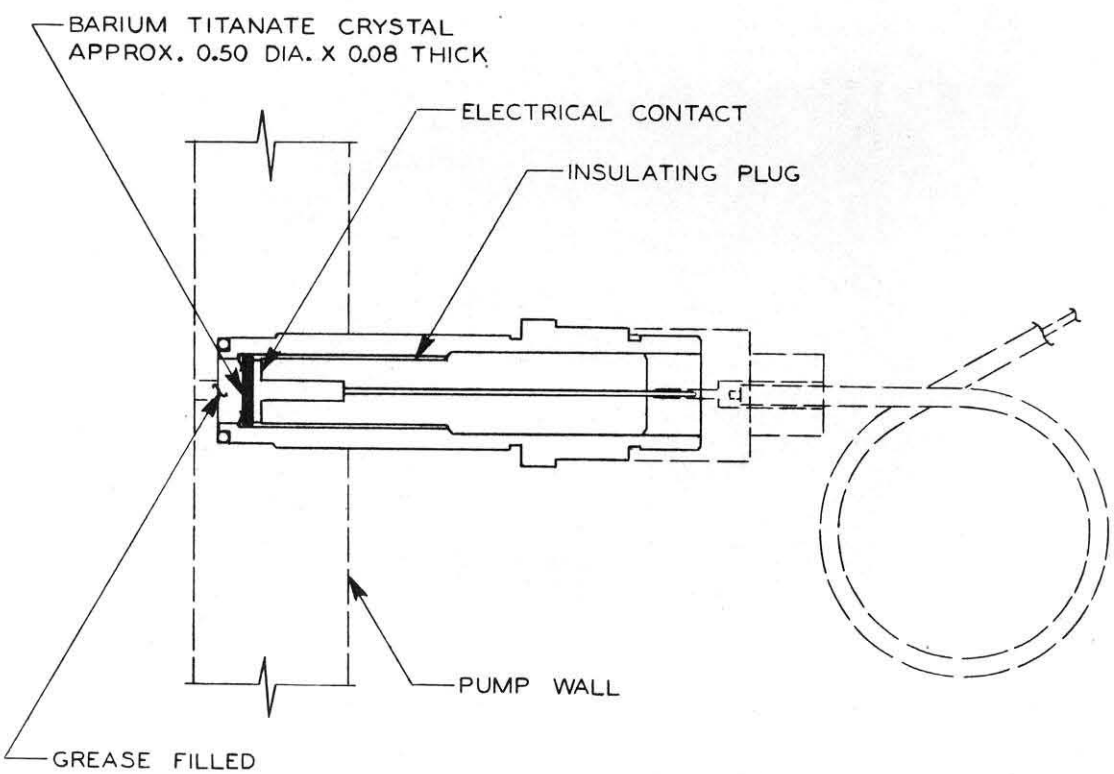

Fig. 13 Pressure Gage.

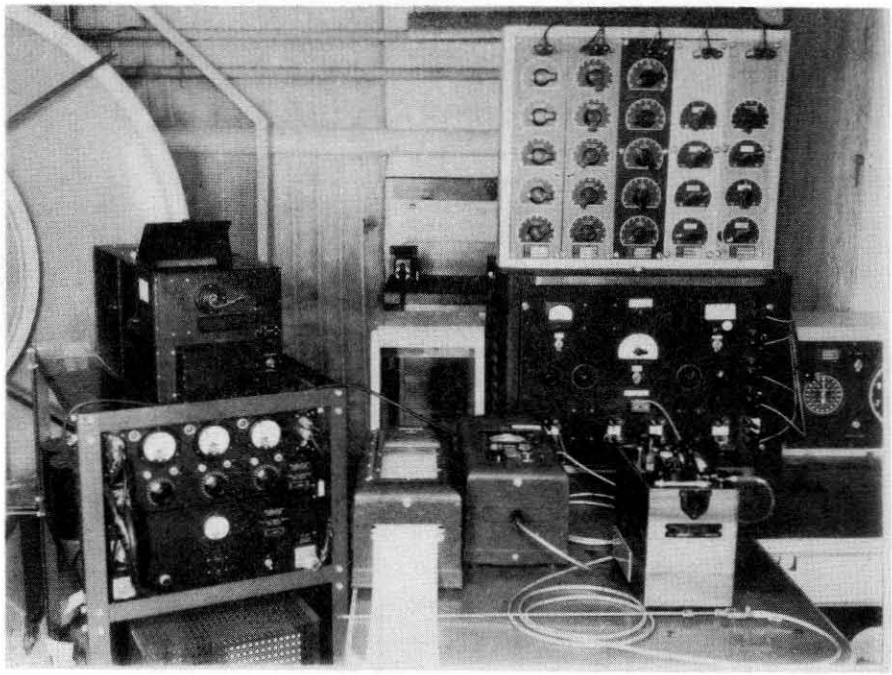

Fig. 14 Instrumentation:
Miller Amplifier and Oscillograph,
Brush Amplifier and Oscillograph,
Constant Current Hot-Wire Anemometer.

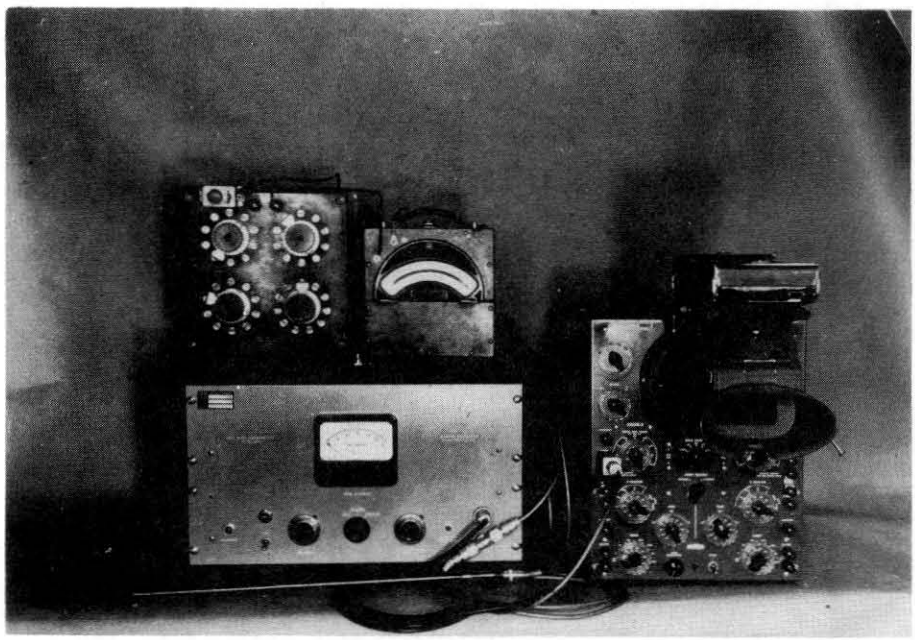

Fig. 15 Instrumentation:
Constant Temperature Hot-Wire Anemometer,
Precision Milliammeter,
Oscilloscope and Land Camera.

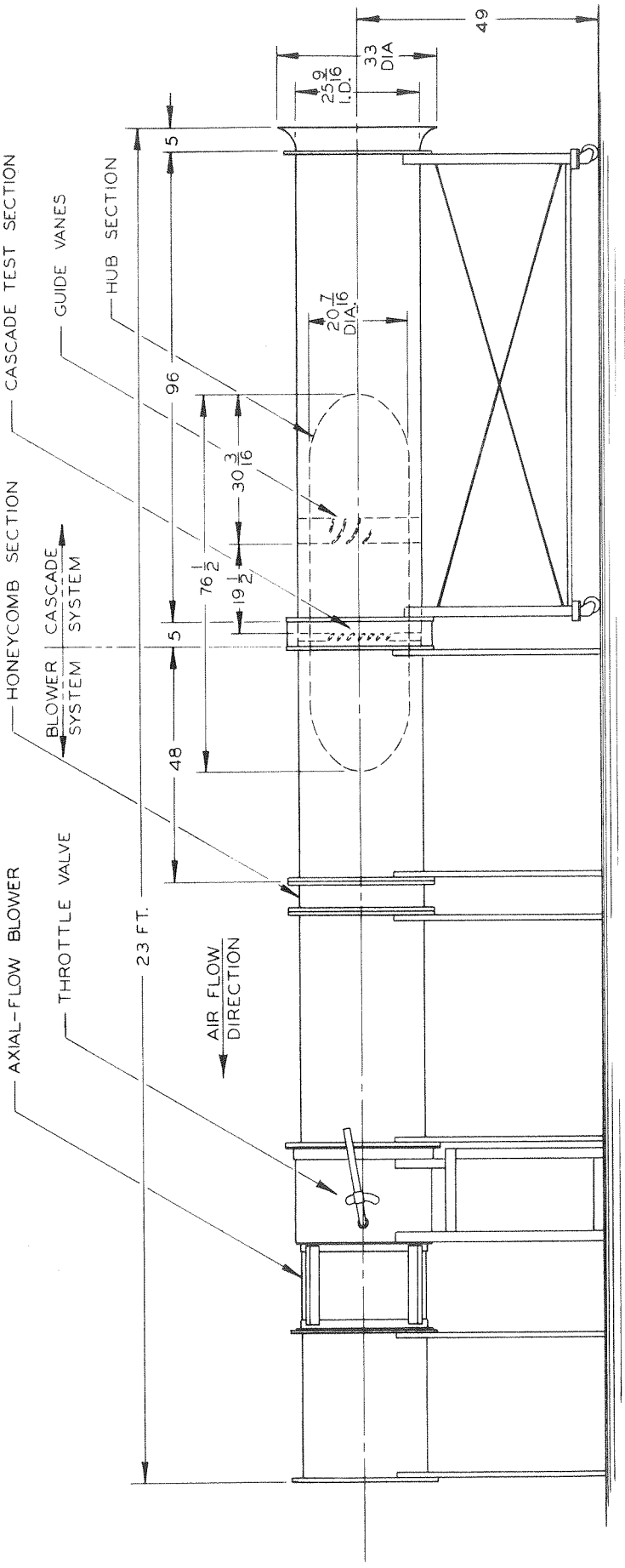

Fig. 16 Annular Cascade Tunnel

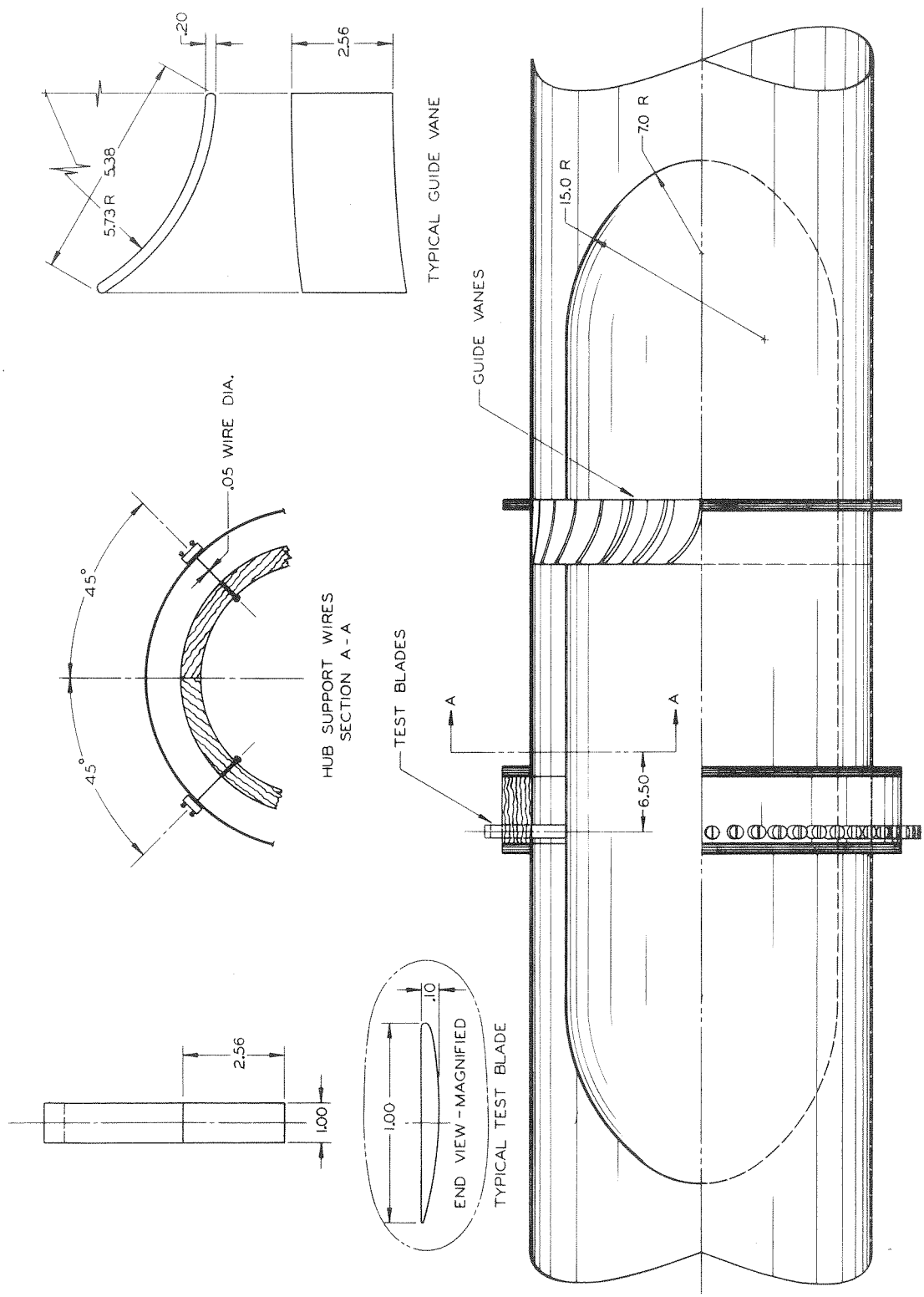

Fig. 17 Details, Annular Cascade

PRINCIPAL DIMENSIONS

NOMINAL TIP DIAMETER	36.000 INCHES
HUB DIAMETER	21.600 INCHES
HUB RATIO	.60
BLADE LENGTH	7.20 INCHES
BLADE CHORD	2.00 - 3.40 INCHES
NUMBER OF ROTOR BLADES	30 PER ROW
NUMBER OF STATOR BLADES	32 PER ROW
STAGES	1 TO 3
SPEED RANGE	0 TO 1800 R.P.M.
TIP SPEED RANGE	0 TO 283 FT./SEC.
AXIAL SPACING BETWEEN ROTOR & STATOR ℄	2.875 INCHES
AVERAGE AXIAL CLEARANCE BETWEEN ROTOR & STATOR	.80 INCHES

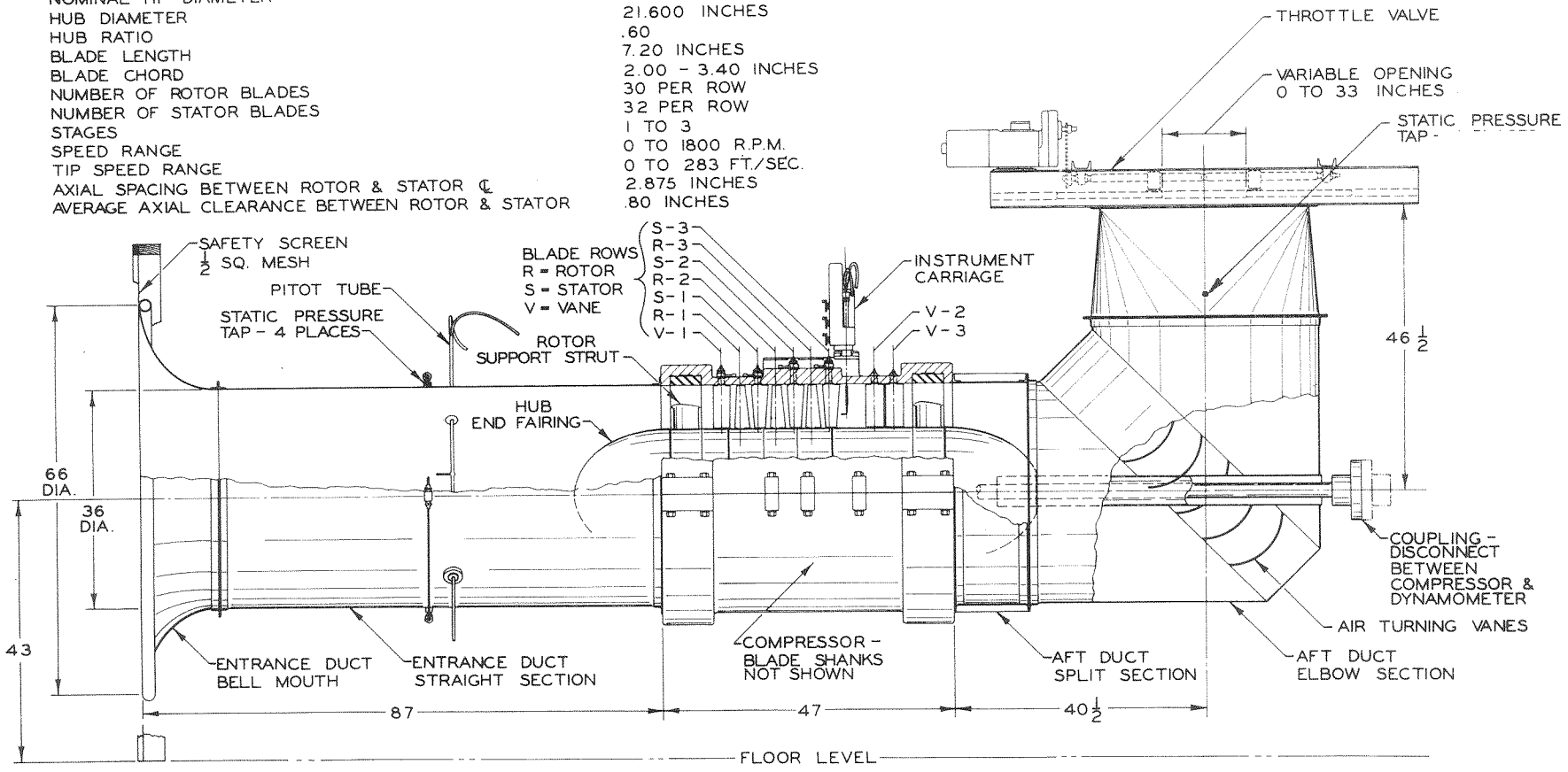

Fig. 18 Axial-Flow Compressor

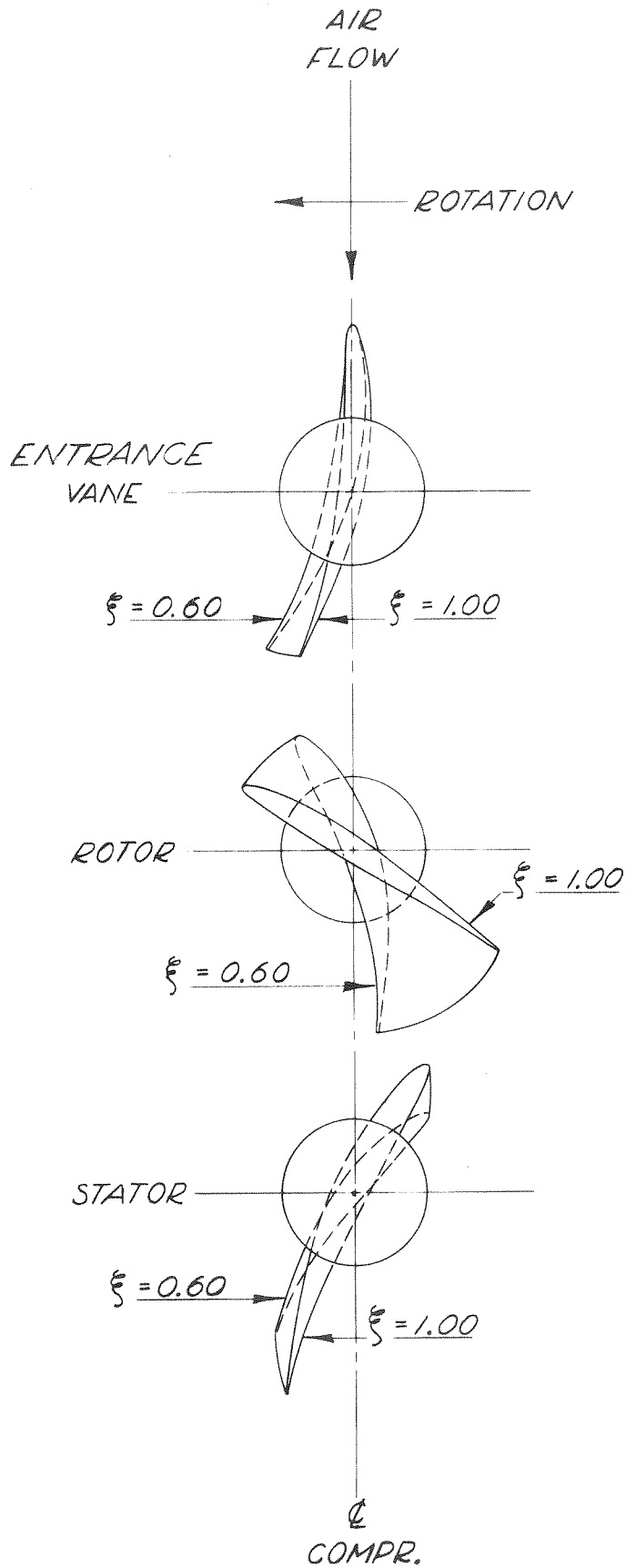

Fig. 19 Root and Tip Sections, Free-Vortex Blading for Axial-Flow Compressor

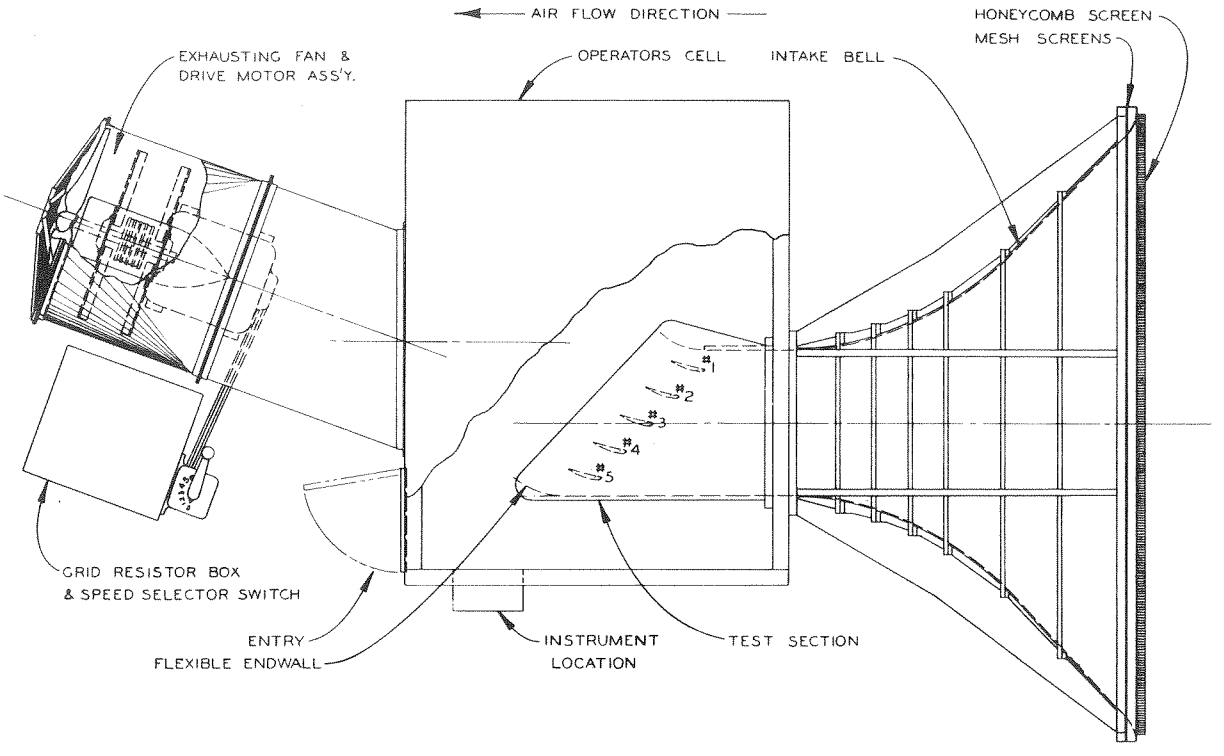

Fig. 20 Rectangular Cascade Tunnel

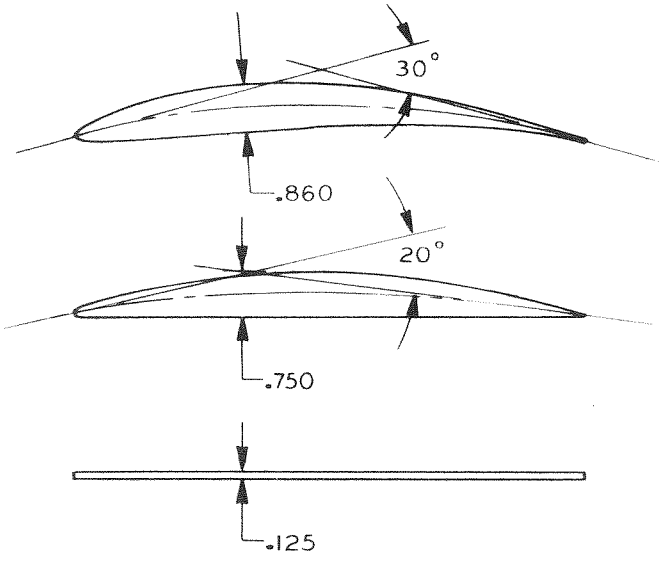

DESIGN BLADE PROFILE

INTERMEDIATE BLADE PROFILE

FLAT PLATE BLADE PROFILE

NOTE: FOR ALL BLADES
CHORD = 8.50 IN.
SPAN = 24.0 IN.

Fig. 21 Test Blade Profiles

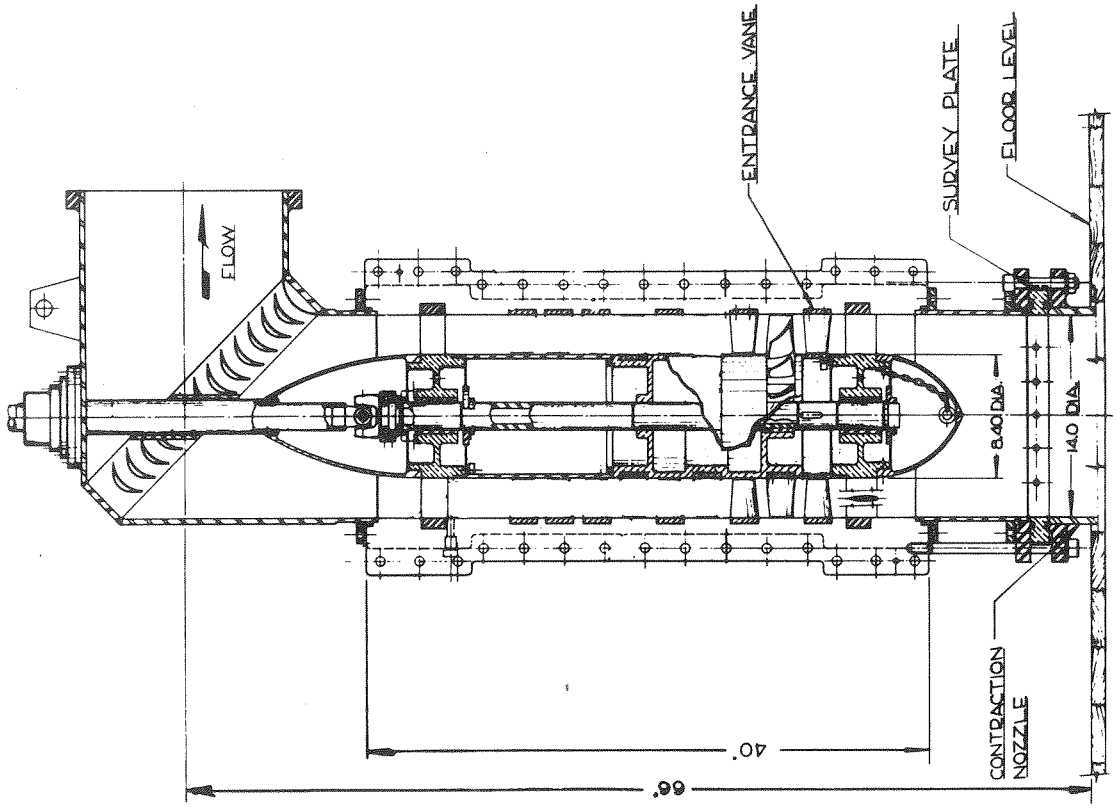

Fig. 23 Details, Axial-Flow Pump

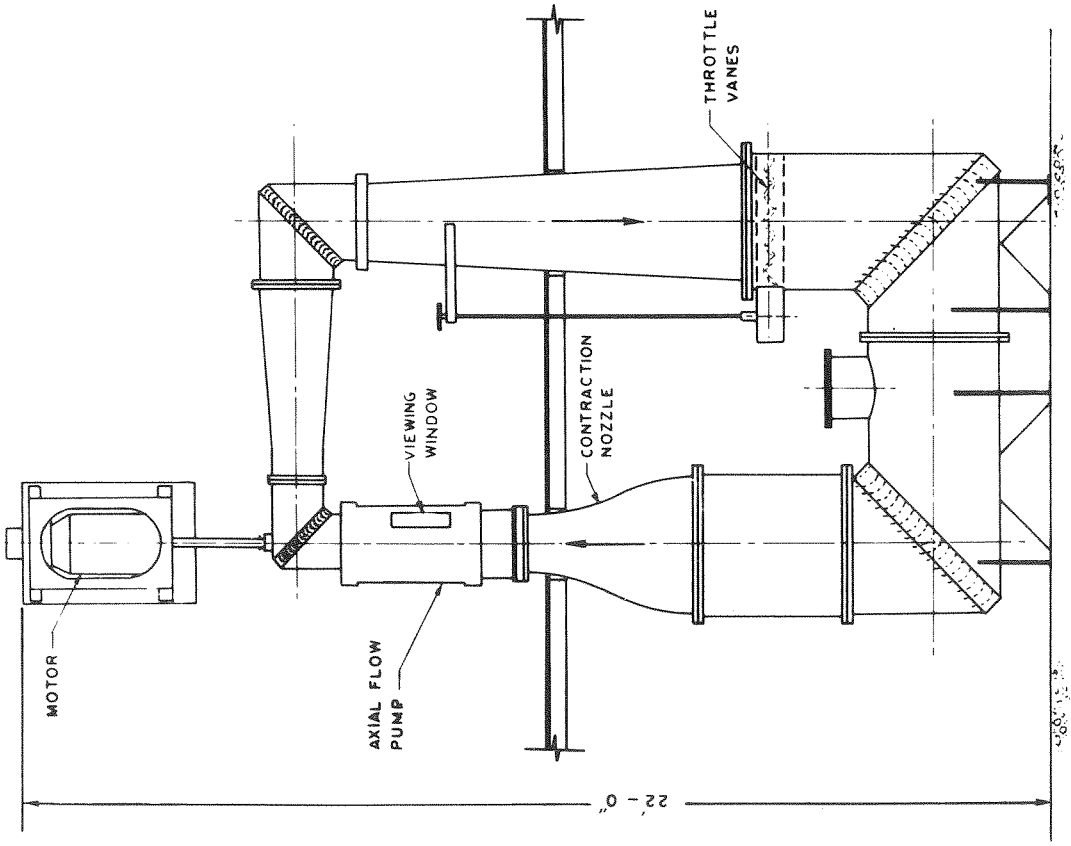

Fig. 22 Axial-Flow Pump

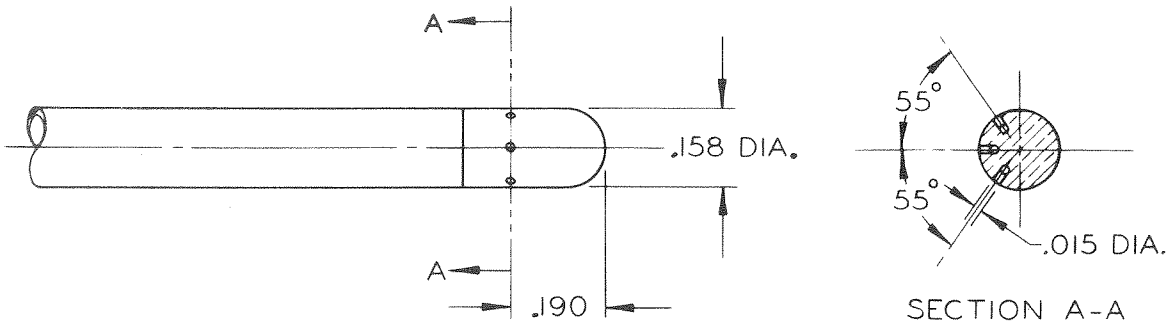

(A) 3 HOLE CYLINDRICAL YAW PROBE

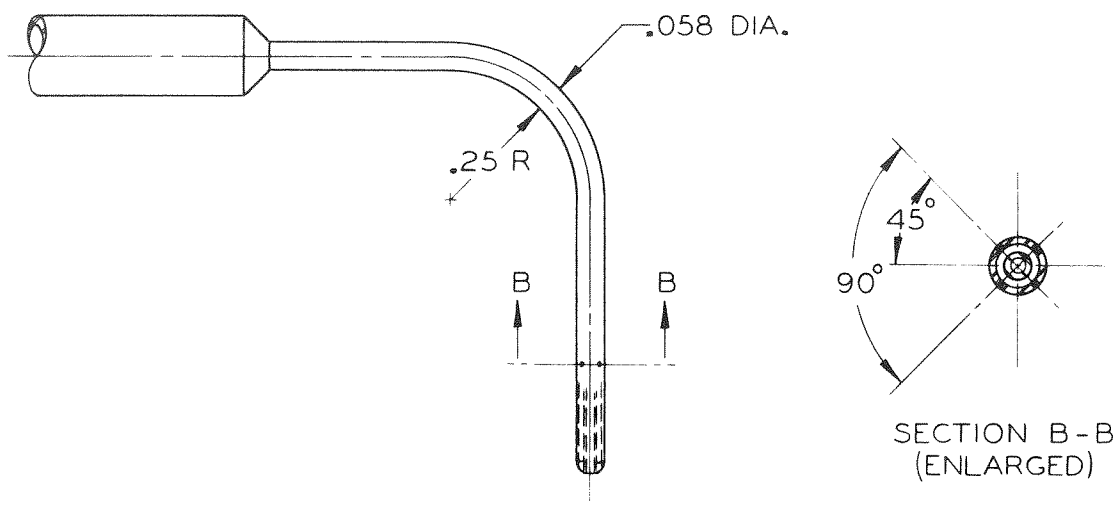

(B) PITOT STATIC PROBE

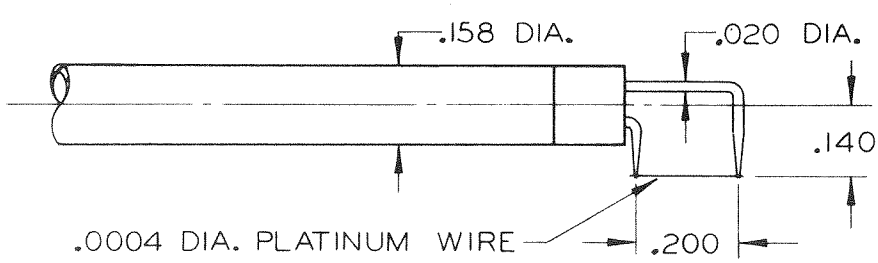

(C) HOT-WIRE PROBE

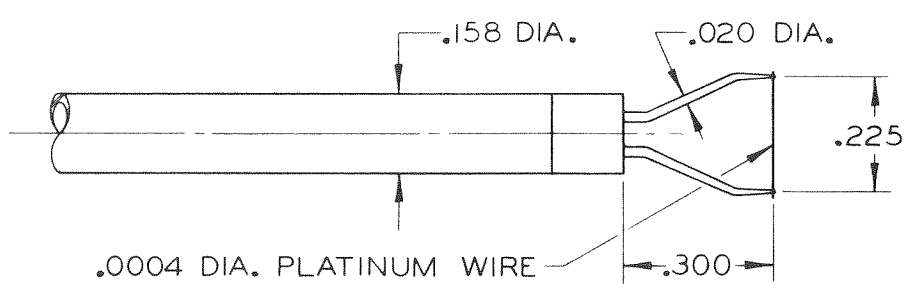

(D) HOT-WIRE PROBE

Fig. 24 Survey Probes

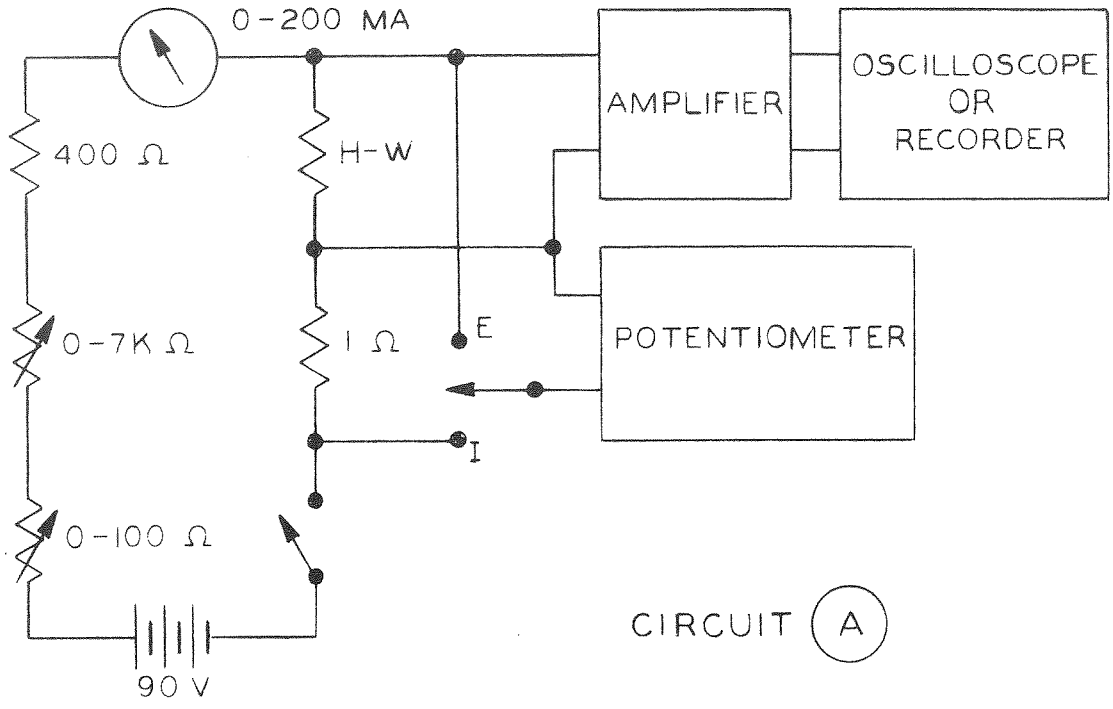

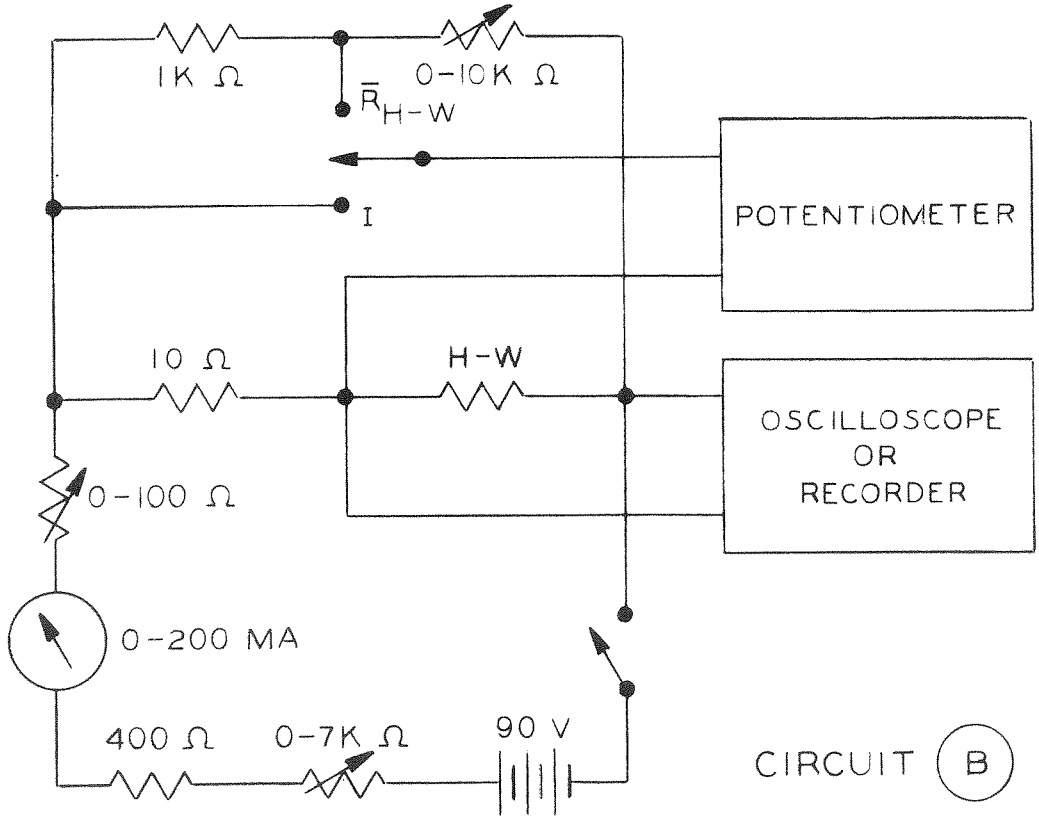

Fig. 25 Constant Current Hot-Wire Anemometer Circuits

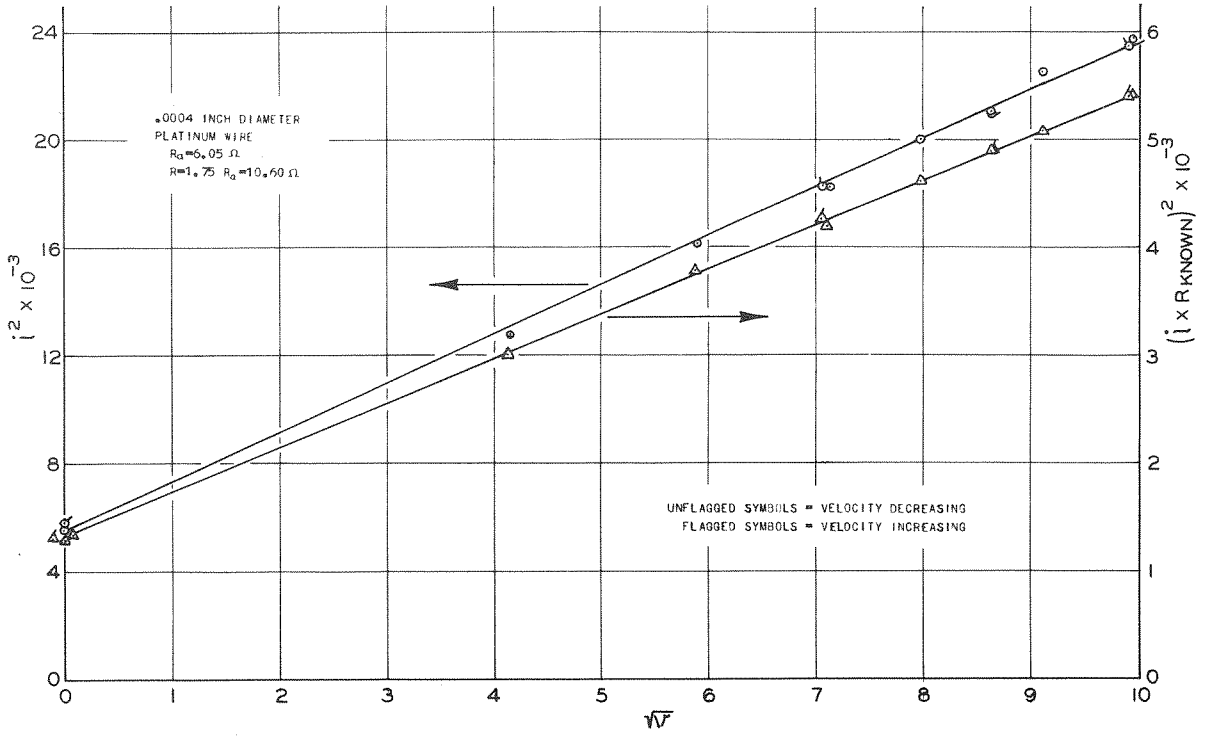

(a)

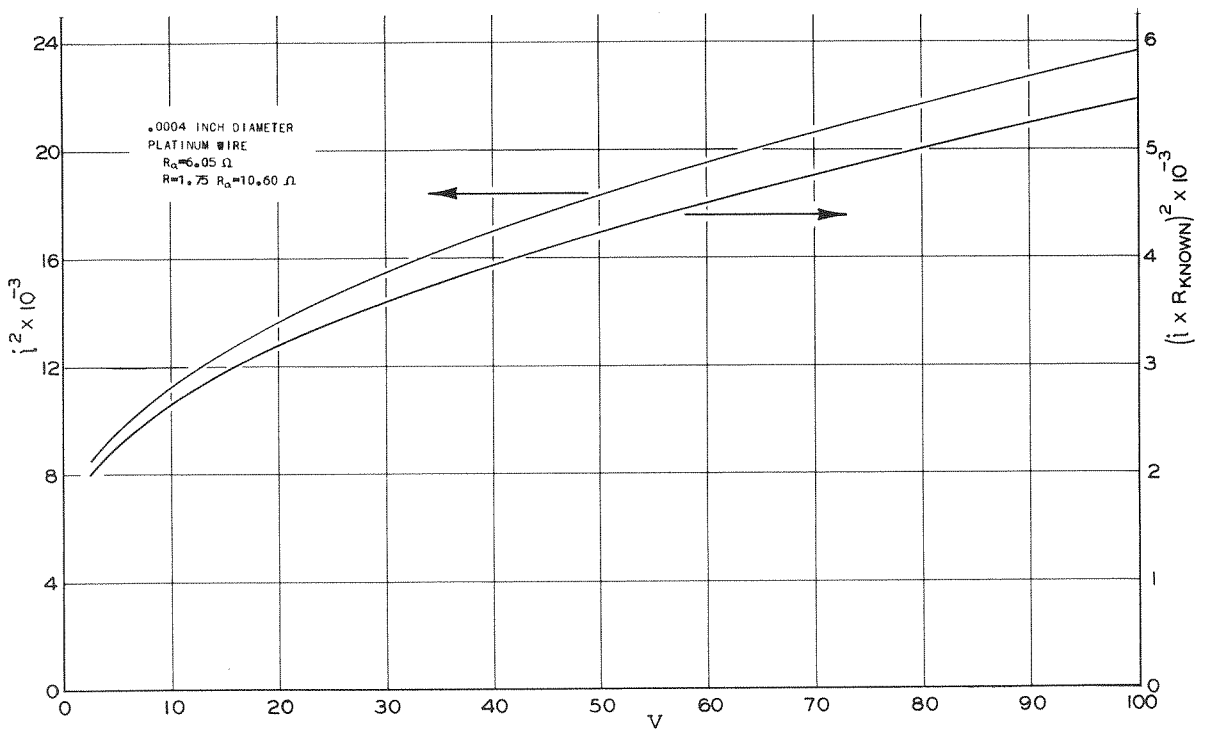

(b)

Fig. 26 Hot-Wire Calibration
Constant Temperature Operation

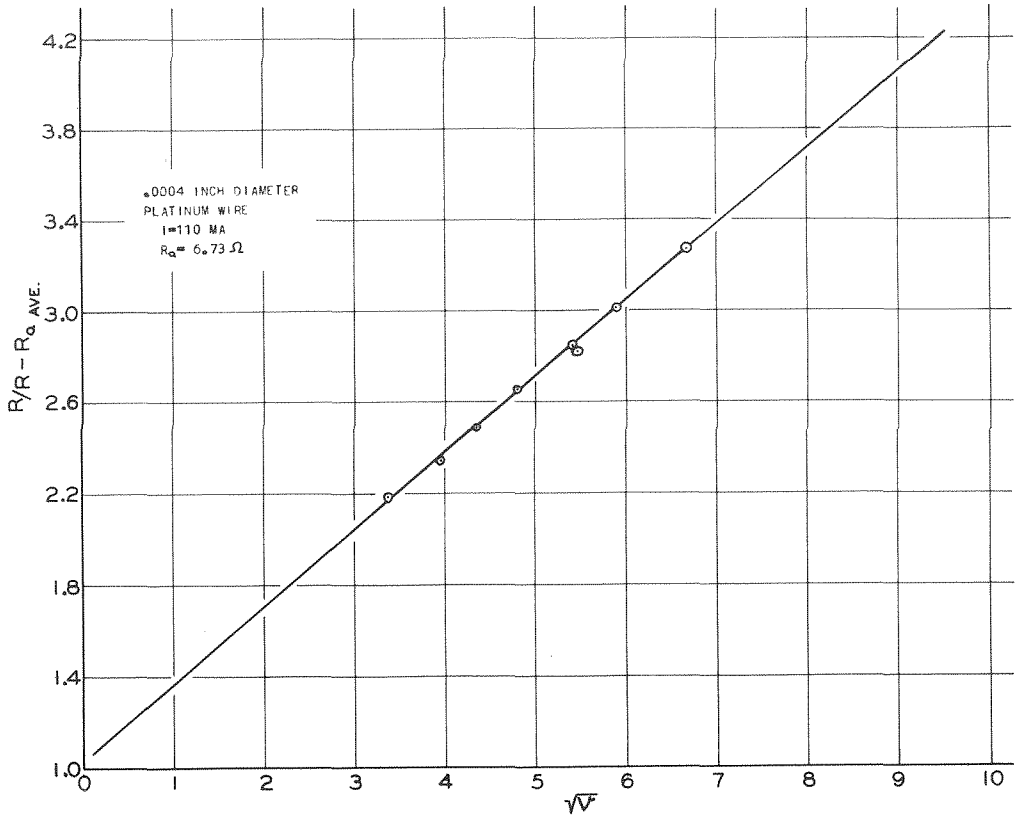

(a)

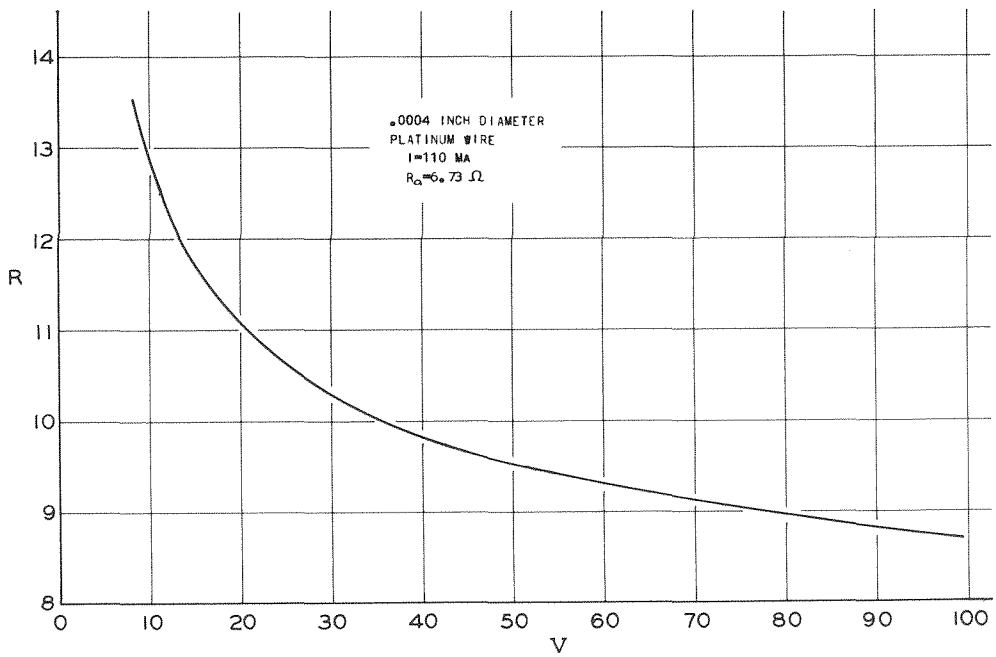

(b)

Fig. 27 Hot-Wire Calibration
Constant Current Operation

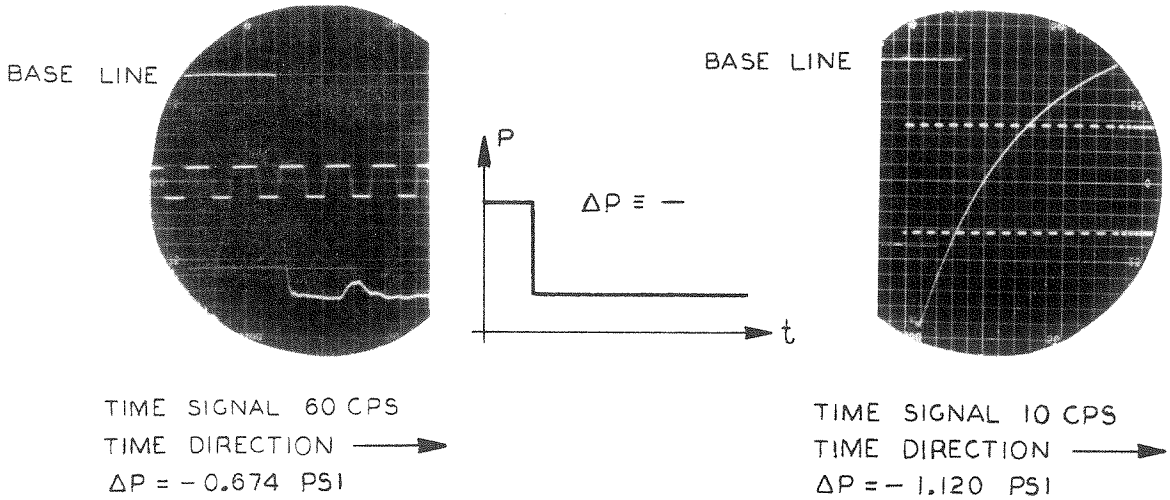

(a) Pressure Pick-Up Calibration Run

(b) Decay of Pressure Pick-Up Signal

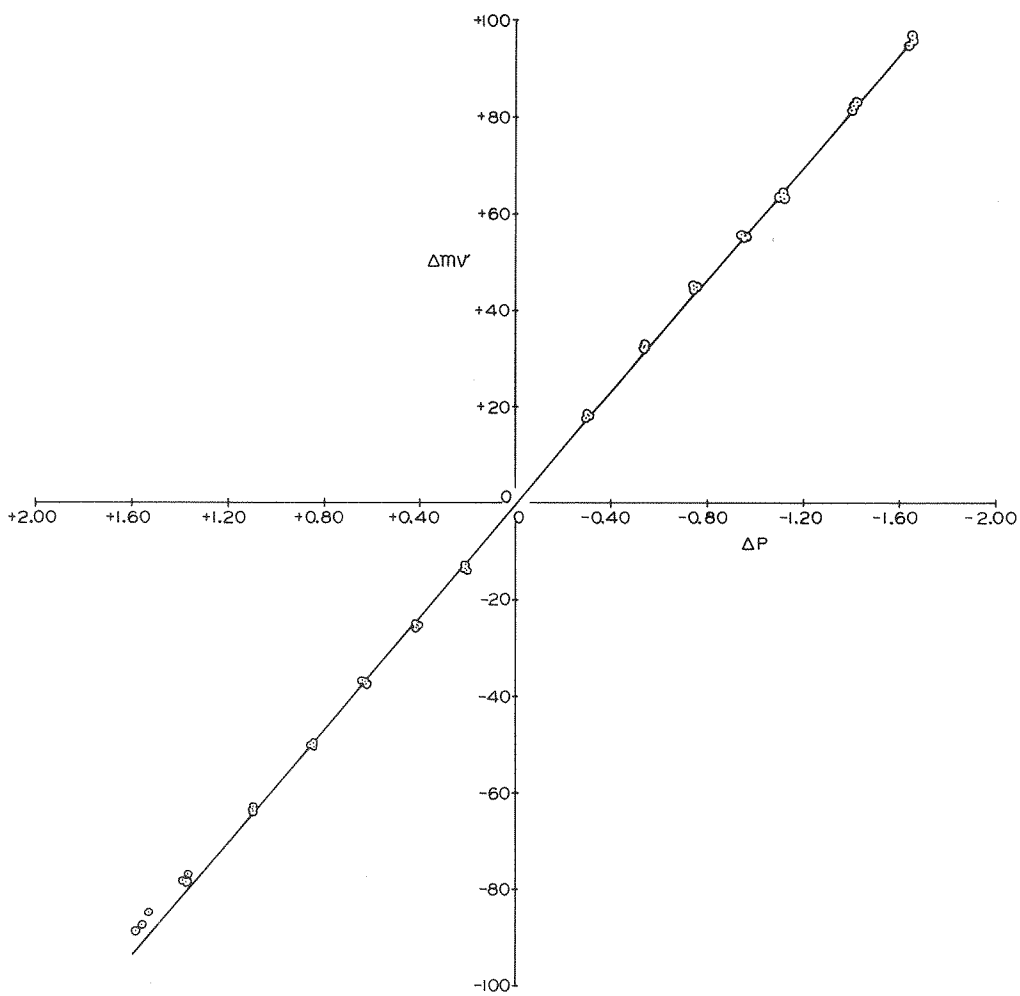

Fig. 28c Pressure Pick-Up System Calibration
(Barium Titanate Crystal Plus Cathode Follower)

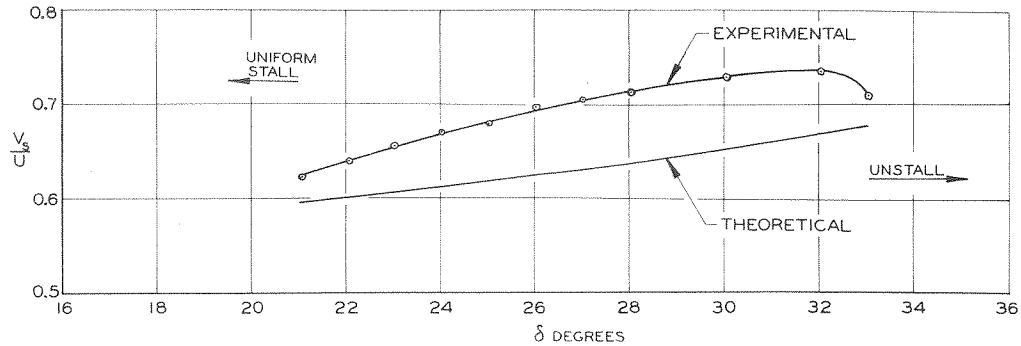

(a) $\sigma/\sigma_0 = 1,\ \xi = 0.896,\ \beta_1 \approx 47.5°$

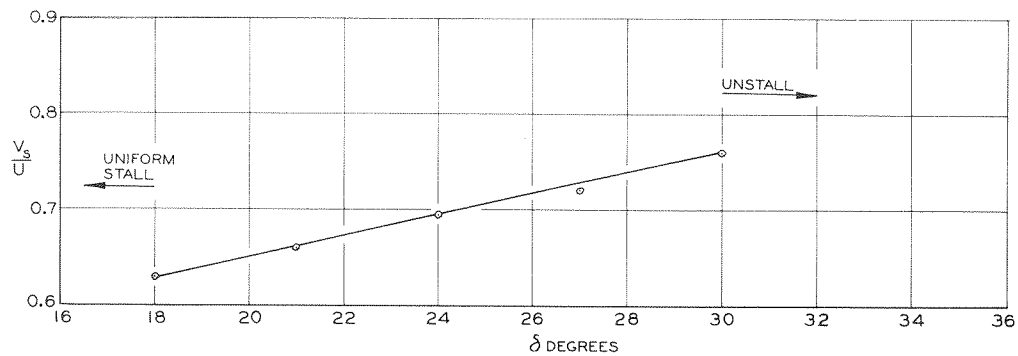

(b) $\sigma/\sigma_0 = 5/6,\ \xi = 0.896,\ \beta_1 \approx 47.5°$

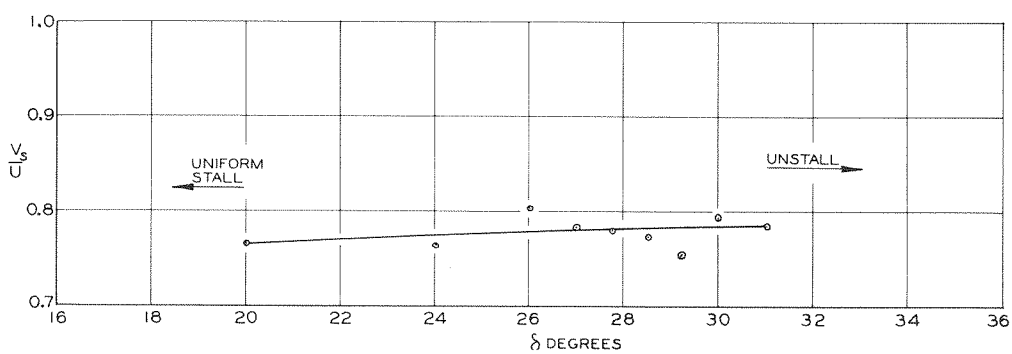

(c) $\sigma/\sigma_0 = 2/3,\ \xi = 0.896,\ \beta_1 \approx 47.5°$

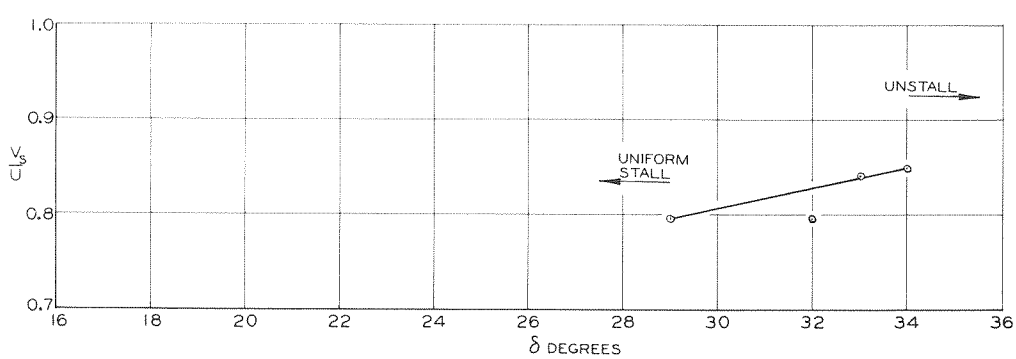

(d) $\sigma/\sigma_0 = 1/2,\ \xi = 0.896,\ \beta_1 \approx 47.5°$

Fig. 29 Variation of propagating stall speed ratio with stagger angle. Annular cascade.

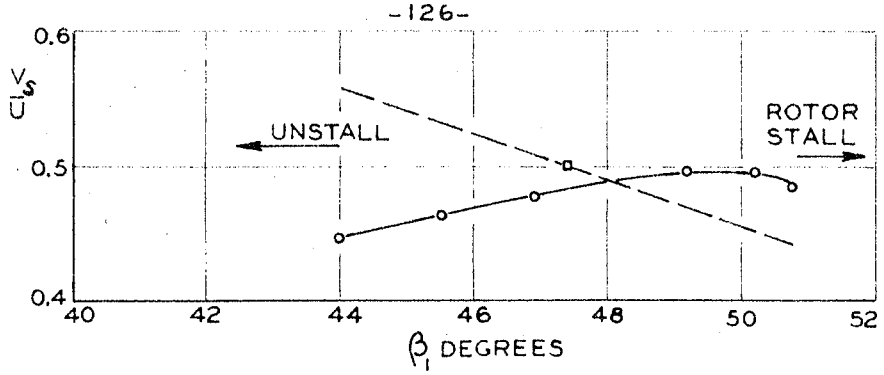

(a) $\sigma/\sigma_0 = 1$, $\Delta\delta = -10^\circ$, $\xi = 0.80$

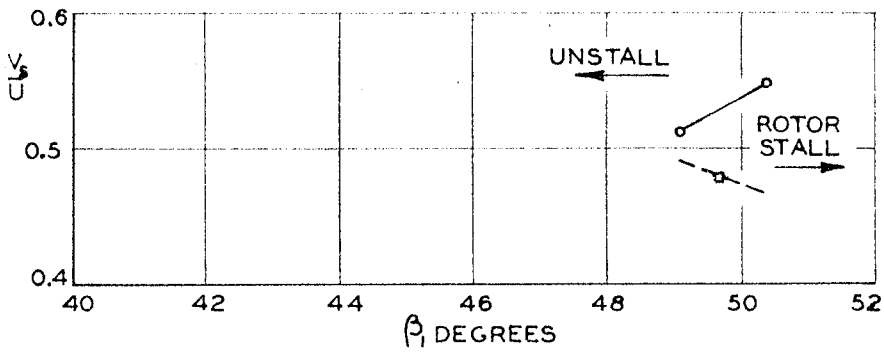

(b) $\sigma/\sigma_0 = 1$, $\Delta\delta = -5^\circ$, $\xi = 0.80$

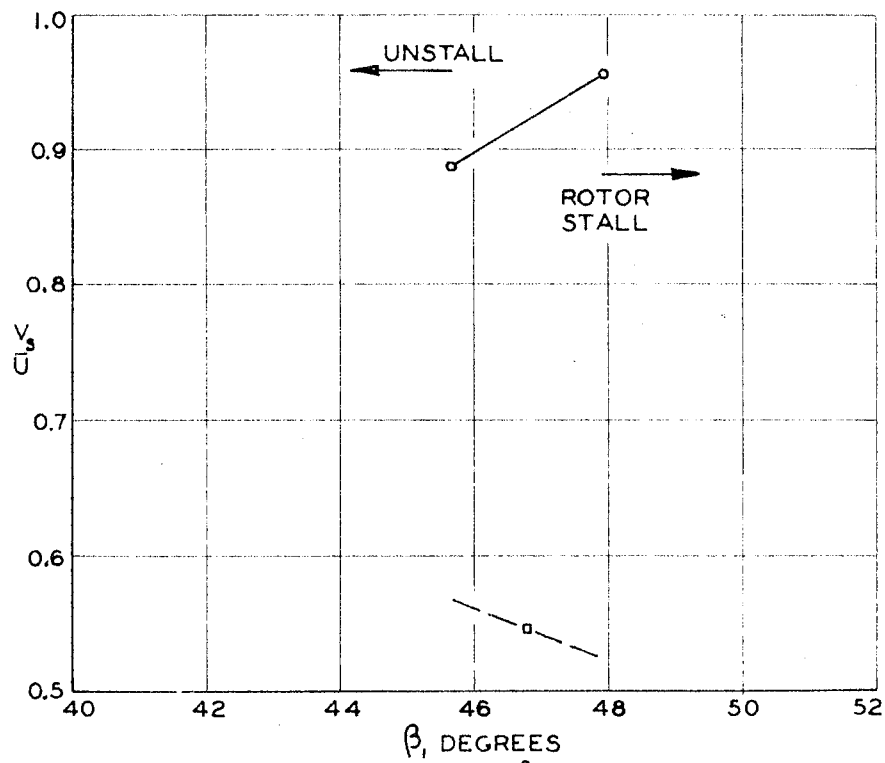

(c) $\sigma/\sigma_0 = 1/2$, $\Delta\delta = -10^\circ$, $\xi = 0.80$

Fig. 30 Comparison of theoretical and experimental propagating stall speed ratio variation with inlet angle. Axial-flow compressor cascade, stator row. —o— Theory —o— Experiment

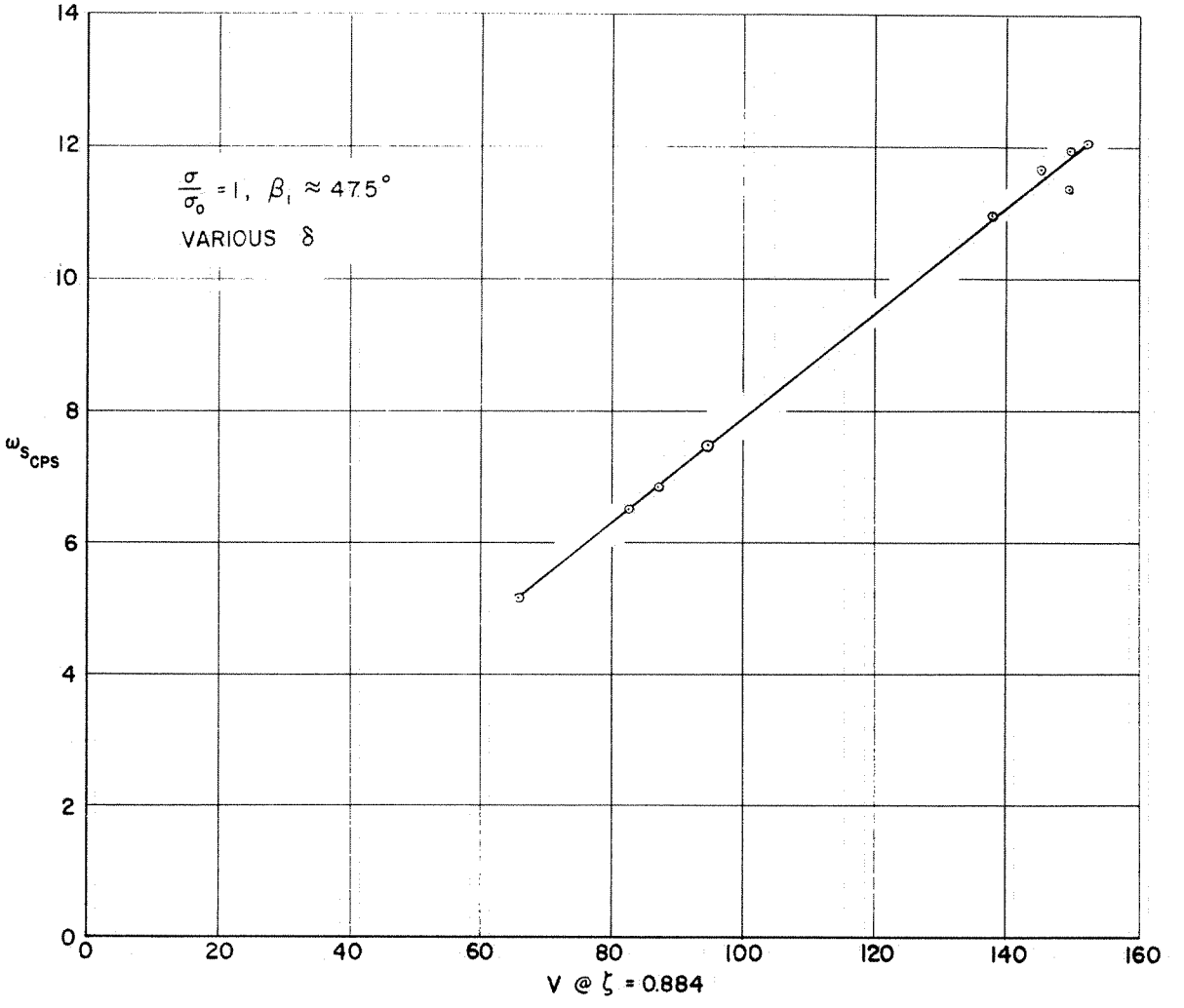

Fig. 31 Variation of absolute propagating stall frequency with velocity. Annular cascade. Data ~ 1 in. before cascade.

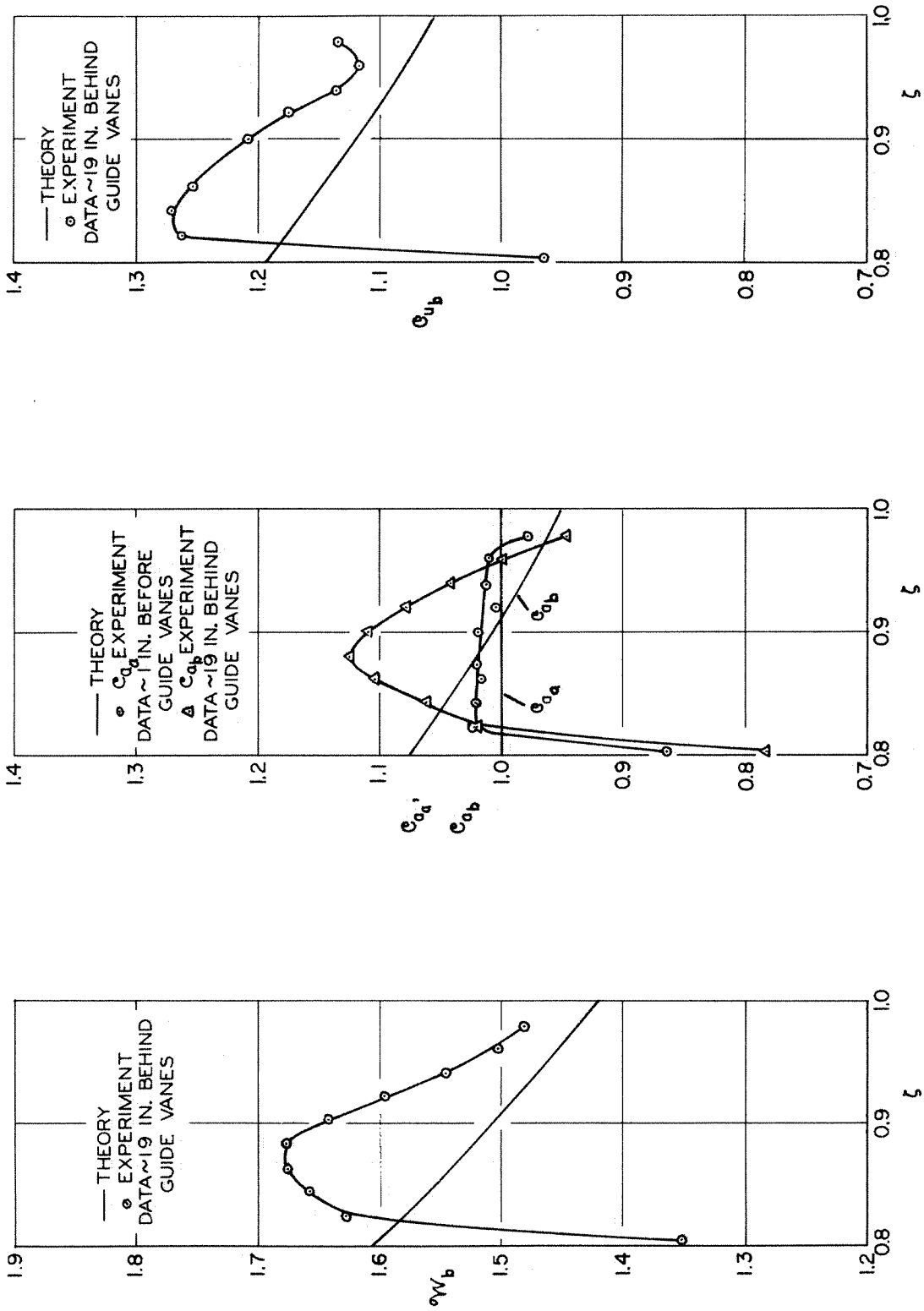

Fig. 32 Comparison of theoretical and experimental velocities. Annular cascade.

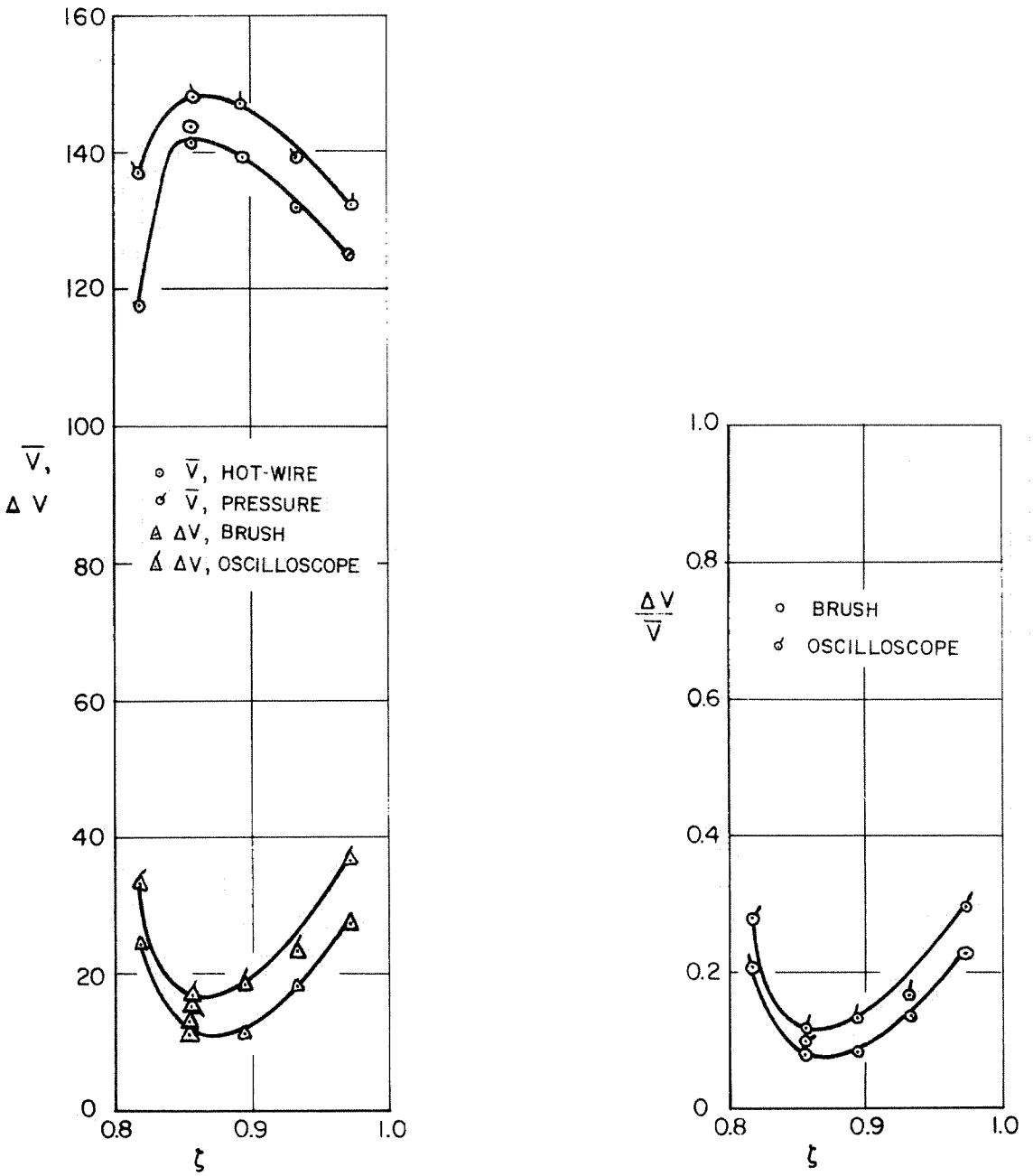

Fig. 33 Variation of velocity, velocity fluctuation and velocity fluctuation ratio with radius ratio.
Annular cascade.
Propagating stall.
Data ~ 1 in. before cascade.
$\frac{\sigma}{\sigma_0} = 1$, $\delta = 29°$, $\beta_1 \sim 47.5°$

$\frac{\sigma}{\sigma_0} = 1$, $\delta = 29°$, $\beta_1 \approx 47.5°$

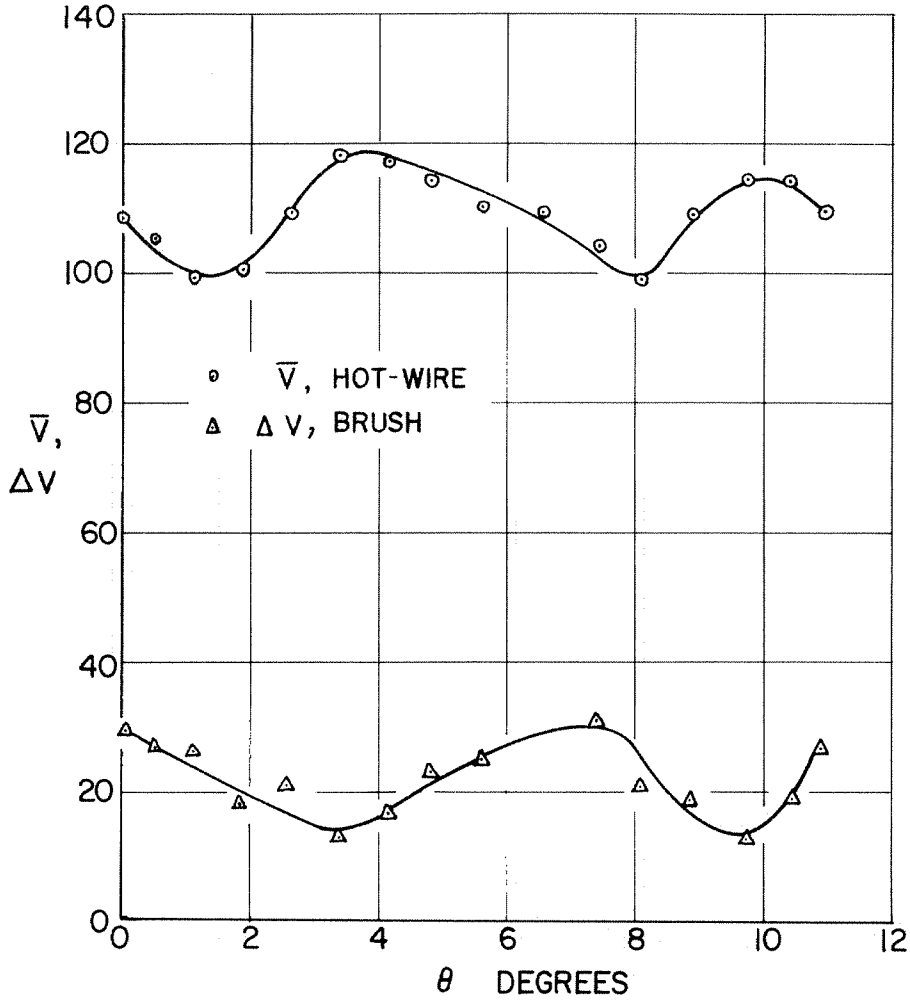

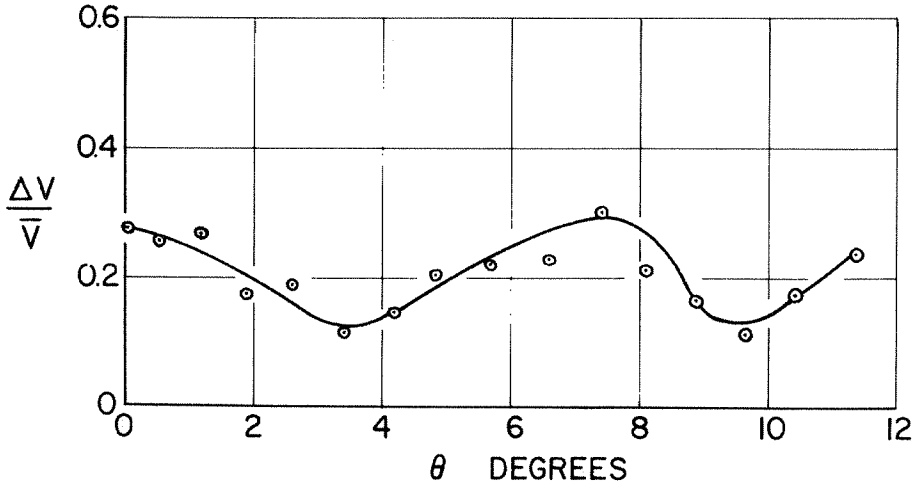

Fig. 34 Variation of velocity, velocity fluctuation and velocity fluctuation ratio with circumferential angle. Annular cascade. Propagating stall.
Data ~ 1 in. behind cascade.

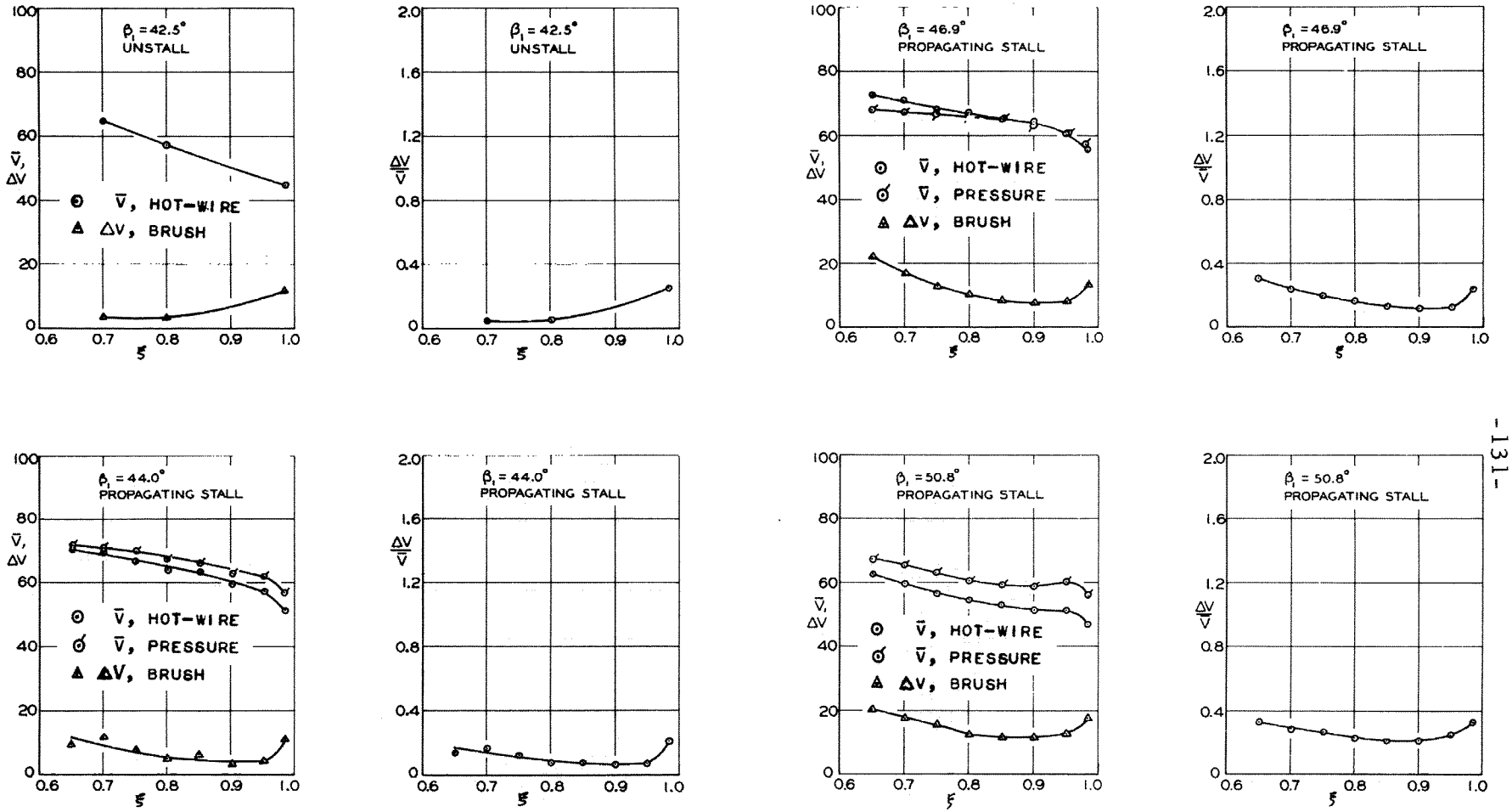

Fig. 35 Variation of velocity, velocity fluctuation and velocity fluctuation ratio with radius ratio. Axial-flow compressor cascade, stator row.

Data ~ 1/4 in. before stator row. $\sigma/\sigma_0 = 1$, $\Delta\delta = -10°$, β_1 = NOTED

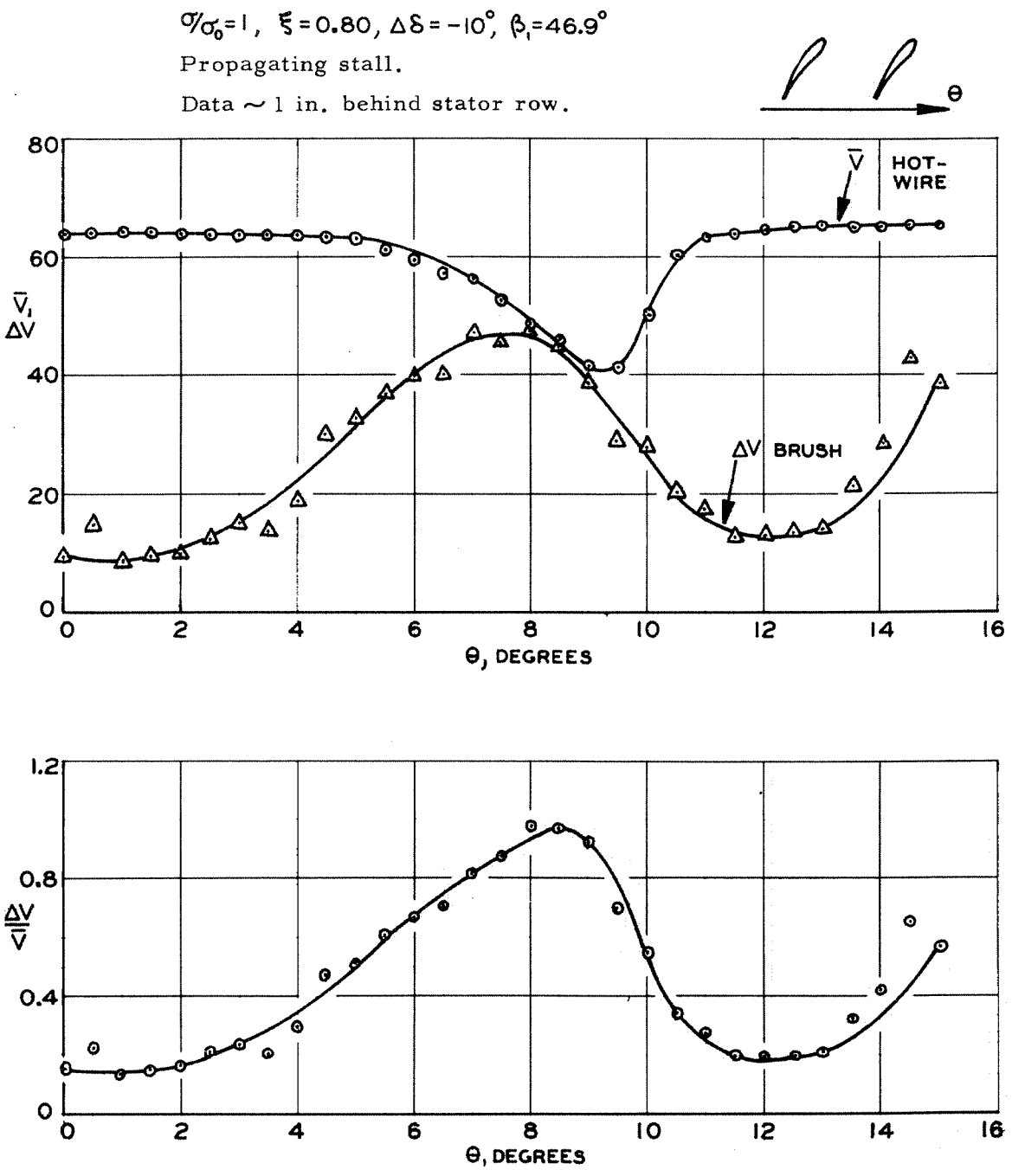

Fig. 36 Variation of velocity, velocity fluctuation and velocity fluctuation ratio with circumferential angle. Axial-flow compressor cascade, stator row.

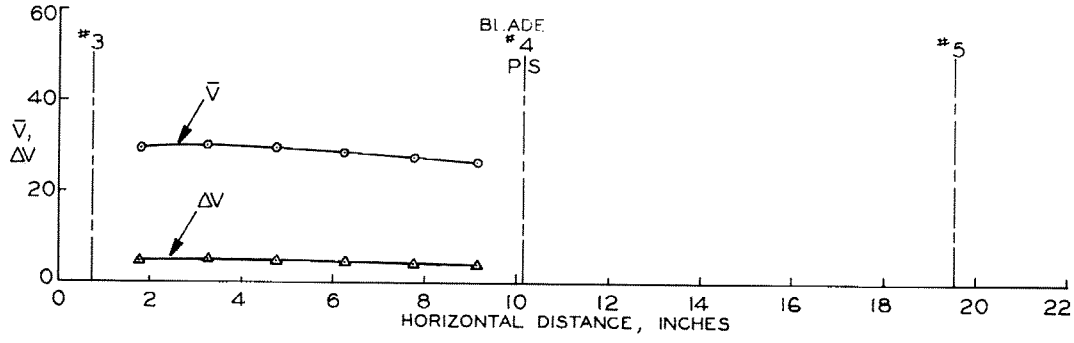

(a) Data ~ 2 in. before cascade.

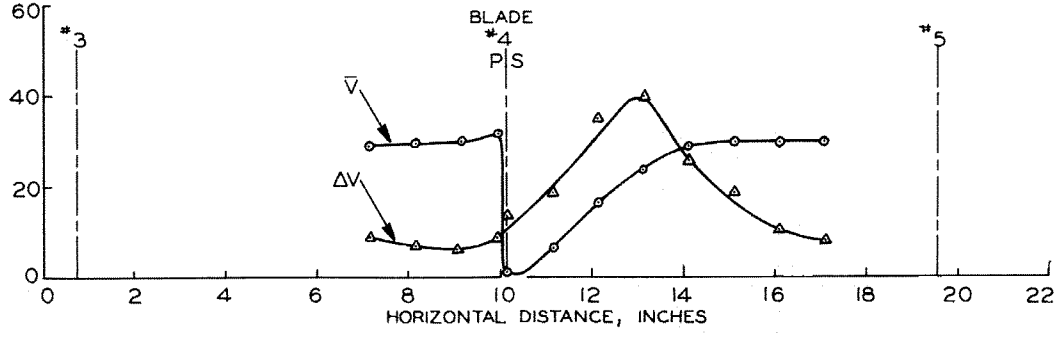

(b) Data ~ 1/8 in. behind cascade.

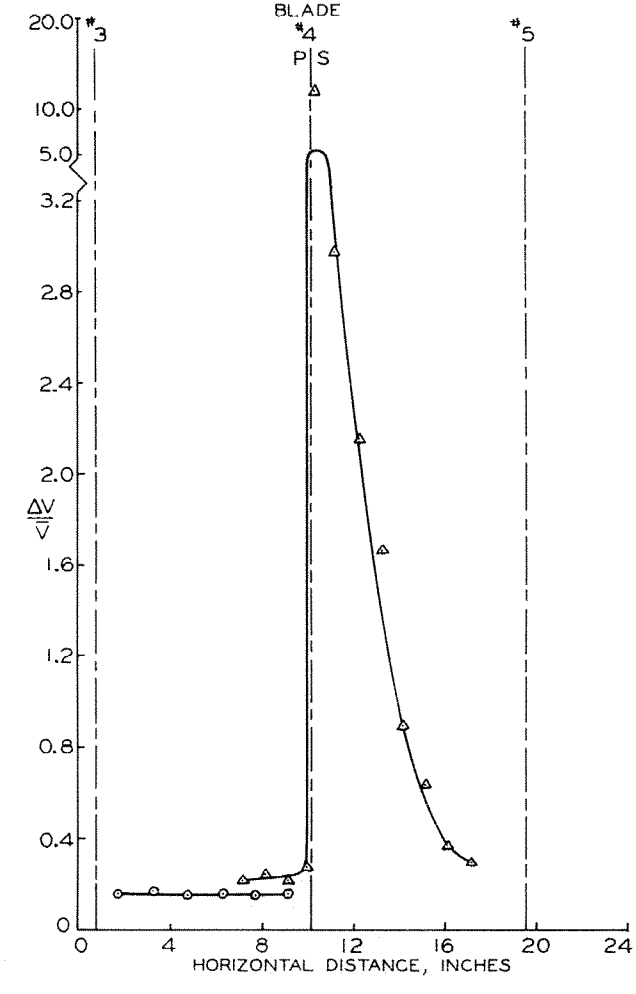

(c) ⊙ Data ~ 2 in. before cascade.
▲ Data ~ 1/8 in. behind cascade.

Fig. 37 Variation of velocity, velocity fluctuation and velocity fluctuation ratio with horizontal distance. Rectangular cascade.

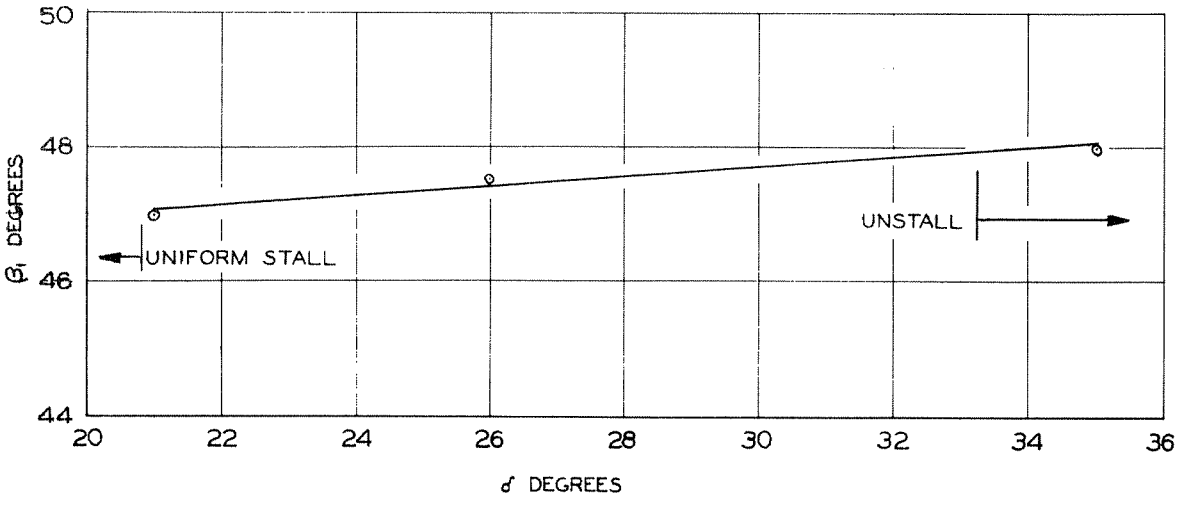

(a) Data ~ 1 in. before cascade. $\sigma/\sigma_0 = 1$, $\xi = 0.896$.

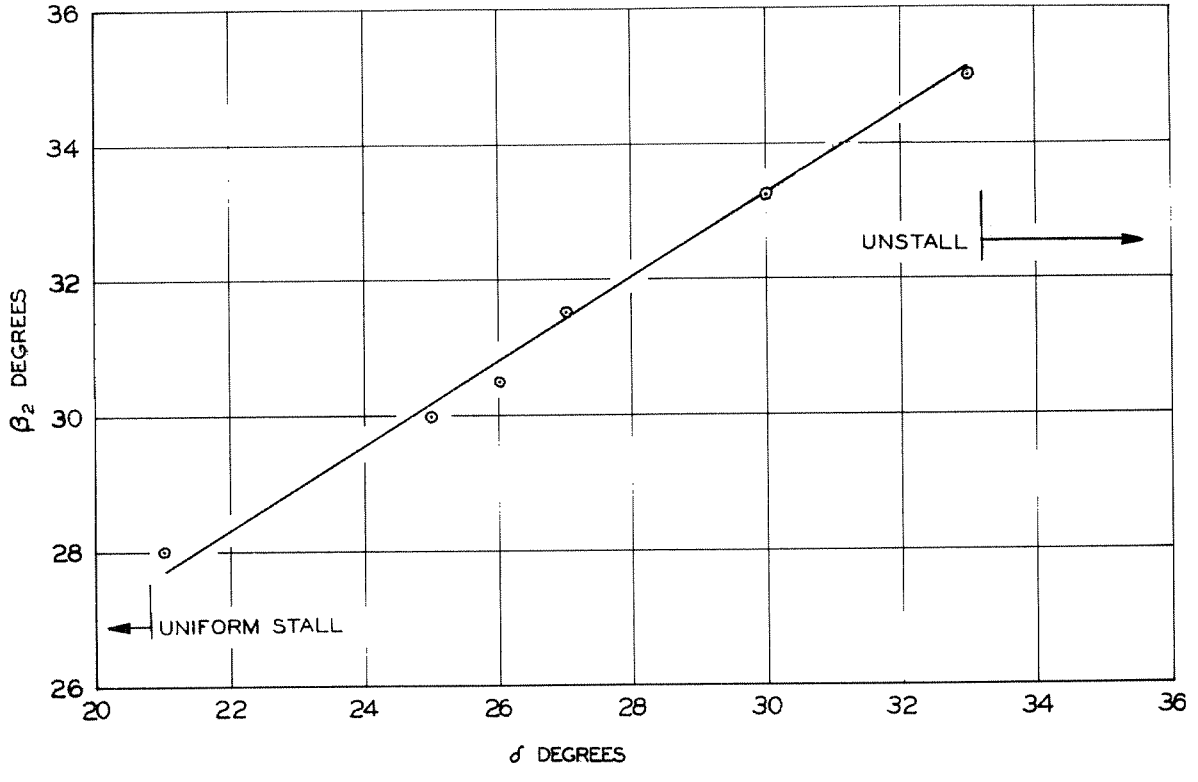

(b) Data ~ 1 in. behind cascade $\sigma/\sigma_0 = 1$, $\xi = 0.896$.

Fig. 38 Variation of inlet angle and exit angle with stagger angle. Annular cascade.

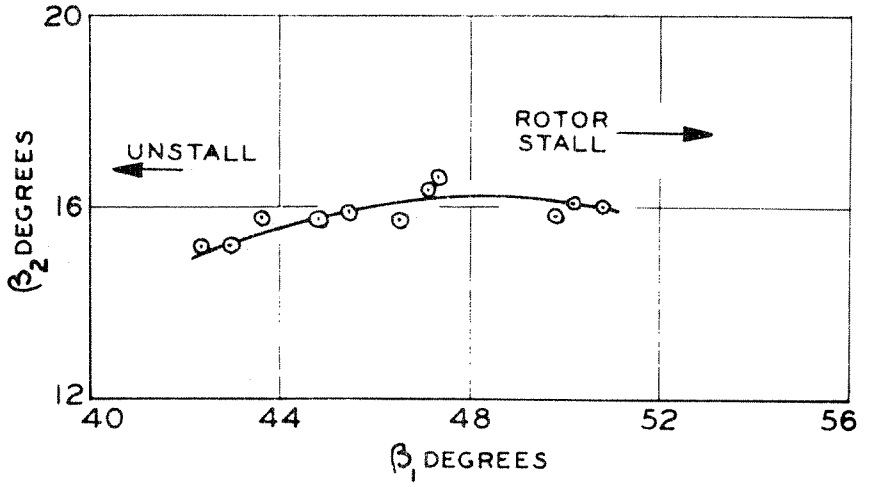

(a) $\sigma/\sigma_0 = 1$, $\Delta\delta = -10°$, $\xi = 0.80$

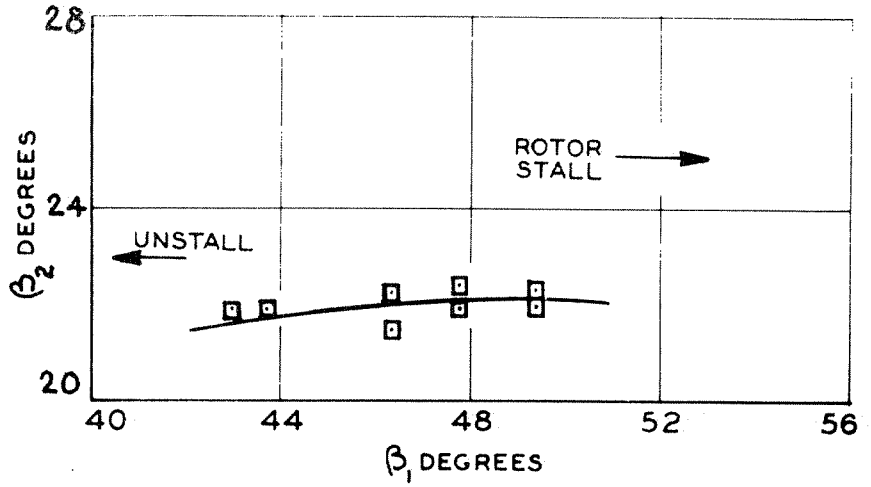

(b) $\sigma/\sigma_0 = 1$, $\Delta\delta = -5°$, $\xi = 0.80$

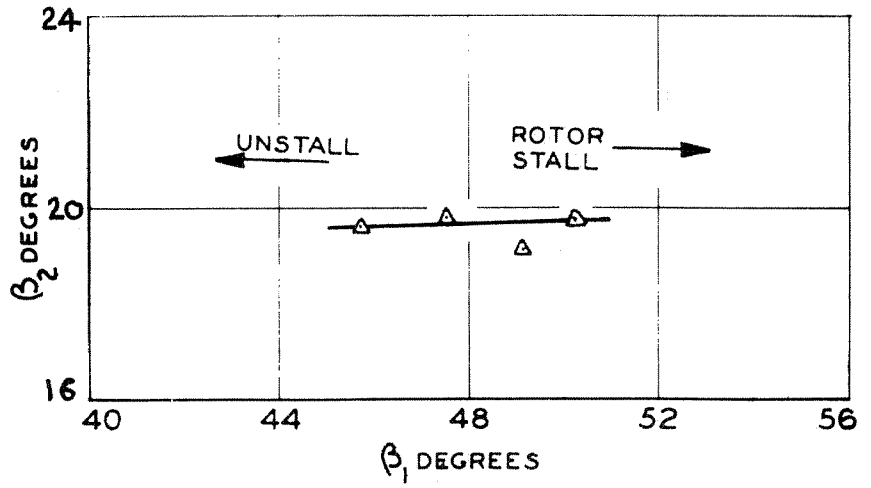

(c) $\sigma/\sigma_0 = 1/2$, $\Delta\delta = -10°$, $\xi = 0.80$

Fig. 39 Variation of exit angle with inlet angle. Axial-flow compressor cascade, stator row.

β_1 measured ~ 1/4 in. before stator row.
β_2 measured ~ 1/4 in. behind stator row.

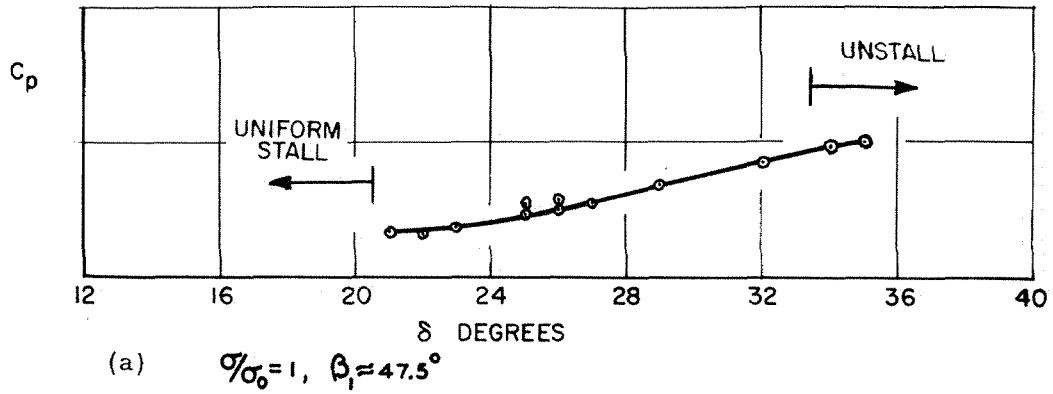

(a) $\sigma/\sigma_0 = 1$, $\beta_1 \approx 47.5°$

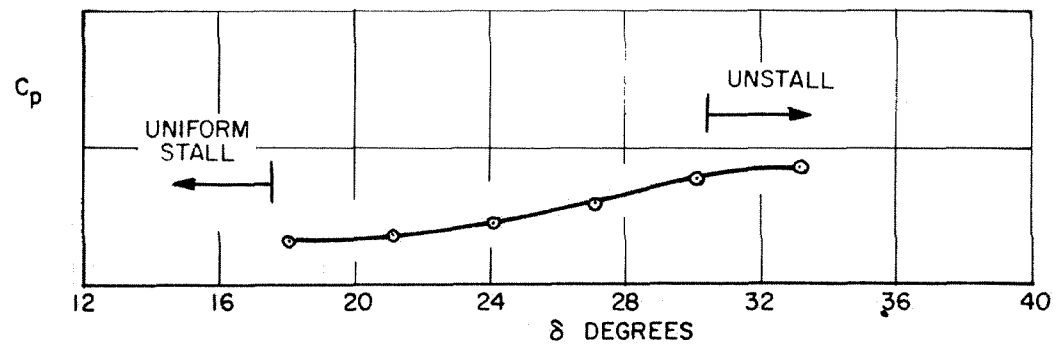

(b) $\sigma/\sigma_0 = 5/6$, $\beta_1 \approx 47.5°$

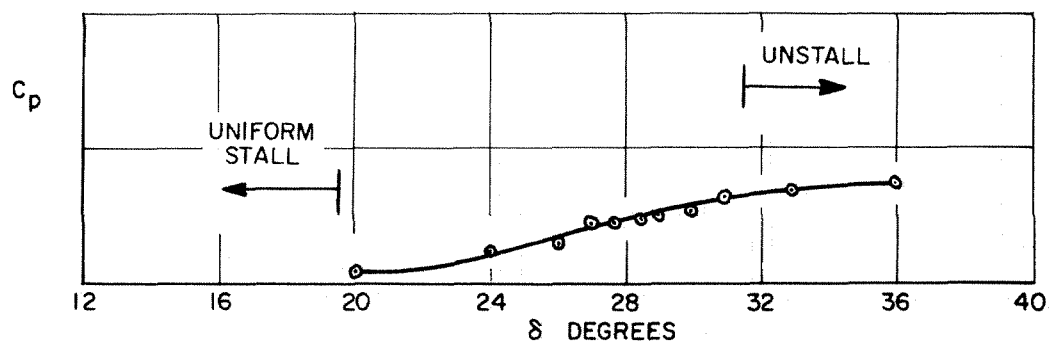

(c) $\sigma/\sigma_0 = 2/3$, $\beta_1 \approx 47.5°$

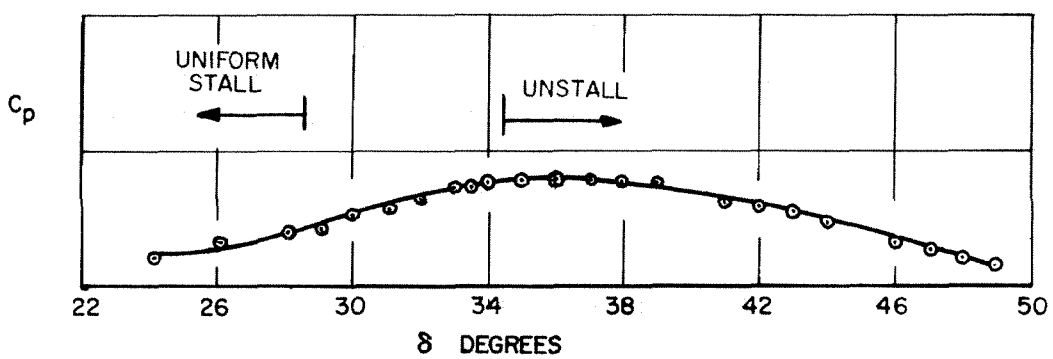

(d) $\sigma/\sigma_0 = 1/2$, $\beta_1 \approx 47.5°$

Fig. 40 Variation of static pressure rise coefficient with stagger angle. Annular cascade.

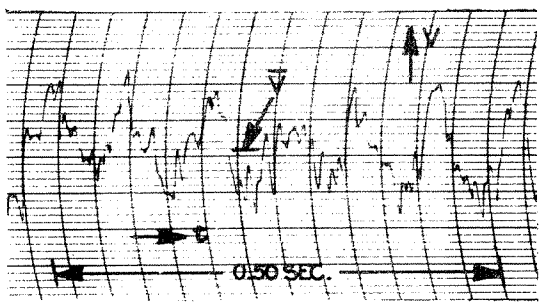

$\xi = 0.818, \frac{\Delta V}{\bar{V}} = 0.21$

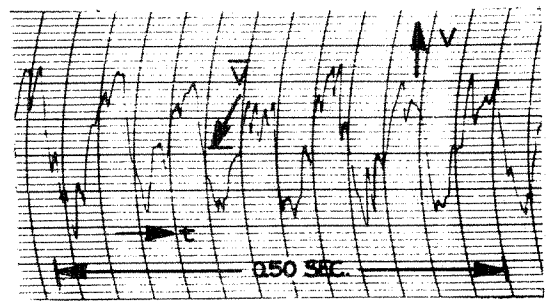

$\xi = 0.855, \frac{\Delta V}{\bar{V}} = 0.08$

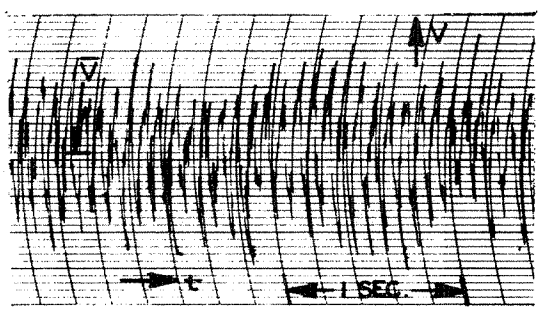

$\xi = 0.894, \frac{\Delta V}{\bar{V}} = 0.09$

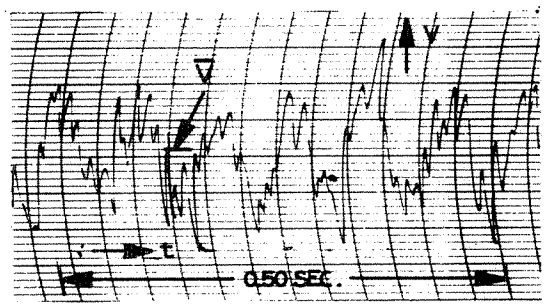

$\xi = 0.894, \frac{\Delta V}{\bar{V}} = 0.09$

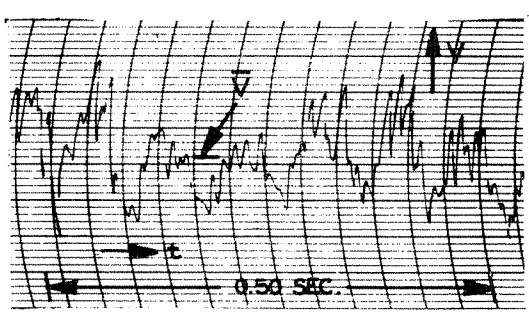

$\xi = 0.934, \frac{\Delta V}{\bar{V}} = 0.14$

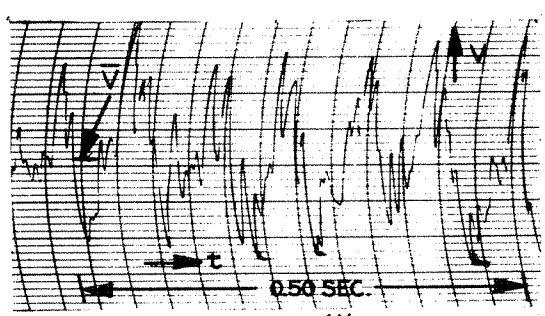

$\xi = 0.972, \frac{\Delta V}{\bar{V}} = 0.23$

Fig. 41 Small amplitude propagating stall.
Annular cascade. $\delta = 29^{\circ}$, $\beta \approx 47.5^{\circ}$, $N_s = 1$
Data $\sim$ 1 in. before cascade.

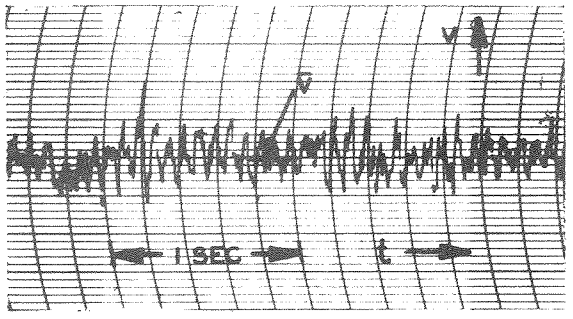

(a) $\sigma/\sigma_0 = 2/3$, $\delta = 28.5°$, $\Delta V/\bar{V} \sim 0.1$

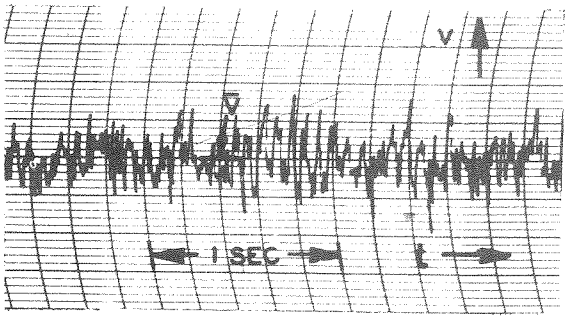

(b) $\sigma/\sigma_0 = 1/2$, $\delta = 32.0°$, $\Delta V/\bar{V} \sim 0.1$

Fig. 42 Small Amplitude Propagating Stall, Annular Cascade
$\xi = 0.894$, $\beta_1 \approx 47.5°$, $N_S = 1$ Data ~ 1 in. Before Cascade

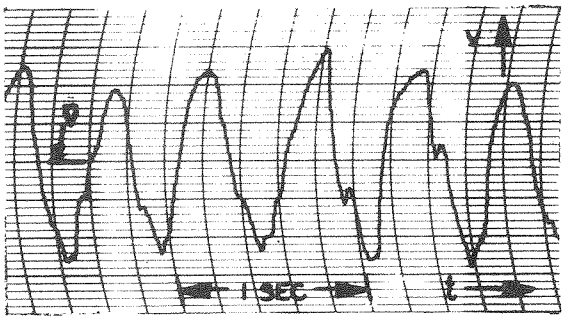

Near Suction Surface
~ 2 in. Before Cascade
$\Delta V/\bar{V} = 0.15$

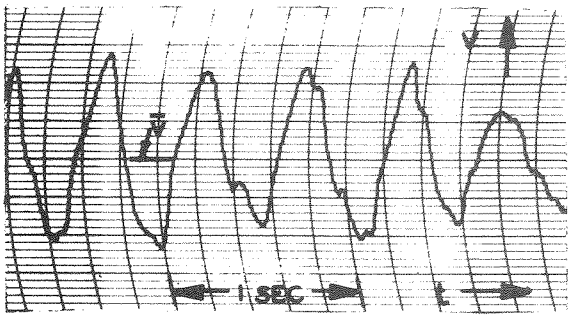

Near Pressure Surface
~ 2 in. Before Cascade
$\Delta V/\bar{V} = 0.15$

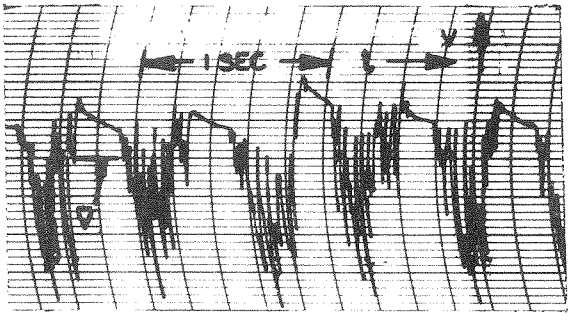

Near Suction Surface
~ 1/8 in. Behind Cascade
$\Delta V/\bar{V} = 2.16$

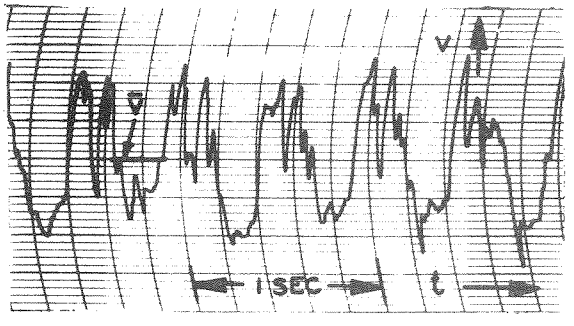

Near Pressure Surface
~ 1/8 in. Behind Cascade
$\Delta V/\bar{V} = 0.20$

Fig. 43 Small Amplitude Propagating Stall, Rectangular Cascade
$\beta_1 \approx 45°$, $N_S = 1$ Data ~ Mid-Height

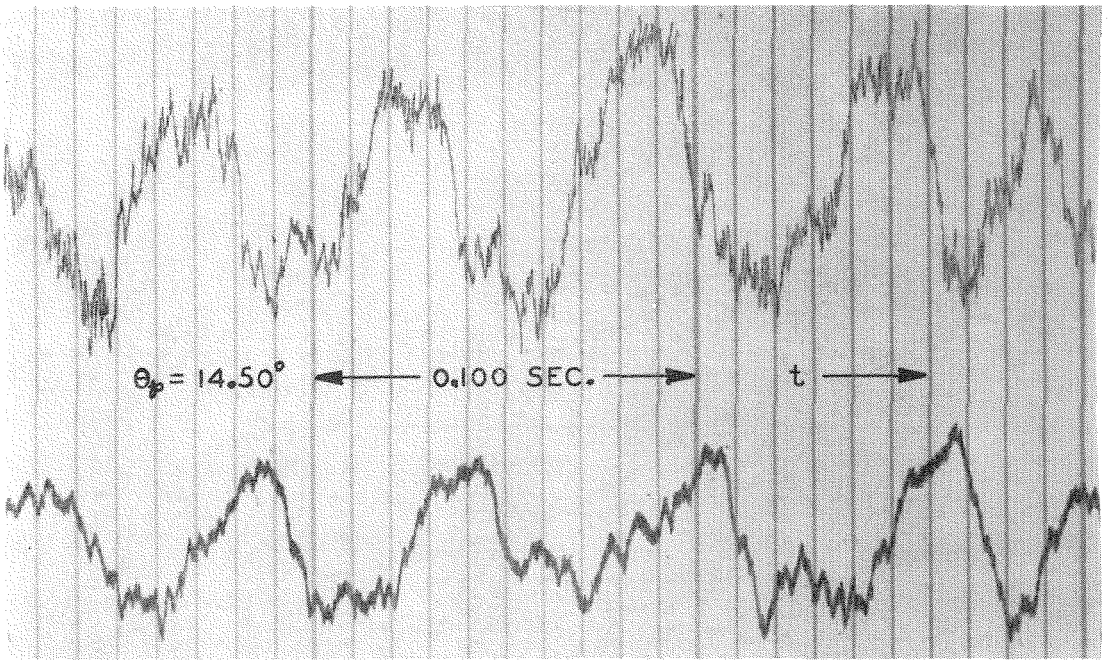

(a) $\sigma/\sigma_0 = 1$, $\xi = 0.700$, $\beta_1 = 47.0°$, $\Delta\delta = -10°$, $\Delta V/\bar{V} = 0.34$, $N_s = 7$

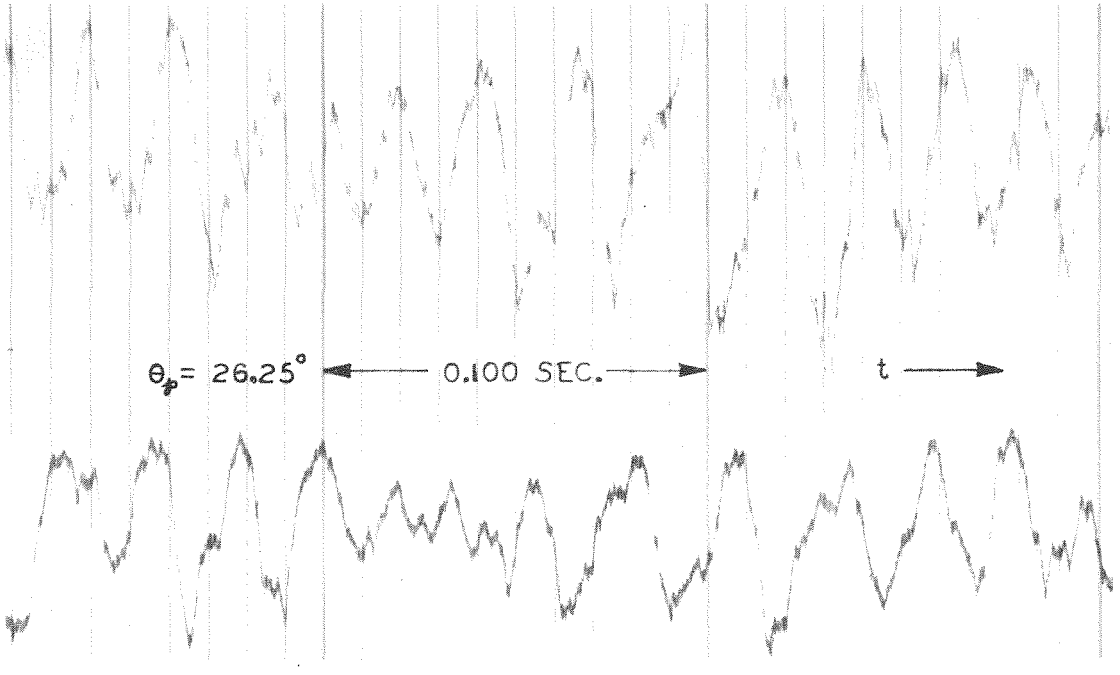

(b) $\sigma/\sigma_0 = 1/2$, $\xi = 0.700$, $\beta_1 = 47.8°$, $\Delta\delta = -10°$, $\Delta V/\bar{V} = 0.21$, $N_s = 10$

Fig. 44 Small amplitude propagating stall. Axial-flow compressor cascade, stator row. Data ~ 1/4 in. before stator row.

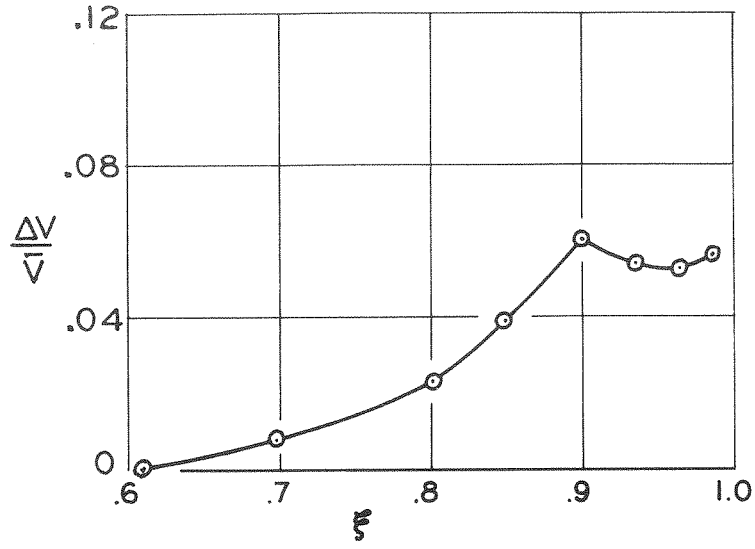

Partial stall $\bar{\Phi}$ = 0.298

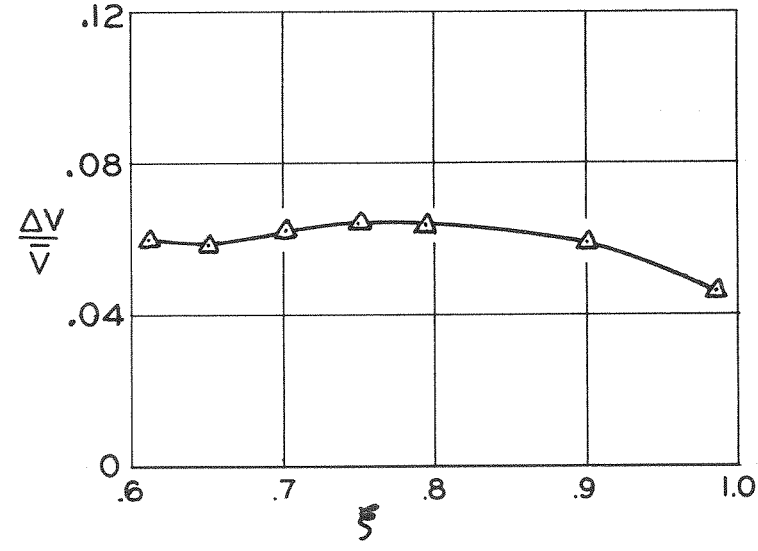

Full stall $\bar{\Phi}$ = 0.112

Fig. 45 Variation of velocity fluctuation ratio with flow coefficient. Axial-flow compressor, single-stage configuration.
Data ~ 3/8 in. behind rotor row.
σ/σ_0 = 1 (from Iura and Rannie)

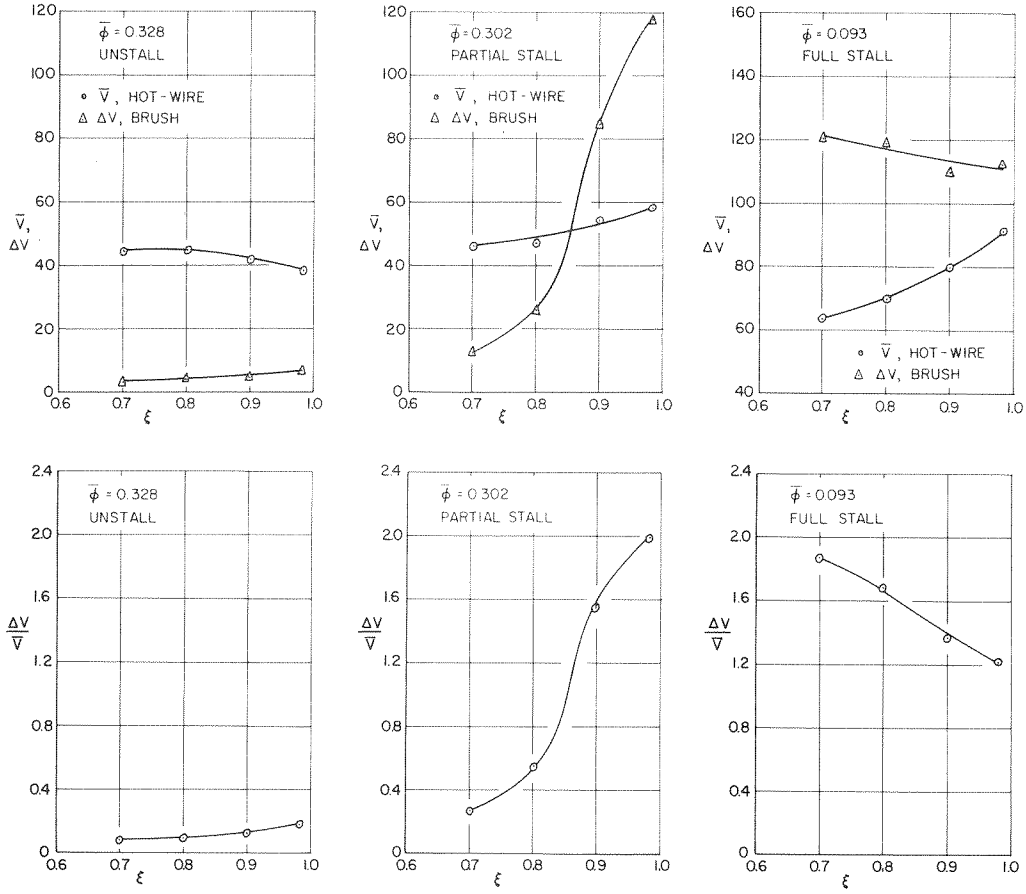

Data ~ 3/8 in. before rotor row.

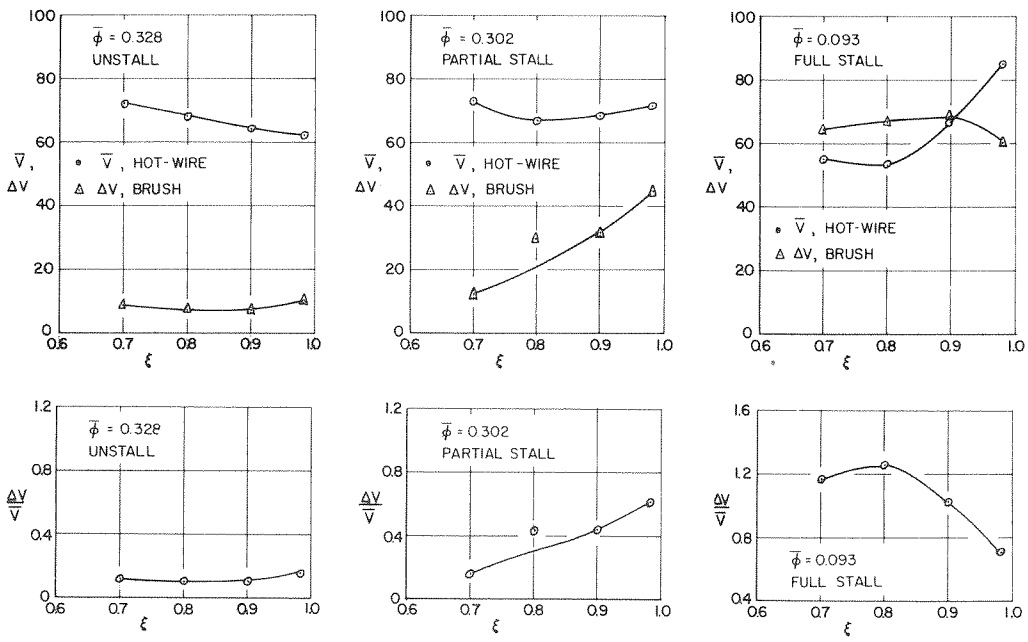

Data ~ 3/8 in. behind rotor row.

Fig. 46 Variation of velocity, velocity fluctuation and velocity fluctuation ratio with radius ratio. Axial-flow compressor, single-stage, expanded configuration. $\sigma/\sigma_0 = 1$

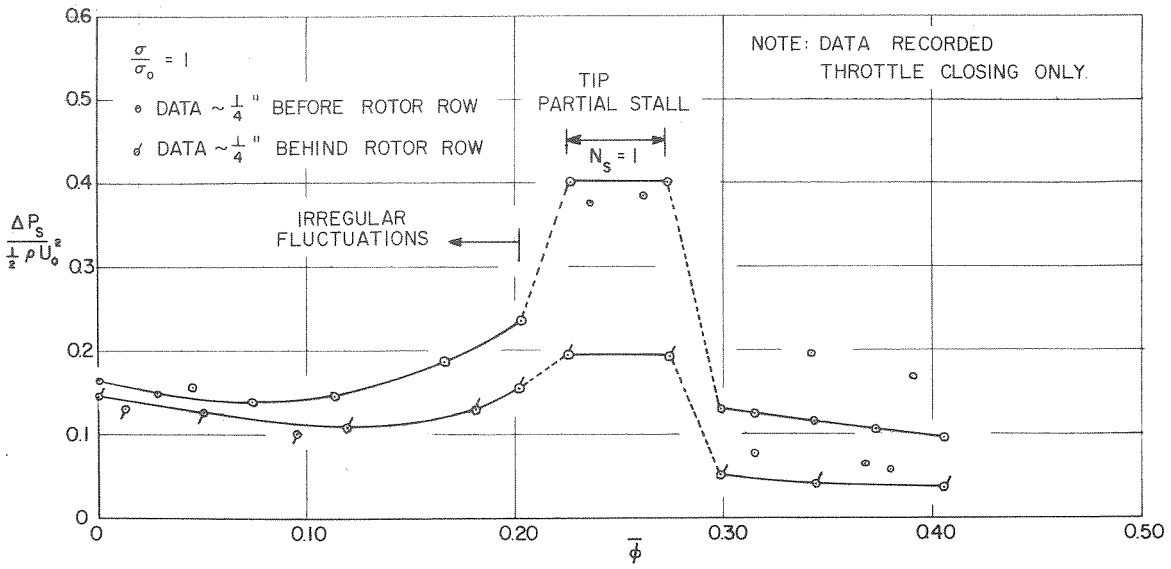

(a) Single-stage configuration.

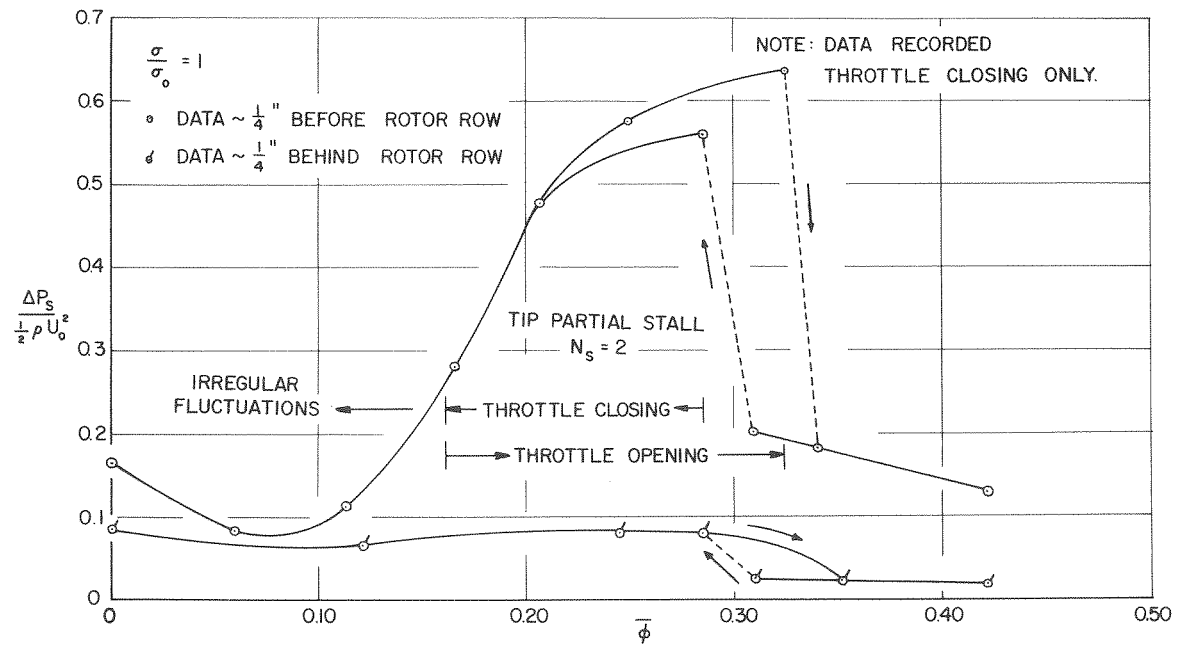

(b) Single-stage expanded configuration.

Fig. 47 Variation of static pressure fluctuation ratio with flow coefficient. Axial-flow pump.

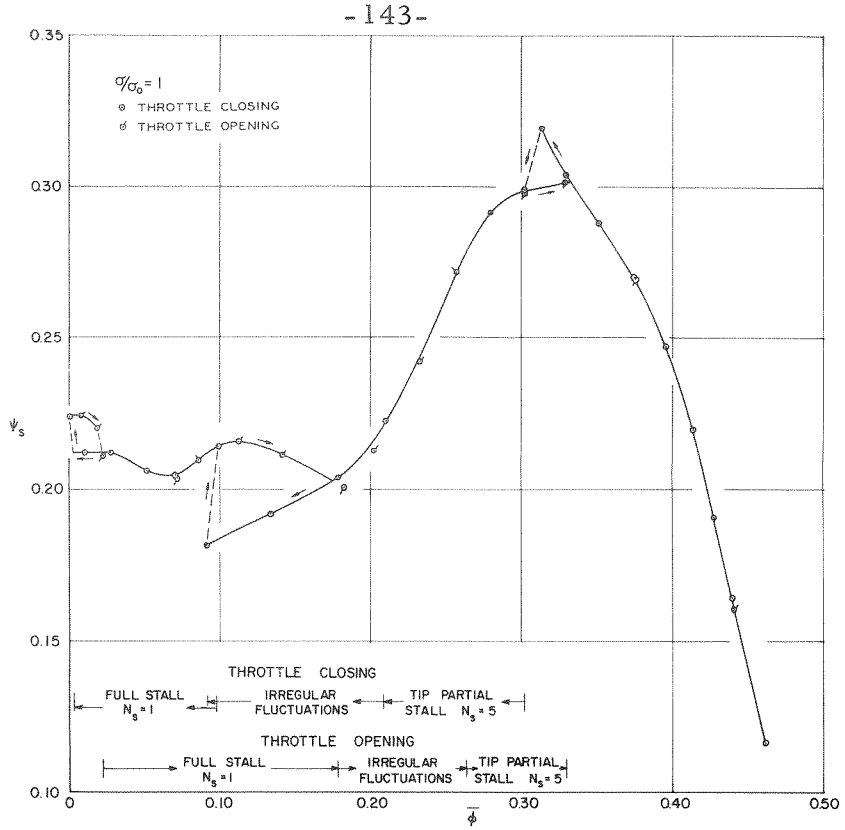

Fig. 48 Variation of exit-duct wall static pressure rise coefficient with flow coefficient. Axial-flow compressor, single-stage, expanded configuration.

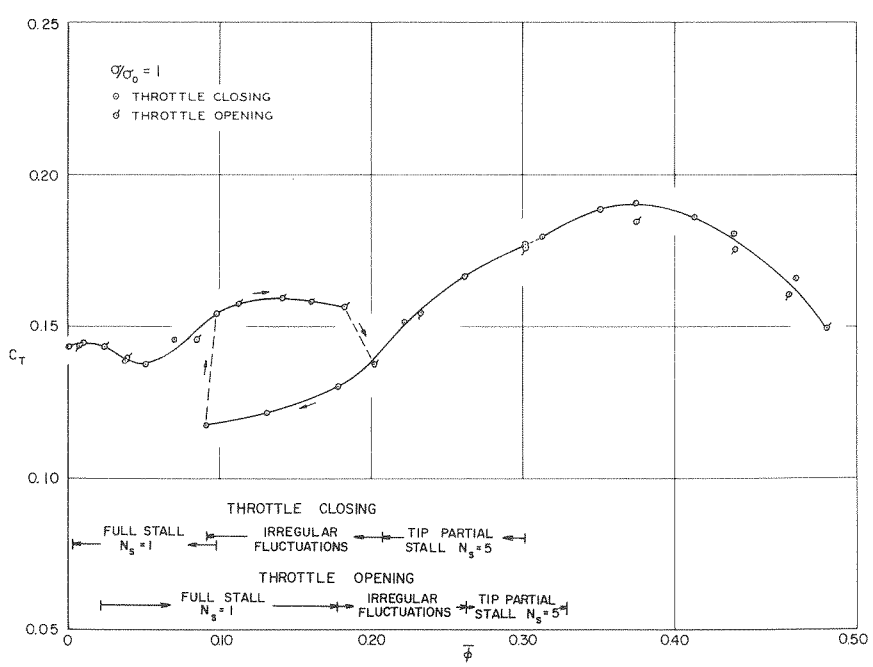

Fig. 49 Variation of torque coefficient with flow coefficient. Axial-flow compressor, single-stage, expanded configuration.

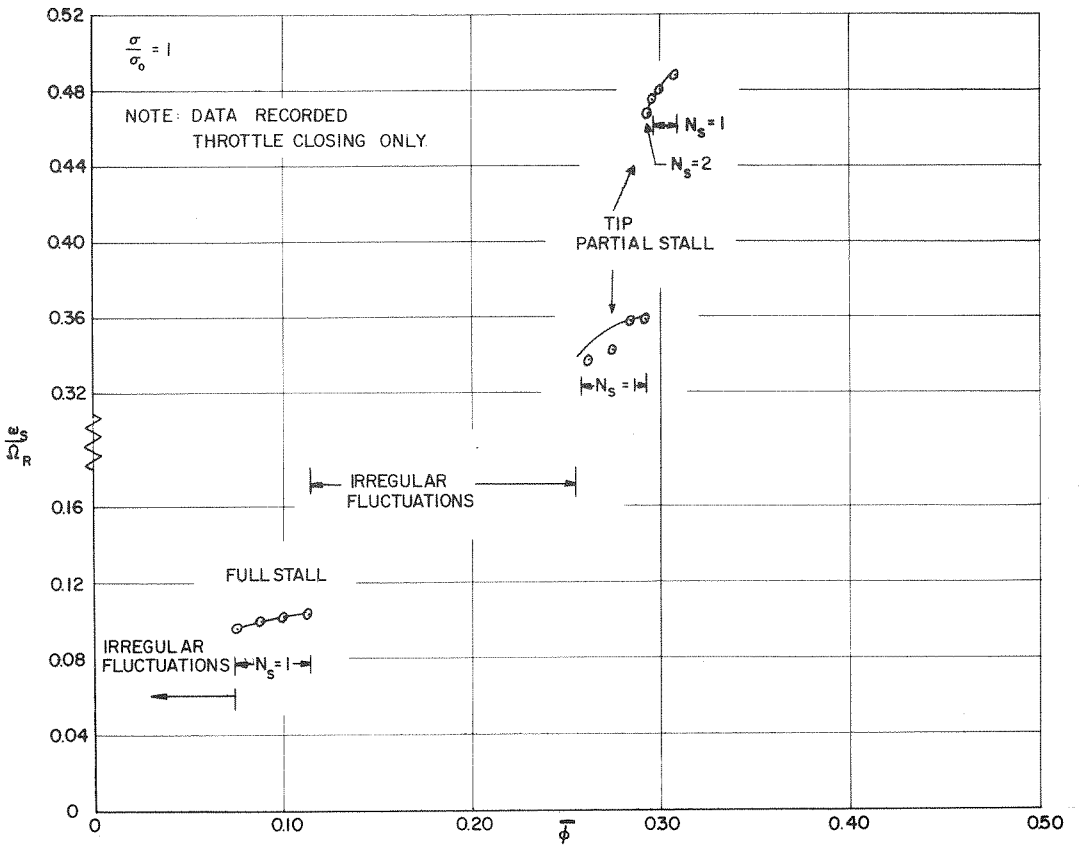

(a) Single-stage configuration (from Iura and Rannie)

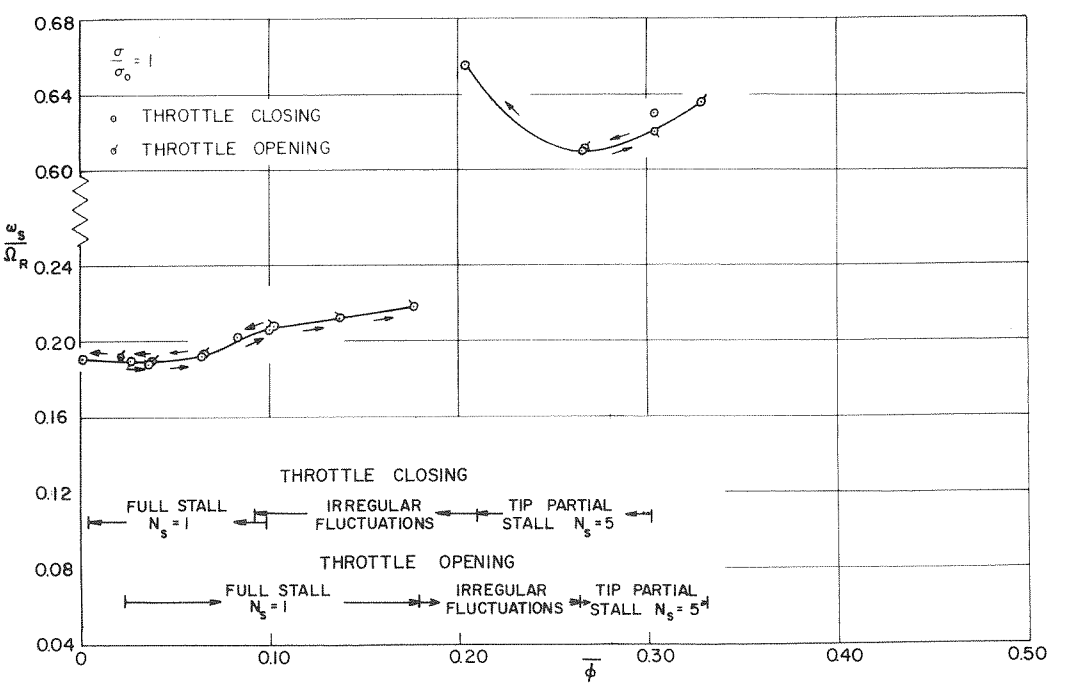

(b) Single-stage expanded configuration.

Fig. 50 Variation of absolute propagating stall frequency ratio with flow coefficient. Axial-flow compressor.

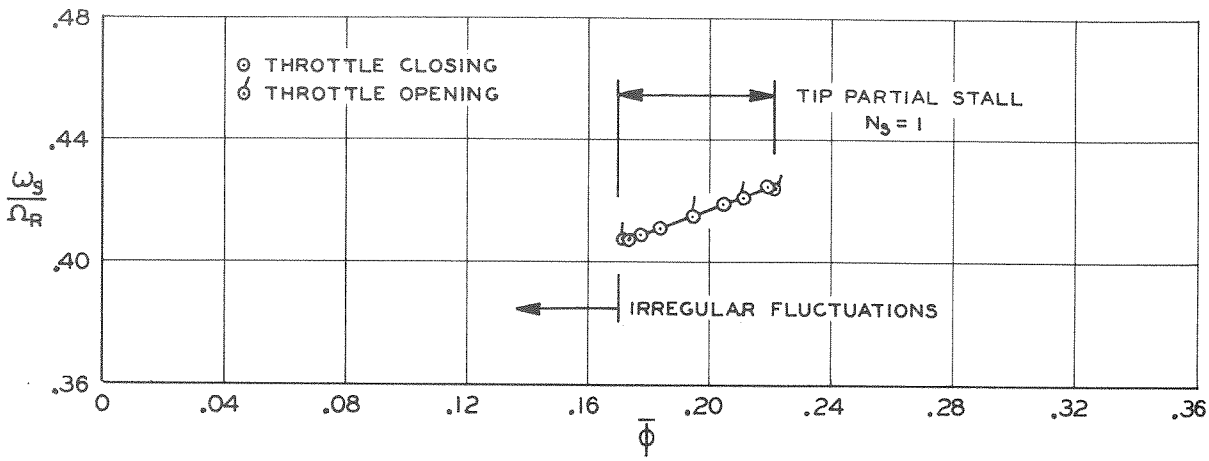

(a) Single-stage configuration.

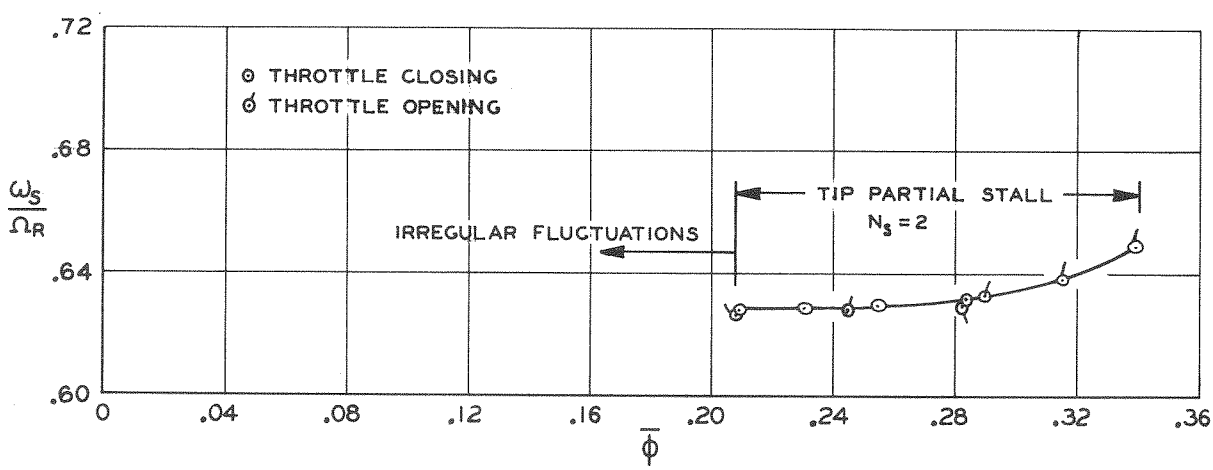

(b) Single-stage, expanded configuration.

Fig. 51 Variation of absolute propagating stall frequency ratio with flow coefficient. Axial-flow pump. $\sigma/\sigma_0 = 1$

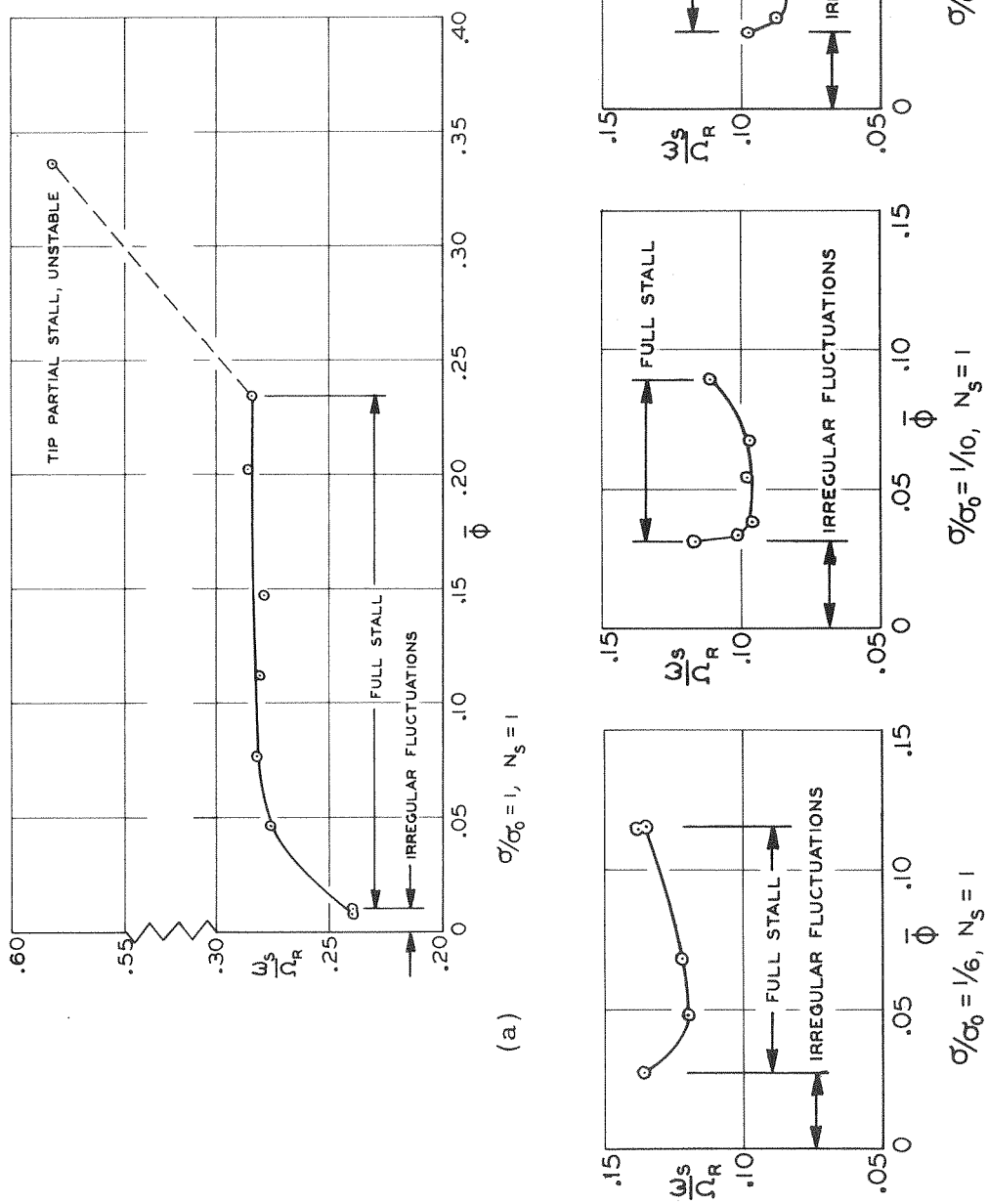

Fig. 52 Variation of absolute propagating stall frequency ratio with flow coefficient. Axial-flow compressor, isolated rotor row configuration. Data from throttle closing surveys.

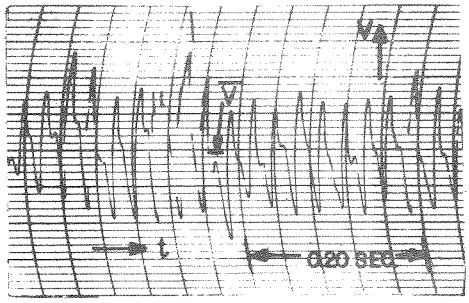

$\xi = 0.700, \frac{\Delta V}{\bar{V}} = 0.27$

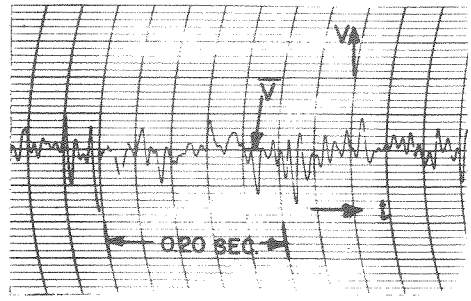

$\xi = 0.700, \frac{\Delta V}{\bar{V}} = 0.17$

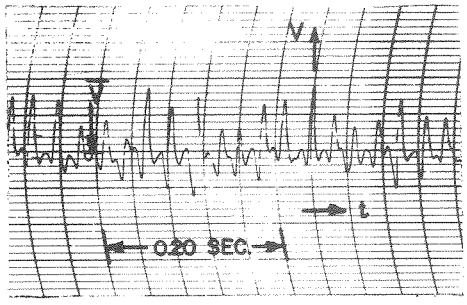

$\xi = 0.800, \frac{\Delta V}{\bar{V}} = 0.53$

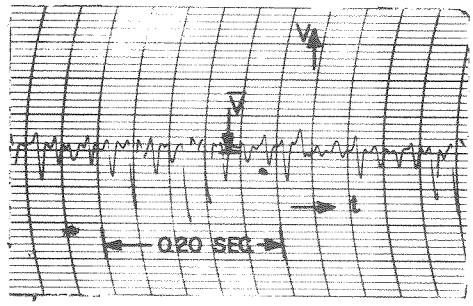

$\xi = 0.800, \frac{\Delta V}{\bar{V}} = 0.32$

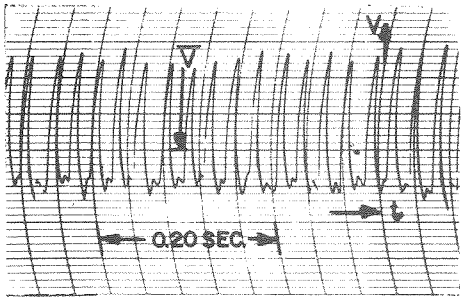

$\xi = 0.983, \frac{\Delta V}{\bar{V}} = 2.10$

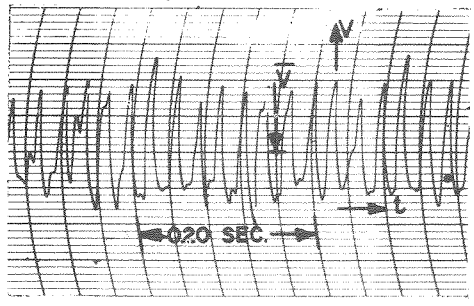

$\xi = 0.983, \frac{\Delta V}{\bar{V}} = 0.63$

Data ~ 3/8 in. before rotor.

Data ~ 3/8 in. behind rotor.

Fig. 53 Large amplitude propagating stall. Axial-flow compressor, single-stage, expanded configuration. Partial stall, $N_s = 5$, $\bar{\Phi} = 0.302$.

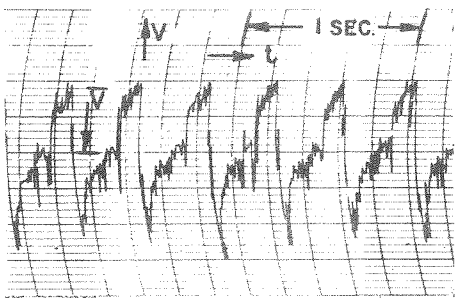

$\xi = 0.700$, $\frac{\Delta V}{\bar{V}} = 1.88$

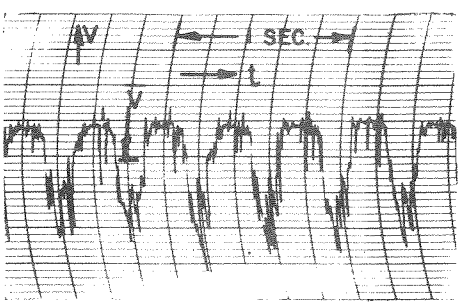

$\xi = 0.700$, $\frac{\Delta V}{\bar{V}} = 1.17$

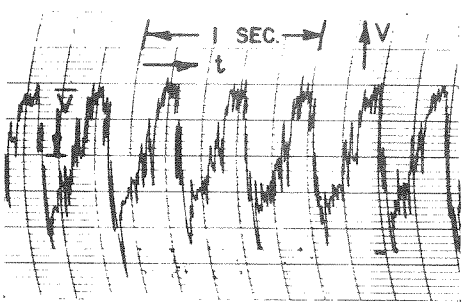

$\xi = 800$, $\frac{\Delta V}{\bar{V}} = 1.67$

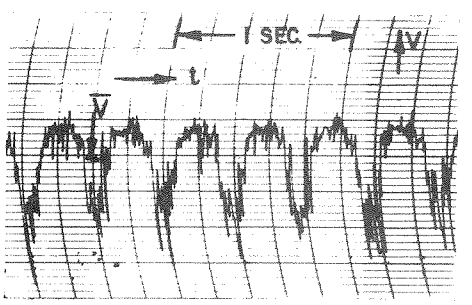

$\xi = 0.800$, $\frac{\Delta V}{\bar{V}} = 1.26$

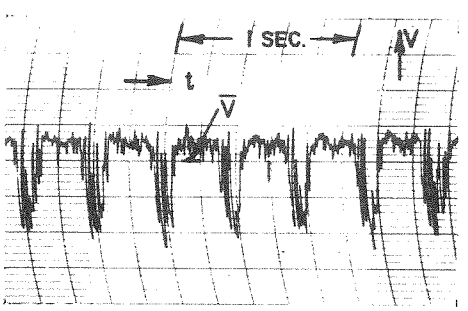

$\xi = 0.983$, $\frac{\Delta V}{\bar{V}} = 1.22$

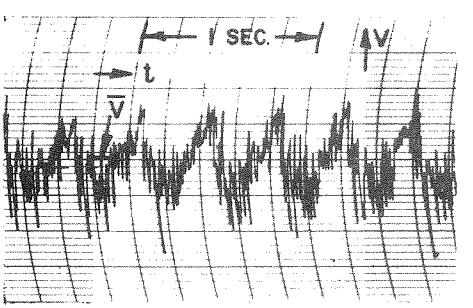

$\xi = 0.983$, $\frac{\Delta V}{\bar{V}} = 0.71$

Data ~ 3/8 in. before rotor.

Data ~ 3/8 in. behind rotor.

Fig. 54 Large amplitude propagating stall. Axial-flow compressor, single-stage, expanded configuration. Full stall, $N_s = 1$, $\bar{\Phi} = 0.093$.

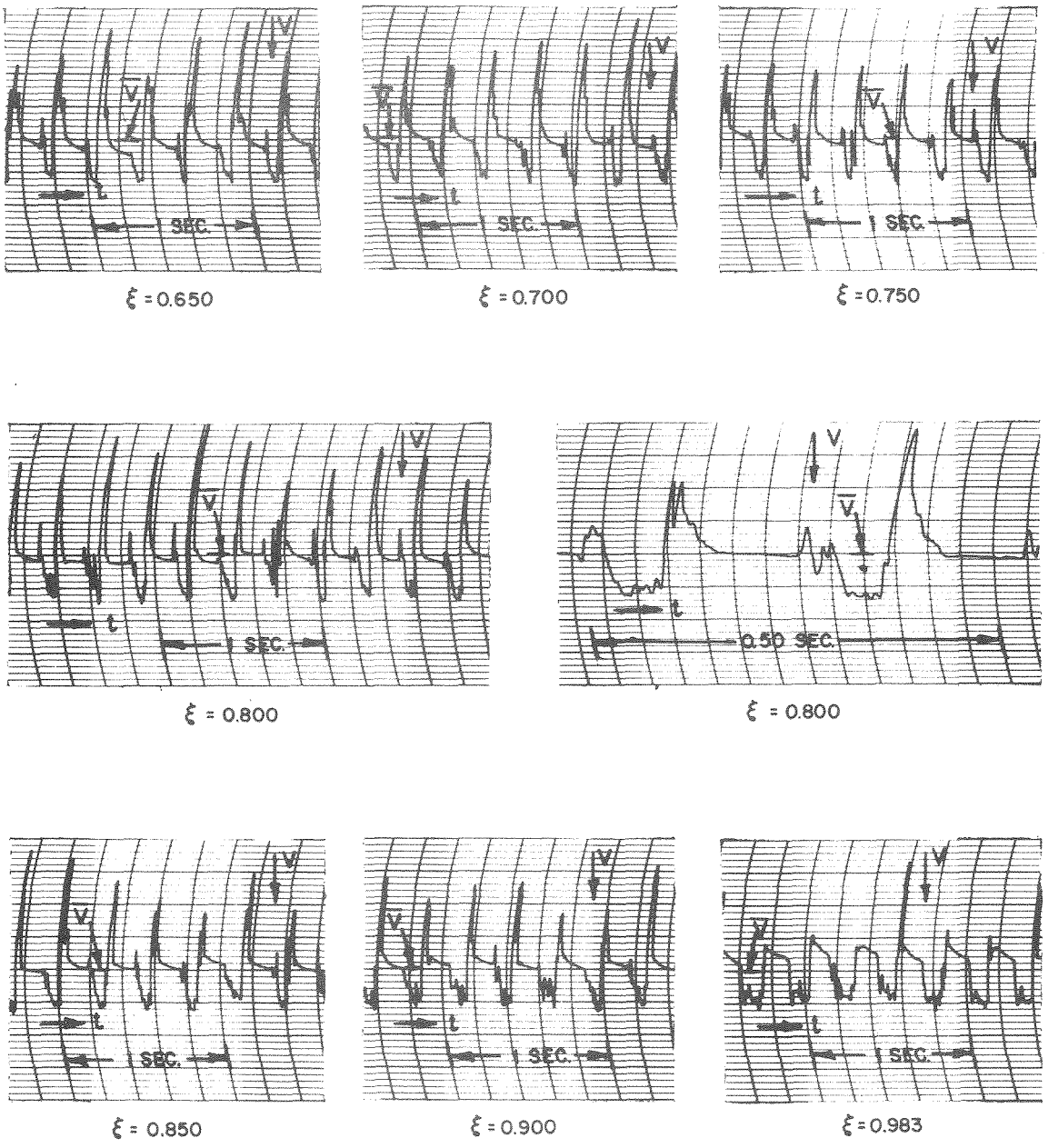

Fig. 55 Large amplitude propagating stall. Axial-flow compressor, isolated rotor row configuration. Full stall, $N_s = 1$, $\bar{\phi} = 0.234$, $\Delta V/\bar{V} \sim 1.8$.

Data ~ 3/8 in. before rotor row.